2007

Structured illumination as a processing method for controlling photopolymerized coating characteristics

Peter Daniel Ganahl
University of Iowa

STRUCTURED ILLUMINATION AS A PROCESSING METHOD FOR CONTROLLING PHOTOPOLYMERIZED COATING CHARACTERISTICS

by

Peter Daniel Ganahl

An Abstract

Of a thesis submitted in partial fulfillment of the
requirements for the Doctor of Philosophy degree
in Chemical and Biochemical Engineering in
the Graduate College of
The University of Iowa

May 2007

Thesis Supervisors: Professor Alec B. Scranton and
Adjunct Associate Professor Chris N. Coretsopoulos

ABSTRACT

The most prevalent polymerization methods are those which fall under the category of thermal polymerizations. The ease of initiation and the abundant knowledge present for these long time standards make implementation straightforward. However in some applications, the drawbacks may be numerous and the use of light induced polymerizations may be advantageous. Because of distinct advantages obtained using photopolymerizations as opposed to the more conventional thermally induced polymerizations science continues to further the knowledge and applications of photopolymers. Structured illumination is one such expansion of photopolymer knowledge and is a method by which variations in light intensity set up differential reaction rates evolving in the migration of monomer. The method can be tailored to produce cured systems with enhanced properties such as the reduction of stress or the control of gloss.

Polymerization shrinkage is important for many applications since it leads to residual stresses which can deform a system and undermine its optical or mechanical properties. Also, while photopolymerized coatings are generally high in gloss, it is a characteristic of a polymer system that can have great impact on its function and appearance. Utilizing the simple method of structured illumination, and thereby controlling the coating system for both reductions of stress and gloss, can lead to great advantages for the finished product. This contribution looks at not only producing coatings using the method of structured illumination but also characterizes their properties by standard and unconventional means, alike. Mathematical modeling of the shrinkage, stress and monomer migration is also present in this work.

Abstract Approved: _____

Thesis Supervisor

_____

Title and Department

_____

Date

_____

Thesis Supervisor

_____

Title and Department

_____

Date

STRUCTURED ILLUMINATION AS A PROCESSING METHOD FOR CONTROLLING PHOTOPOLYMERIZED COATING CHARACTERISTICS

by

Peter Daniel Ganahl

A thesis submitted in partial fulfillment of the
requirements for the Doctor of Philosophy degree
in Chemical and Biochemical Engineering in
the Graduate College of
The University of Iowa

May 2007

Thesis Supervisors: Professor Alec B. Scranton and
Adjunct Associate Professor Chris N. Coretsopoulos

Graduate College
The University of Iowa
Iowa City, Iowa

CERTIFICATE OF APPROVAL

PH.D. THESIS

This is to certify that the Ph. D. thesis of

Peter Daniel Ganahl

has been approved by the Examining Committee for the thesis requirement for the Doctor of Philosophy degree in Chemical and Biochemical Engineering at the May 2007 graduation.

Thesis Committee:_____
Alec Scranton, Thesis Supervisor

_____
Chris Coretsopoulos, Thesis Supervisor

_____
John Wiencek

_____
David Rethwisch

_____
Ned Bowden

To my loving wife and daughter

ACKNOWLEDGMENTS

Many have contributed to my success here at the University of Iowa and I would like to express my sincere appreciation to those who have been most influential. First, I would like to start off by thanking my advisors, Dr. Chris Coretsopoulos and Dr. Alec Scranton. Without their energy and spirited discussion, my research would have not nearly been as successful. I am also indebted to the undergraduate research assistants who have helped with the many tasks involved in everyday research. I hope the experiences we shared have been as thought provoking and enlightening for them as they were for me. I am grateful for the diverse research group in which I have been involved, both past members who have moved on and those I leave behind. I wish them all well. Of course none of my this research would be possible without funding and the source of my funding came from an excellent group of companies who's individual representatives were responsible for mentoring me and giving me a chance to present my work to many brilliant minds in the field of photopolymerization. And most importantly, I would like to thank my wife and daughter for their love and support throughout my time at the University of Iowa.

TABLE OF CONTENTS

LIST OF TABLES

LIST OF FIGURES

CHAPTER 1: INTRODUCTION AND MOTIVATION

Introduction to Photocurable Processes and their Advantages over Thermal Processes

The most prevalent polymerization methods are those which fall under the category of thermal polymerizations. The ease of initiation and the abundant knowledge present for these long time standards make implementation straightforward. However in some applications, the drawbacks may be numerous and the use of light induced polymerizations may be advantageous. With the more common thermal polymerizations heat is used to start the reactions and the energy input into these reactions is immense when compared to the more efficient use of energy present in photopolymerizations. Thermal polymerization initiations are also limited by the rate of heat transfer. Initiation takes place at elevated temperatures and getting to the required temperature takes time which is dependent on the transfer of heat. Conversely, photopolymerizations are initiated immediately upon illumination and, depending on the chemistry, can be made to either terminate or continue when the light is removed. Thermal polymerizations take time to cease and can be difficult to control. Directing light on a photopolymerizable sample also gives rise to spatial control of reaction. Directed light is easily accomplished using lasers or masks. Matching this capability using heat is a difficult if not impossible task.

A summary of the common advantages of photopolymerizations includes high reaction rates at room temperature, ability to use solvent free formulations to avoid environmental or contamination issues, both spatial and temporal control of initiation and polymerization, low energy input because of the more efficient use of light energy rather than thermal energy, and finally the chemical versatility afforded by an ever increasing interest and research base in the photopolymer field.

Commercial and Industrial Applications of Photopolymers

Because of the advantages listed photopolymers have been used as an industrial standard in a wide array of products and processes for many years with new applications being implemented regularly. Such standard applications of photopolymers include printing, whether applied as photoreactive inks which take far less time to "dry" than conventional inks[1, 2] or to make printing plates for flexographic printing. Photopolymers have also found permanent homes in optical data storage[3, 4] and holography[5]. Rewritable CDs and DVDs use a laser to change the color or reflectivity of photoresponsive dyes while holograms use lasers for photopolymerization and take advantage of the difference of index of refraction between a monomer and the polymer it produces or two separate polymers to create images[6]. Dentistry is an area in which a large volume of research has been conducted involving photopolymers for use in dental restoratives[3, 7-9]. Dental researchers have proven that even thick cure systems are possible with some systems using a photobleaching initiator[10]. With all photopolymers have to offer it is no wonder that their applications are growing daily.

Thin films and coatings are another area where photopolymers excel. With thin geometries, the added heat from reactions is dissipated quickly, and high reaction rates at room temperature allow for solidification and further processing at very rapid rates, thereby eliminating the need of storage space for annealing, cooling or drying products. At one time the rate limiting step for producing optical fibers was the curing of the polymer cladding which was greatly enhanced by the use of photopolymers. The rate limiting step now tends to be winding the fibers for shipment. A newer and possibly less well know application for photopolymers is in the personal care industry. Fingernail polishes and coatings are now being photopolymerized[11, 12]. Also home use of photopolymers is being employed by fishermen for sealing a knot on a fishing line or applying various colors to their jigs to attract fish. These photopolymers have the capability of harnessing the energy of the sun for a simple and useful purpose.

Another common use for photopolymers is in the manufacturing of printed circuit boards used in many electronic devices. The speed and accuracy of photoprocessing a printed circuit board makes photopolymers essential for product competitiveness[13-15]. Optical photopolymers have also been proven useful in certain commercial applications[4]. These last two examples represent technological fields in which photopolymers are important.

Current Limitations of Photopolymer Systems

Polymerization Shrinkage Stress

As with many polymer systems, polymerization shrinkage can cause problems to emerge in a finished product. This shrinkage comes about during polymerization and is a function of the density being higher in the polymer than in the original monomer. In the case of unconfined systems such as films and prototyping, this shrinkage can lead to visible deformities in the product[16]. For confined systems such as dental restorations or coated surfaces[17, 18] the shrinkage is restrained and a stress is realized. This stress can have painful effects for a person with a restored tooth or coated fingernail. In the case of a dental restoration internal stresses can cause micro cracks to form between the tooth and restoration providing sites for additional decay. During or after a manicure, stresses built up from a thick coat of glossy finish can cause pain and a weakening of the coated fingernail[12]. Industrially, this shrinkage stress is important in the lifetime and durability of coatings[19]. Internal stresses can weaken the coating and in some cases cause loss of adhesion between the coating and the substrate[17, 20].

A vast majority of shrinkage stress related research has been focused in the field of dentistry. Some studies focused on measuring shrinkage and exploring methods to reduce it[21-23], while others have accepted shrinkage and instead measured the stress and researched how to manage it[3, 24, 25]. The issue of polymerization shrinkage stress

has been deemed important enough to have national standards assigned for its measurement[26].

In order to combat polymerization shrinkage and shrinkage stress various formulations have been tried. One field of chemistry applied to photopolymers in order to combat polymerization shrinkage is cationic polymerization. Also bulky pendent groups, oligomers and large monomer molecules have been incorporated so as to reduce the percent volume of reactive groups per molecule. Additives have been used to reduce to percentage of matter undergoing polymerization and hence polymerization shrinkage. Additives can also be used to lower the modulus of the polymer therefore causing less stress to its confinement. Stress absorbing adhesives have been used in dental applications between the tooth and the dental restorative to reduce the stress realized by the tooth. Each of these methods can be used only in specific circumstances where as the use of spatial and temporal patterns of light are applicable to a wide array of photopolymerization applications. Structurally illuminating a photopolymerizable sample will be discussed in great detail throughout this work and specifically in Chapter 5 regarding stress relief.

Gloss Issues in Photopolymerized Coatings

In general, neat photopolymerized coatings are very smooth and glossy. This has tremendous advantages for automotive applications and other applications where high gloss is desirable. Many photopolymerized systems such as those incorporating acrylates also offer the advantages of durability, scratch resistance and good weathering characteristics[20, 27]. These advantages make them desirable in applications many applications regardless of gloss. For low gloss applications additives have been commonly used to lower the apparent gloss of the coating by micro-roughening its surface. This is a common practice in the wood coatings industry for products such as cabinetry, flooring and furniture[28, 29]. With a concentration gradient being setup in a

structurally illuminated sample, one can take advantage of diffusion and shrinkage induced monomer migration to micro-roughen the surface of a coating without incorporating the possible drawbacks of additives. This technique will be discussed in further detail in Chapters 6 and 8.

CHAPTER 2: BACKGROUND

This chapter will discuss free radical polymerizations, specifically that of acrylates, followed by photoinitiation, stress development in polymerizing systems, techniques to measure that stress, methods to reduce it with an introduction of structured illumination, and finally gloss control techniques and how structured illumination may help in this area of research.

Free Radical Polymerizations

The mechanism of free radical polymerizations includes three main steps: initiation, propagation, and termination. In the initiation step, free radicals are formed which start the reaction and subsequent propagation of the free radical to form a polymer chain. Termination occurs via different reactions in order to stop the reaction resulting in a polymerized system.

In a free racial polymerization the initiation step itself consists of two steps. First an initiator molecule must dissociate in order to form two separate, either similar or dissimilar species. The initiating radical must then combine with a single monomer molecule in the association step. The dissociation step can be represented by the following equation where k_d is the dissociation rate constant of the initiator (I-I) into two free radical initiator species (I●)[30]. A free radical initiator species may also be obtained by the abstraction of a hydrogen molecule but will not be discussed here for its use will not be needed by the studies revealed in this work[31].

$$I\text{-}I \xrightarrow{k_d} 2I\bullet$$

Eq 2.1: Dissociation of initiator molecule into free radical initiator species.

The association step can then be represented by the following equation where k_a is the rate constant for monomer association between the monomer (M) and the free radical initiator species.

$$I\bullet + M \xrightarrow{k_a} IM\bullet$$

Eq 2.2: Association of a monomer molecule (M) to the free radical initiator species.

From Equation 2.1 and 2.2 the rate constants, k_d and k_a can be combined to get an overall initiation rate constant, k_i. Propagation then takes place as represented by Eq 2.3.

$$IM_x\bullet + M \xrightarrow{k_p} IM_xM\bullet$$

Eq 2.3: Propagation of free radical to extend the polymer chain length by one monomer unit.

Here, k_p is the propagation rate constant for the addition of a monomer to the growing polymer chain ($IM_x\bullet$). This propagation eventually is halted, generally during the termination step. Termination can occur by three common processes. One is termination by combination which is the process by which two propagating radical chains meet and combine to form one polymer chain.

$$IM_{x-1}M\bullet + \bullet MM_{y-1}I \xrightarrow{k_{tc}} IM_{x-1}M\text{-}MM_{y-1}I$$

Eq 2.4: Termination of propagating radical chains, $IM_{x-1}M\bullet$ and $\bullet MM_{y-1}I$ by combination to form a polymer chain of length x+y.

The propagating radical chains can be of any chain length and their combining occurs by creating a covalent bond between the two species from the radical ends. This process is illustrated in the following equation with k_{tc} as the rate constant for termination by combination.

Termination can also take place by disproportionation leaving two separate and terminated chains. This is illustrated in the following equation where k_{td} is the rate constant of termination by disproportionation.

$$IM_{x\text{-}1}M\bullet + \bullet MM_{y\text{-}1}I \xrightarrow{k_{td}} IM_x + IM_y$$

Eq 2.5: Disproportionation of propagating radical chains in order to form two separate and terminated chains of length x and y.

Growing polymer chains can also be terminated by chain transfer in which a hydrogen is abstracted from an initiator, solvent, monomer or polymer molecule. This reaction is summarized by the following equation.

$$IM_{x\text{-}1}M\bullet + SH \xrightarrow{k_{tr}} IM_{x\text{-}1}MH + S\bullet$$

Eq 2.6: Termination via chain transfer by hydrogen abstraction.

Here k_{tr} is the rate constant of termination by chain transfer and SH represents a solvent or other molecule with an abstractable hydrogen atom. It is also important to note that a polymerization reaction can cease to continue in the event that the radical becomes entrapped within the self made network thereby not allowing it to react further.

Photoinitiation of Free Radical Polymerizations

Photoinitiation refers to a process by which light is used to dissociate the initiator molecule in the first step of a polymerization reaction[32-34]. Dissociation of an initiator molecule can occur through many mechanisms including the use of heat, light and chemical methods as an energy source for dissociation of the initiator molecule. The photoinitiation of an initiator molecule is represented in the following equation where I_a-I_b is an initiator molecule which splits into two separate molecules when light (hυ) is incident upon the system.

$$I_a - I_b \xrightarrow{h\upsilon} I_a \bullet + I_b \bullet$$

Eq 2.7: Dissociation of an initiator molecule by light energy.

Here, I_a can be equal to I_b, but such is not often the case. The overall efficiency of the photoinitiation process is a product of the fraction of incident light absorbed by the photoinitiator, the fraction of photoinitiator reactive excited-state which produces initiator species and the fraction of initiators which initiate polymerization. It is important that the light being emitted by the illumination source be such that it will effectively dissociate the initiator molecule. This effectiveness is a function of the both the wavelength and the intensity of the light illuminating the system. Light being absorbed by the initiator in order to initiate a polymerization reaction can often be absorbed by other components of the system thereby limiting the effectiveness of the initiator. Despite these considerations the efficiency of energy transfer between the light energy and the initiator molecule is quite high making energy input into the system lower than that needed for the more common thermal polymerizations.

The initiators themselves are often quite expensive but are used in very small quantities, generally less than 5% by weight and often at concentrations as small as 0.1%. Utilizing photoinitiators rather than thermal not only cuts down on energy costs but also on solvent costs since in coating applications and the like, solvents are not needed for photopolymer formulations.

Acrylates: A Standard in Industrial Applications

The number of applications in industry involving the use of acrylates is profound. Because of their properties acrylates can be found in applications ranging from durable, weather resistant coatings to dental composites. Acrylates are found in home use products including adhesives and nail polishes while industrial adhesives, coatings and printing inks are also made from acrylates[35-37]. High quality paper finishes, pressure sensitive adhesives, and polymer property modifiers are also among the list of growing fields for acrylate applications.

Being a low viscosity liquid at room temperature[33] thereby providing ease of storage, transportation and application, Hexane Diol DiAcrylate (HDDA) has become an important acrylate monomer in industry. When cured, HDDA has high impact strength, with good weather resistance and scratch resistance[37]. HDDA is a relatively inexpensive photopolymerizable monomer[37] that despite its possible health concerns has yet to be replaced in many industrial applications[35].

Polymerization Shrinkage Stress Development, Measurement and Methods for Reduction

In all polymerizable systems one must contend with the possibility of polymerization shrinkage and the stresses related to that shrinkage. Shrinkage occurs when covalent bonds are formed between monomer molecules. These bonds allow two or more monomer molecules to take up less space than they otherwise would while moving about freely in solution. This concept of polymerization shrinkage is very

important in acrylate systems with a high ratio of reactive bonds to monomer volume, as is the case with HDDA. This shrinkage is a function of the density of the polymer being higher than that of the monomer from which it is made. Knowing the density of the monomer and polymer, one can calculate the shrinkage with Equation 2.8[38] where ρ_p and ρ_m are the polymer and monomer densities, respectively.

$$\text{Shrinkage } (\%) = 100 \times \frac{\rho_p - \rho_m}{\rho_p}$$

Eq 2.8: Percent shrinkage calculated knowing the densities of the polymer and the monomer from which it is made.

There are varying techniques to measure the shrinkage of a photopolymer system including pycnometry, dilatometry[21], the use of a linometer[22], absorbance measurements for films[36] and the like[39], however for this contribution the shrinkage stress is a more important parameter. The stress as a result of polymerization shrinkage is a function of not only the shrinkage and the monomer conversion leading to that shrinkage but also the adhesion to the confinement, the modulus of the polymer system, the modulus of the confinement and, as will be revealed, the manor in which the polymerization occurs.

Shrinkage stresses can hinder the longevity and durability of films and coatings along with causing internal stresses in intricately designed pieces made during photo-fabrication using techniques such as the additive layer method. Shrinkage can also play a role in dentistry during the photopolymerization of pastes used in dental restoratives. Shrinkage in these pastes cause internal stresses between the tooth and the restorative thereby depleting its life. Finding a method simple to reduce such shrinkage stresses would prove quite advantageous.

Common Stress Reduction Techniques

Scientists have been working on this problem and have implemented such techniques as using fillers within the polymer matrix. Fillers are rigid bodies which do not shrink during the polymerization process. With less polymer present per volume there is ultimately less total volumetric shrinkage. This works well for polymers in which their properties are not adversely affected by the filler. Optical properties, for example, are often adversely affected by fillers. In this case the fillers would be considered contaminants. Also the dimensions of the final product must be sufficiently larger than the dimensions of the filler. Thin film coatings for example would not be an area in which large fillers would be much help. Within the field of dentistry scientists have also implemented the use of stress absorbing adhesives. Others have looked at using high molecular weight monomers with either long carbon backbones or bulky pendent groups. In either case the idea is again to reduce the percent of the system that is undergoing reaction and subsequent shrinkage[40].

Preliminary Studies with Stress Measurements

It has been observed, after photopolymerizing a drop of monomer between two glass slides creating a thin film, that Newton's Rings are visible. Newton's Rings come about from the constructive and destructive interference of reflected light waves from both a curved transparent surface and a flat surface. Knowing the wave length of light being reflected and the spacing of the rings one can calculate the radius of curvature of the upper curved transparent surface. During the polymerization of a drop of monomer between two glass slides it is believed that the slides are bending due to the shrinkage and stresses from the polymer. With the use of an ordinary desktop scanner and Adobe Photoshop® one can enhance the visibility of the rings and if a direct correlation between these rings and the stresses involved in photopolymerization could be made then an easy and inexpensive method of measuring polymer stress would be available.

Coming up with such a correlation would be quite valuable and could be easily implemented into experiments involving partial illuminations and multiple step illuminations. One such way in which a correlation between these observed Newton's Rings and shrinkage stress and strains might be made is to use small strain analyzers on the film during photopolymerization. Strain analyzers relate the bending of the analyzer to the impedance of the circuit within the analyzer. Such analyzers can be quite small; on the order of millimeters. These devices may be useful to measure strain during a polymerization and at the same time rings could be counted and a relation could possibly be made.

Considerations for this technique are many. One, the modulus of the strained glass would need to be well known and consistent between the different pieces needed for multiple experiments. Also the cost of the strain analyzers is such that reuse would need to be possible. Permanently affixing them to the glass or polymerizing them between the glass slides would not be affordable. Also the application of the monomer to the glass substrates would need to be very consistent. Inconsistencies in the thickness of the polymerizing monomer would cause variations in the ring count.

Another way to measure the stress development in thin films may be to use a stress gauge normally applied in the semiconductor industry. This gauge relies on knowing the mechanical properties of a thin wafer of silicon and measuring its deflection when a thin layer of monomer is polymerized on its surface. This deflection, with the use of a few simple equations can reveal the stress induced on the silicon substrate by the polymerizing monomer. Getting an old stress gauge to work proved quite difficult and was eventually abandoned. Even if it were to function properly consistent application was still an issue. Attempts to deal with this were made by the use of a spin coater.

Other Techniques for Stress Measurement

Francis et al outlined a method of using a coated elastic substrate and measuring the curvature of deflection of the object[41]. This curvature can be related to the stress placed on the substrate due to the polymerization by knowing the elastic properties of the substrate. The radius of curvature can be monitored using expensive analytical equipment such as scanning laser devices or x-ray diffraction. Without the means for such expensive equipment a simpler and cheaper method is desired.

Stolov et al showed not only a way to measure stress using a cantilever beam but also a way to monitor the reaction taking place causing the stress. This cantilever beam technique again used a sophisticated setup in order to measure deformation of the cantilver beam using a laser and detector[42].

Watts et al used a load cell and a displacement transducer to measure stresses with compliances taken into account[43] similar to one made by Stansbury et al based on a large cantilever beam[25]. Again these techniques would take quite the capital investment in order to begin measurements. Also they were not set up for a film or coating geometry.

ASTM International has also researched methods to measure shrinkage stress. One such method uses small thin strips of metal which curve when a coating is applied to its surface and subsequently cured[44]. This method is relatively inexpensive and easy to implement, however at the onset of this work its creation was not yet complete.

Similar attributes to all the cantilever beam based measurements are that they share use of the Stoney equation[45] and work done by Corcoran[46]. This gives a good place to start in determining the best method for stress measurements for experiments involving structured illumination.

Premise of Structured Illumination

In order to combat the deleterious effects of polymerization shrinkage stress in a confined geometry such as a coating, the method of structured illumination was devised. This method involves the use of patterned light chosen specifically for a selected monomer/initiator system taking into account key factors such as viscosity and reaction rate. The temporal sequence of illumination is also matched with the pattern to give the proper final properties of the cured polymer. The premise is that structurally illuminated light followed by flood cure will leave a system with the same conversion as if it were simply flood cured, yet the properties of system will have been changed for the better due to monomer migration having alleviated much of the stress found otherwise in a conventionally cured sample. This work will show that monomer migration does indeed alleviate polymerization shrinkage stress without significantly changing the conversion profile and that optimizing a pattern and temporal sequence for the structured illumination scheme is possible for differing monomer/initiator systems.

The concept of monomer migration is that during polymerization monomer molecules flow from masked or non-polymerizing zones within the sample to the illuminated and therefore polymerizing regions. During polymerization there is an overall volumetric shrinkage that occurs, driving monomer to migrate towards the affected area. Under correct conditions of structured illumination stress is relieved by monomer migration. This relief has been shown in thick films on the order of 0.6 mm in height for samples of HDDA.

General Guidelines for Stress Reduction via Structured Illumination

It is believed that certain general guidelines can be drawn in order to help choose the correct pattern for a particular application. Below are some examples of masks along with a cross-section of the proposed monomer migration and surface morphology

resulting from structured illumination. In order to maximize stress relief, it is proposed that there be enough monomer migration to alleviate all of the stress in the structurally illuminated regions and also that the fully stressed regions which only undergo illumination during the flood cure, be as small as possible. It is currently thought that small, discontinuous regions of stressed polymer will cause less stress to be seen by the substrate. The following figure shows what is likely to happen when the area being illuminated is so large that monomer migration does not occur over a long enough length scale to maximize stress relief in the structurally illuminated regions.

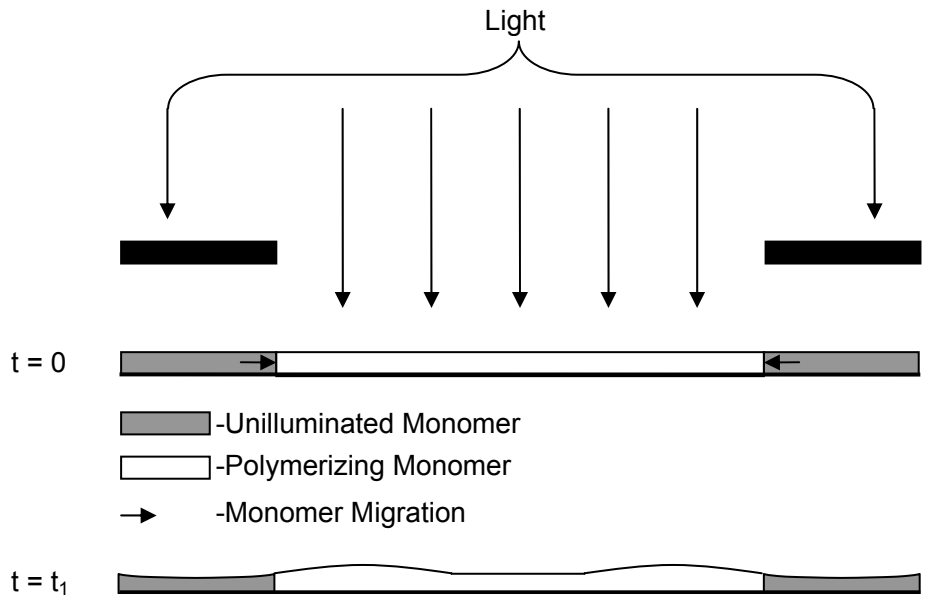

Figure 2.1: Proposed illustration representing structured illumination of a film of monomer where the light is turned on at time zero and subsequent monomer migration occurs before time t_1. Here migration did not occur along the entire length of the illuminated region before conversion of the monomer to polymer limited migration of monomer.

Shown above, the polymerization finished before the monomer movement could occur across the entire length of the illuminated region. Without sufficient monomer

migration maximal stress relief in the structurally illuminated region is not achieved. The following figure shows a system in which the migration is sufficient for maximum stress relief in the structurally illuminated regions.

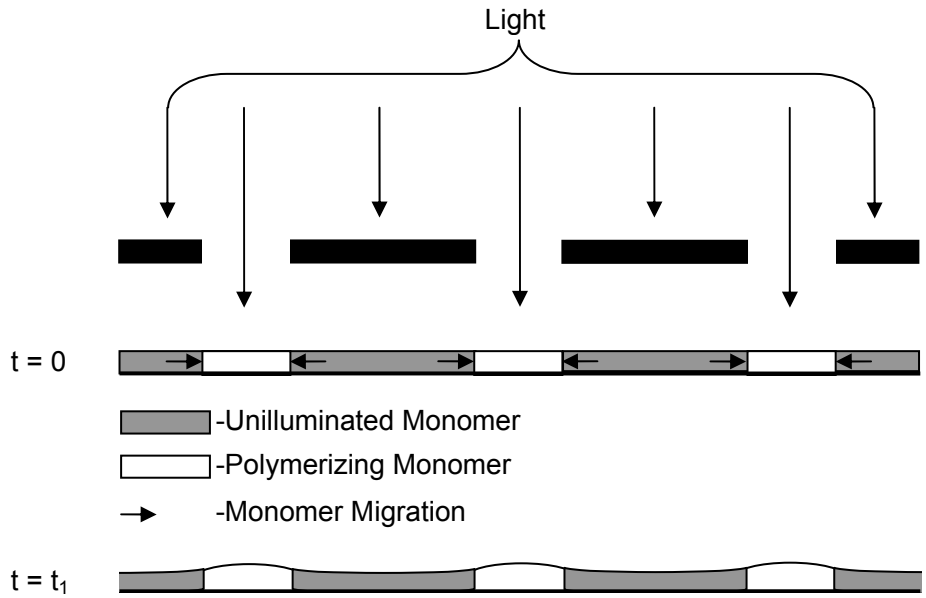

Figure 2.2: Proposed illustration representing structured illumination of a film of monomer where the light is turned on at time zero and subsequent monomer migration occurs before time t_1. Here there was sufficient migration for maximum stress relief in the structurally illuminated regions, however with the large masked regions, subsequent flood cure created stressed zones that are relatively large.

The problem with Figure 2.2 is that the area of uncured monomer left to be polymerized in the final flood-cure stage will contribute a great deal to the final stress between the coating and substrate. These areas must be minimized. So as to minimize the effects of stress in the final flood cure step, Figure 2.3 illustrates smaller masked areas and the potential problem. Here a sufficient coating is not realized following the flood cure step.

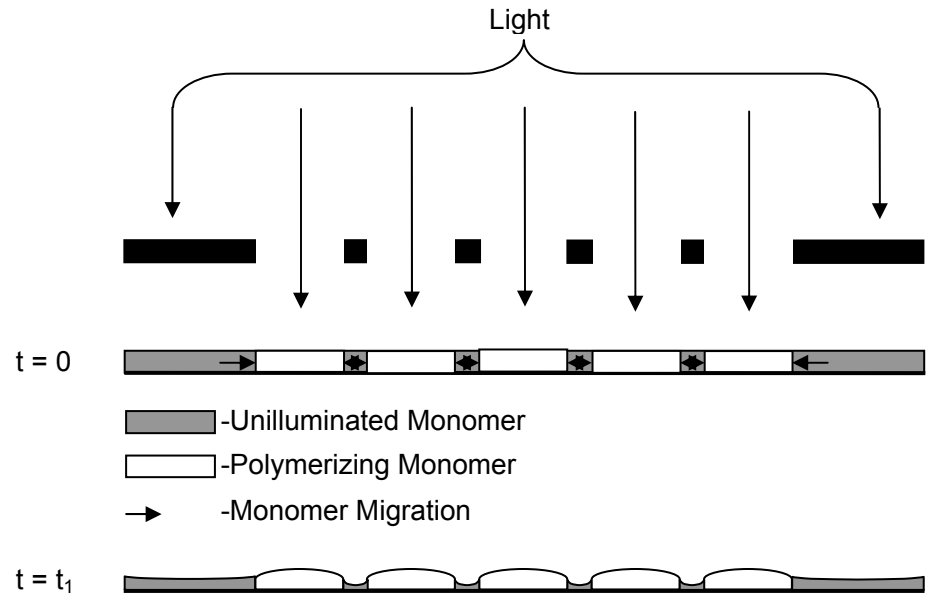

Figure 2.3: Proposed illustration representing structured illumination of a film of monomer where the light is turned on at time zero and subsequent monomer migration occurs before time t_1. Here there may not have been sufficient migration for maximum stress relief in the structurally illuminated regions. The small masked regions, which are subsequently cured during flood illumination, create very little stress; however they may not coat the substrate sufficiently.

If the areas masked off during the structured illumination step are too small, then there will not be sufficient monomer for migration and maximum stress relief. What little monomer which may be left for flood cure may not make for an acceptable coating. There is also the potential for completely depleting the monomer beneath the mask. This concept may be useful in other areas, such as lithography, to eliminate a wash step; however for a coating application depleted monomer regions is likely unacceptable.

With no limitations on migration the minimum percent area masked, that would still allow for maximum stress relief, would be equal to the percent shrinkage. This application would not suffice for a coating, because there would be no remaining monomer beneath the masked portions for subsequent flood cure. It is, however, a good place to start in our calculations to find the minimum masked, and therefore stressed,

regions for optimum stress relief. Still with no limitations on migration, the optimum percent masked area is a function of needed coating thickness and percent shrinkage of the given system. With the limitation to migration given by the uncured monomer viscosity and the change in diffusivity of the monomer into the curing polymer, the system becomes far more complex.

Gloss Reduction in Photopolymerized Coatings

The reduction or control of apparent gloss for coating applications is sometimes seen as a value added characteristic. A glossy finish may cheapen the look of richer deeper looking woods. Utilizing a low gloss coating allow for the richness and texture of the wood to show through giving an apparent increase in value to the finished product. Low gloss finishes are also popular for wood coatings because they are effective in masking blemishes, scratches and defects on wood surfaces. With the application of photopolymerized coatings making a large impact in the wood coatings industry, combating or controlling the apparent gloss of inherently glossy UV-cured coatings is an issue which has been researched. The most common technique to reduce gloss is to micro-roughen the surface of the coating through the use of additives such as silica and micronized waxes. Upon polymerization of the monomer coating the additives protrude from the surface causing irregular distortions. These distortions lead to a randomizing of the reflected light providing a diffuse reflection. This diffuse reflection is seen as an apparent low gloss finish. Consistent gloss reduction with current additive techniques is often difficult, specifically switching a line operation between low and high gloss finishes. As with any coating additive, incorporation, proper loading and optimization is needed to ensure a quality product. In order to produce both low and high gloss finishes, generally two separate production lines are implemented to eliminate turnover time between runs with differing gloss values.

Despite the many considerations for the use of photopolymerized coatings their incorporation into main stream industry has seen great gains due to its favor with the United States Environmental Protection Agency (EPA). With little to no volatile organic carbons (VOC's) being emitted during their use, photopolymers have made great strides in lessening the industrial impact of coatings on our environment. This aspect alone makes their ever expanding use a priority for many coating companies. This contribution will look at ways to utilize the concept of structured illumination to provide facile control of gloss for photopolymerizable coatings while not compromising other characteristics through the use of additives.

CHAPTER 3: OBJECTIVES

Dissertation Research Objectives

With the significant industrial applications discussed in Chapter 1, a fundamental understanding of the advantages and limitations for the use of photopolymers in industrial processes is very important. One major limitation, which is often dependent on the selection of monomer and not on the photopolymerization process, is the shrinkage stress that must be either tolerated or contested. Other work has examined methods to combat shrinkage stress involving the use of additives, specialty chemistry or stress absorbing layers between the substrate, bonded or filled material and polymer sample. Because photopolymers inherently provide a high gloss surface, obtaining a low gloss finish is also an issue which some have been forced to face. Again additives have been used to solve this problem in most applications. The spatial control available in a photocurable system allows for unique possibilities to control a polymerization reaction in order to change the final characteristics of a polymer sample. Photopolymerizing a sample with a specified illumination pattern and sequence in order to address the aforementioned problems, until now, has not been researched in depth. This processing method has the clear advantage of changing surface characteristics without the use of additives or specialty chemistry and will be shown to be quite simple in its application to not only laboratory processes but also continuous processes found in many industrial applications involving films, laminates, coatings and the like.

This thesis will attempt to reveal the work completed during dissertation research at the University of Iowa on structurally illuminating polymer samples in order to enhance coating characteristics by either reducing the polymerization shrinkage stress or by controlling the apparent gloss of a coating. It will also tackle the subject of conversion and its possible influences on photopolymer sample characteristics. Finally

this writing will attempt to depict a fundamental understanding of monomer migration and its effects on surface morphology through mathematical modeling.

CHAPTER 4: A SIMPLE, INEXPENSIVE AND EFFECTIVE METHOD FOR POLYMERIZATION SHRINKAGE STRESS MEASUREMENTS IN PHOTOPOLYMERIZED COATINGS

Motivation for Cantilever Beam Setup

Polymerization shrinkage is important for many applications since it leads to residual stresses which can deform a system and undermine its optical or mechanical properties. This paper describes a simple, inexpensive, and effective method for characterizing polymerization shrinkage stresses in photopolymerized coatings. The method, which is based upon the deflection of a thin brass cantilever, can be used with any initiating light source, and is ideally suited for screening of monomer formulations since it can quickly and easily generate comparative data. The theoretical basis and design of the apparatus is presented and considerations for accurate stress measurements are discussed.

Introduction

Photopolymerization has recently become an industrial standard in many high through-put applications because of its efficient use of light energy to rapidly initiate polymerizations at room temperature. Both free-radical and cationic photopolymerizations[47, 48] are used in applications that range from thin coatings to thick films[10, 49], and from emulsion polymerizations[50, 51] to nanostructured materials produced using lyotropic liquid crystals[52]. Photopolymerization is also an area of active research designed to address current issues and enable new applications. Examples include research on methods for overcoming oxygen inhibition[53], and new initiation systems using less energetic visible light[54].

The density of the final polymer coating is invariably greater than that of the original monomer liquid, and the resulting polymerization shrinkage stress may deform the coated product or undermine its optical or mechanical properties. For example, the

coating could warp low modulus substrates or cause delamination or micro-crack formation[41]. The polymerization stresses developed in a given system depend upon a number of factors, including: the molar volume change upon polymerization, the conversion profile, the geometry of the system, the modulus of the cured material and the modulus of the substrate or confinement. For many applications, a simple, inexpensive and effective method for measuring the polymerization shrinkage stress in photopolymerized coatings is important because it will allow the shrinkage stress resulting from different monomer formulations to be quickly compared for screening purposes. This paper describes such a method for characterizing polymerization shrinkage stresses in photopolymerized coatings. The method, which is based upon the deflection of a thin brass cantilever, can be used with any initiating light source and photopolymerization system.

Principles of the Cantilever Method for Coating Stress Measurements

The measurement of polymerization shrinkage stress through the deflection of a cantilever is a simple concept illustrated schematically in Figure 4.1. Polymerization of the coating leads to shrinkage in the plane of the cantilever. Because the coating is constrained by adhesion to the cantilever, a stress is transferred to the cantilever, causing it to deform. Cocoran *et al* studied stresses in organic coatings in the 60's and developed a relationship between the cantilever deflection and internal stresses in the organic coating. This relationship was based on Stoney's equation[45, 55] and includes the moduli and Poisson ratios of the coating and the cantilever.

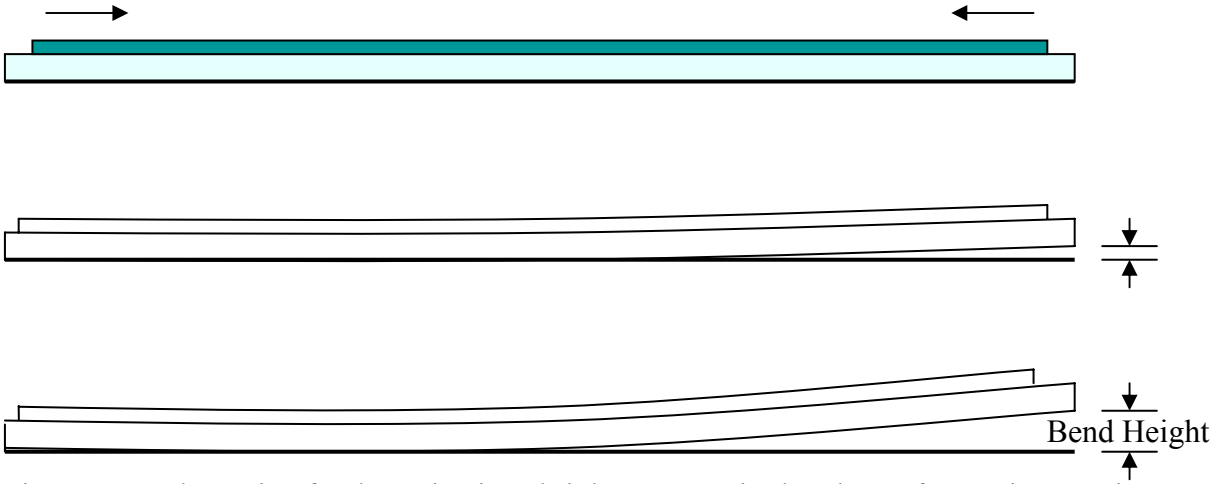

Figure. 4.1 Schematic of polymerization shrinkage stress in the plane of a coating causing a vertical deflection of a cantilever.

Equation 1 shows a modified version of Corcoran's relationship that will be used in this paper:

$$S = \frac{hE_s t^3}{3L_s L_c c(t+c)(1-\gamma_s)} + \frac{hE_c(t+c)}{L_s L_c(1-\gamma_c)}$$

Eq 4.1: Stress related to bend height and physical properties

In this equation: S represents the internal stress; h is the deflection of the cantilever; E_s *and* E_c correspond to the modulus of elasticity for the substrate and coating, respectively; γ_s and γ_c are Poisson's ratio of the cantilever substrate and the coating, respectively; L_s denotes the length of the substrate between the edge point at which it is clamped and point at which deflection is measured; L_c is the length of the coating; t denotes the thickness of the cantilever substrate; and c represents the thickness of the coating. The second term in Equation 1 gives a value for the stresses removed as a result

of the cantilever deformation while the first term gives a value for the stresses remaining in the coating[46]. Equation 1 is based on the assumption that the coated portion of the cantilever lies centered along the cantilever's length.

Selection of Cantilever Materials and Dimensions

The dimensions and mechanical properties of a cantilever for stress measurements depend upon the magnitude of the stress to be measured. It is desired that the cantilever deflection be easily measurable, but remain within the elastic deformation regime. In addition, it is imperative to have good adhesion between the substrate and polymer coating, and the cantilever must not react with or dissolve in the monomer liquid. Many plastic substrates were eliminated due to the latter consideration. Based upon all of these considerations, a brass cantilever substrate was chosen with characteristics listed in Table 1. With this design photopolymerization shrinkage stresses generated by acrylates lead to cantilever deflections on the order of 10mm.

Table 4.1: Brass cantilever properties.

Description	Formable Cartridge Brass (Alloy 260), 25 ft roll, McMaster order #90355K223
Thickness	0.051 ± 0.008 mm (0.002 ± 0.0003 in)
Width	12.7 mm (0.5 in)
Length	5 cm

The selected brass alloy was obtained in a standard roll, and cantilevers were cut to the desired length using a small precise table-mounted shear (Figure 4.2). To ensure adhesion between the cantilever and the coating, each brass cantilever was thoroughly cleaned using the following procedure. Oils from machining and handling of the brass

were removed by washing in soap and water, followed by a rinse in de-ionized water then a rinse with acetone before being stored in sealed vials of acetone.

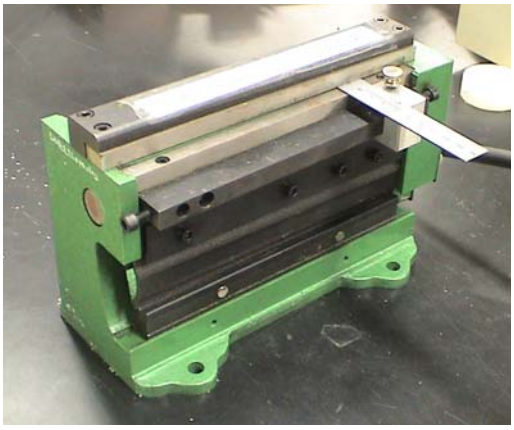

Figure 4.2: Shear for cutting brass cantilever strips for use in stress measurements.

Placing the strips in a vial with the curvature of the strips in alternating directions allows for good contact between the cantilever and the acetone solvent and also for easy removal during stress measurements.

Figure 4.3: Picture of brass cantilever strips stored in acetone so as to keep clean and allow for consistent adhesion during stress measurements.

Original Cantilever Setup

It is important, in the setup of a stress measuring device, that all variables be accounted for. Reaction rate and conversion of the photopolymerized coating will directly affect the stress in the coating. Care must be taken to ensure that the intensity and distance of the lamp from the sample are consistent. The preliminary set-up used for the cantilever beam experiments utilized an Oriel 200W Hg/Xe arc lamp as the illumination source. Brass cantilevers were positioned on a scribed block of aluminum, 10 cm from the edge of the beam turner.

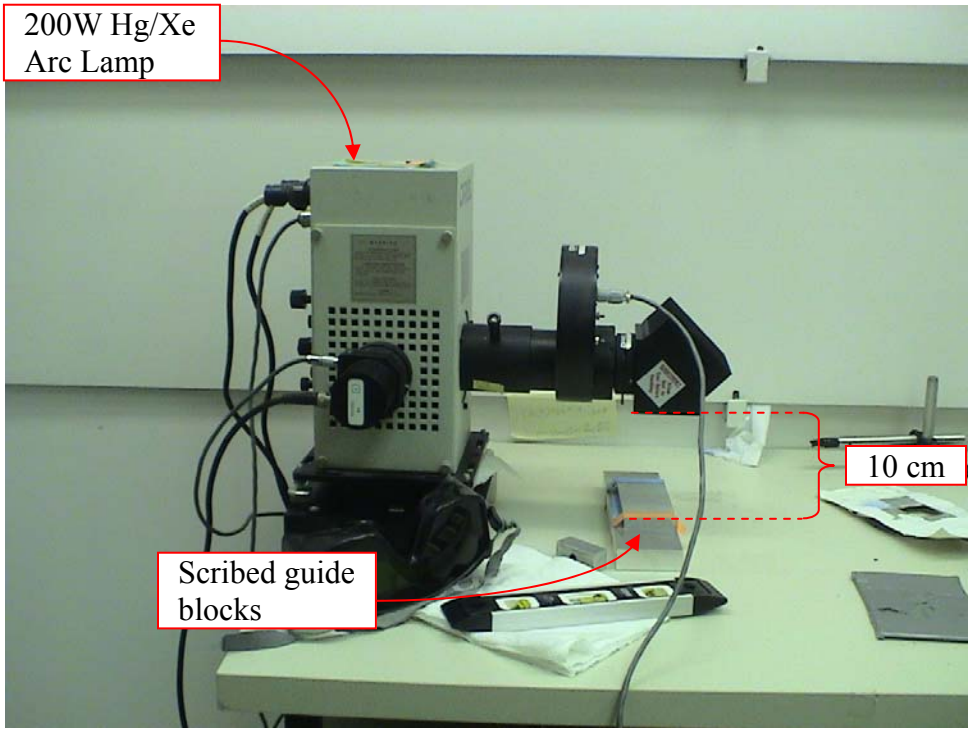

Figure 4.4: Original setup for cantilever beam experiments.

The beam of the arc lamp is focused to a point on the cantilever beam, and the brass strip is aligned using scribed lines within the lower aluminum block.

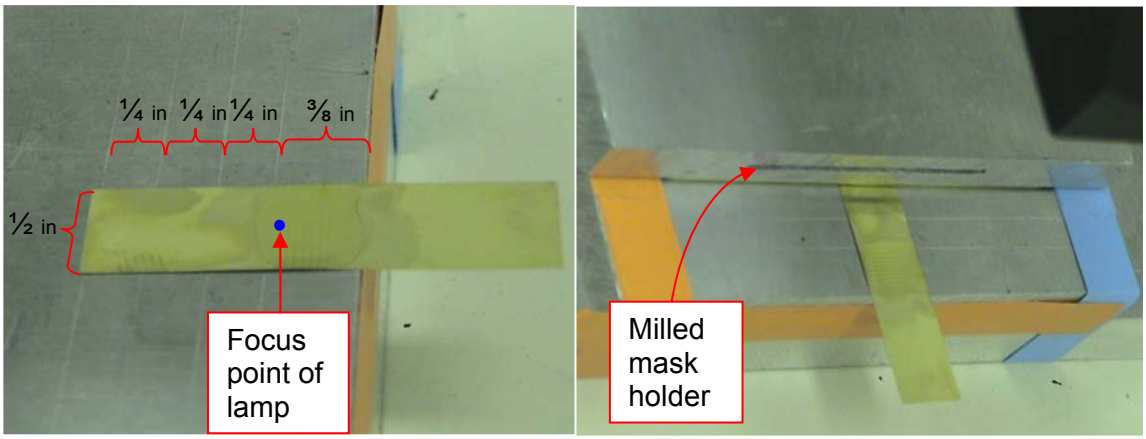

Figure 4.5: Guide blocks with brass cantilever and polymer shown placed correctly using scribed lines on the bottom aluminum block.

The cantilever is placed between the scribed lines and another aluminum block is placed on top of the cantilever to restrict its motion at one end and keep the strip in place. The block has a groove milled out of it in order to hold masks used in the structured illumination process described in various chapters within this work.

After polymerization through illuminating the sample for a particular timeframe, the deflection of the beam is measured.

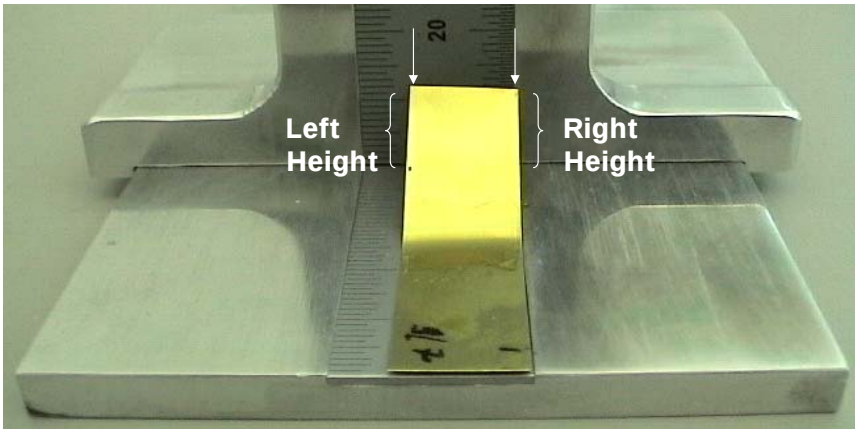

Figure 4.6: Measurement device for accurate and consistent measurements of deflection in the cantilever beams.

The total deflection is recorded on each side of the beam as shown in Figure 4.6. The initial deflection, due to the curvature of the brass strips cut from a role (generally 1-2 mm), is then subtracted from the value measured to obtain the net deflection, or the deflection due to stress, of the cantilever beam.

Modified Stress Measurement: Setup and Procedure

Photopolymerizations were initiated using a 1000 W Hg/Xe arc lamp equipped with optics (Newport Corporation, Irvine, CA) which directed the light downward toward the substrate. A mechanical shutter was used to control the length of illumination and the light was passed through a water cooled IR filter to reduce heating from the lamp. A cantilever holder was machined from a block of poly(vinyl chloride) and used to secure one end of the brass cantilever so that the free end could be measured using the mounted rule. A picture of the experimental apparatus is shown in Figure 4.8 along with a diagram in Figure 4.7 showing a detailed view of the custom machined parts. In Figure 4.8 the cantilever holder is shown in the position where monomer is applied. The aluminum platform including the cantilever holder and optional filter holder is slid into place beneath the lamp prior to illumination

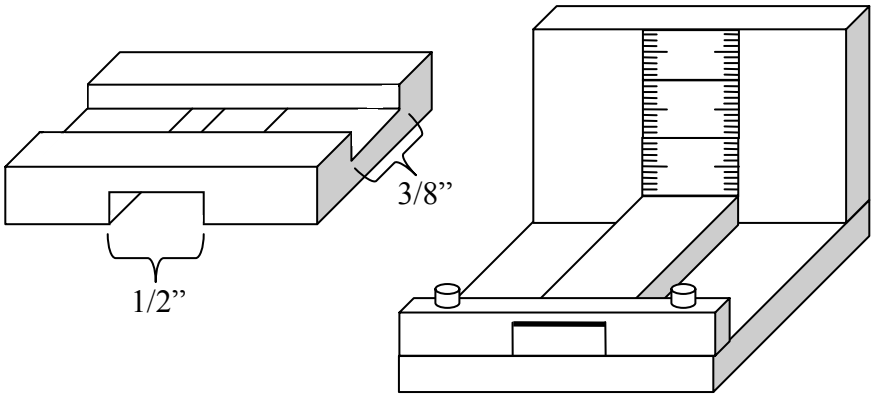

Figure 4.7: Diagram showing both the cantilever holder and the application guide.

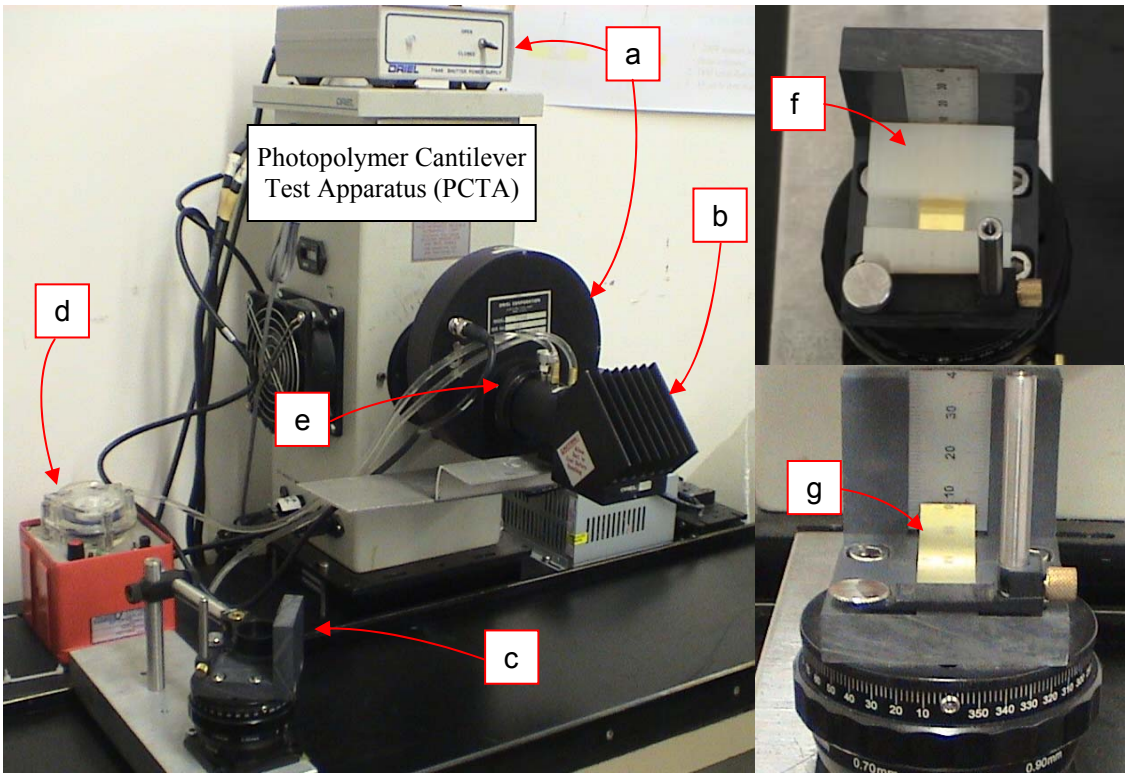

Figure 4.8: Pictures of the cantilever setup for the stress measurements reported in this contribution. (a) shutter device, (b) light beam turner, (c) cantilever holder, (d) water pump, (e) water-cooled IR filter, (f) application guide, (g) deflected cantilever.

The repeatable application of the monomer to the cantilever substrate was found to be an important step in the stress measurement process. Consistent application was ensured using a micropipette to apply precise amounts of monomer (20 μL) to the substrate, and a custom machined guide to spread the monomer over a specified area measuring 1/2" by 3/8" in a specified location in the center of the brass cantilever substrate. Figure 4.7 shows the various custom machined components. The two thumb screws are used together for tightening the cross member which holds down one end of the cantilever strip. The white applicator guide is used along with a micropipette in order to consistently apply the monomer coating which is to be photopolymerized and subsequently measured for stress. The machined guide is removed before

photopolymerization occurs so as not to hinder the deformation of the cantilever substrate.

In the first step of the stress measurement procedure a single brass strip is removed from the storage media and dried using a delicate task wipe to remove the solvent. The brass strip is then inserted into the holder so that the curvature of the strip is concave up. Next the machined guide is placed atop the strip and monomer is applied in a defined area. Then the machined guide is removed and the bend height of the cantilever due to natural curvature of the strip is recorded. The coated cantilever strip is then centered beneath the lamp by sliding the holder into place. With the optics aligned and focused properly, the coating is illuminated for a specified amount of time to give consistent monomer conversion between samples. The bend height for both the left and right side of the cantilever strip is measured and recorded. The original bend height is subtracted from that measured after polymerization to obtain net deflection of the cantilever. These values can either be compared between experiments to show which systems result in greater stress or they can be used in Equation 1 to obtain a stress value.

For structured illumination studies a mask was used to control the intensity of light illuminating the various regions of the coating surface. Making masks worked best using Adobe PhotoShop & Adobe Image Ready. Alternately, Microsoft PowerPoint has been used to make masks. The masks are printed on a high resolution, Xerox Tektronix Phaser 7300 D/N (2400 DPI) printer on acetate (transparency paper). In order to hold the masks, they were cut and placed into photo slide holders. The holder was then placed in a milled slot in the top aluminum block in the original setup. For the setup used in reported experiments in this work, masks were punched out in one inch diameter circles and held by a fixed mask holder shown below.

When designing masks, line thickness and spacing are the key variables. When using software such as PowerPoint, it is only possible to space lines based on center to center spacing, or edge to edge. Also, the thickness of the lines is only controllable by

font size, which is problematic when estimating the actual thickness of the lines. Therefore, using Adobe software is desirable, since line thickness and blank space can be easily controlled by selecting a specified resolution (i.e. pixels/length) and controlling the line thickness by controlling the number of pixels used to create the line thereby obtaining a characteristic length for masked areas. Illuminated areas are controlled by the number of pixels between printed pixels.

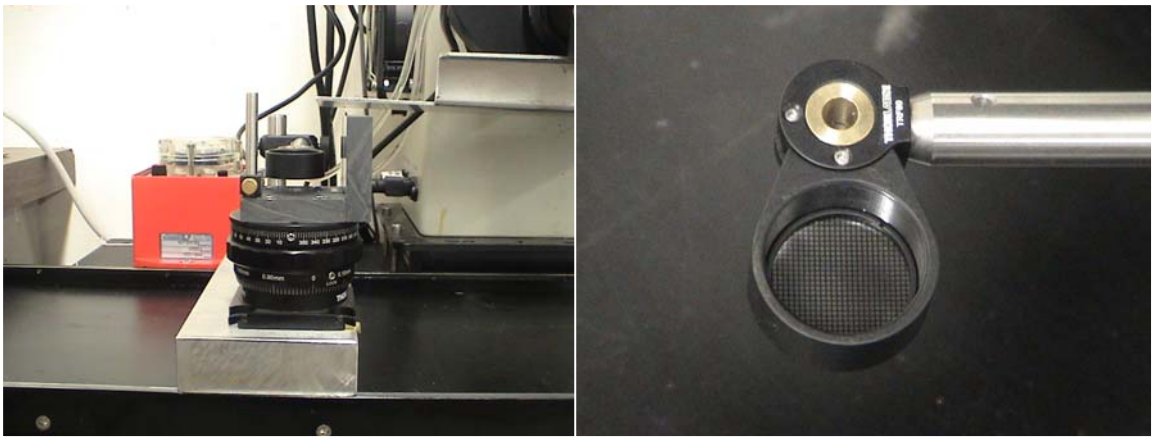

Figure 4.9: Mask holder used for stress measurements shown from above (right) and side view (left). The distance the mask is held from the sample is kept constant for a series of experiments.

Conclusions

In this contribution, a simple and inexpensive cantilever apparatus for photopolymerization shrinkage stress measurements is described. The apparatus, which is designed for stresses typically encountered in photopolymerizations of acrylates, can provide a very consistent means of comparing the shrinkage stresses that arise from different coating formulations. The method can be used with any initiating light source, and is ideally suited for screening of monomer formulations since it can quickly and

easily generate comparative data. This apparatus and method was used for a systematic study of photopolymerization shrinkage stress presented in the next chapter.

CHAPTER 5: STRUCTURED ILLUMINATION FOR REDUCTION OF POLYMERIZATION SHRINKAGE STRESS IN PHOTO-CURED ACRYLATE COATINGS

Introduction to Stress Reduction in Polymer Coatings

Light-induced polymerizations have become the standard for high through-put coating applications on a variety of substrates including paper, metal, plastic, glass, and wood. Advantages of photopolymerization include solvent-free formulations, high reactivity at room temperature, spatial and temporal control of initiation, a wide variety of commercially available monomers, and initiators effective in the visible and ultraviolet regions of the spectrum. The solvent-free nature of photopolymerization minimizes shrinkage due to evaporation; however, stresses may occur due to the polymerization shrinkage associated with the increase in density as the liquid monomer is converted to a solid polymer coating. Homopolymerizations of acrylates exhibit polymerization shrinkage as high as 20% as a result of the double bond consumption during the polymerization reaction. The combination of polymerization shrinkage and the constraints of a rigid substrate due to adhesion of the coating can lead to significant stresses which can undermine the properties of the coated system. Current techniques for reducing polymerization shrinkage stress generally focus on limiting the polymerization shrinkage by either reducing the fraction of the system that undergoes polymerization (through use of fillers, large monomers, oligomers or bulky pendent groups[7, 56, 57]), or by using specialized reactions such as ring-opening polymerizations[58, 59]. These techniques rely on specific low-shrinkage formulations and are not generally applicable since they do not encompass all photopolymerizable monomers.

In this contribution, a novel approach for reduction of polymerization shrinkage stress is presented. This new method, in contrast to methods which are based upon a change in the formulation to reduce the total amount of shrinkage, is focused on reducing

the stress produced by the shrinkage that will inevitably occur. Specifically, the "structured illumination" method is based upon a two-stage illumination process in which the coating is first illuminated in a pattern of light and dark regions. Since active centers are produced only in the illuminated region, these are the areas in which the polymerization occurs. During this structured illumination stage, unreacted monomer from the dark region will migrate in response to the polymerization shrinkage and concentration gradient setup by the reaction, thereby limiting the development of stress. At the end of the structured illumination stage, the system contains patterned regions of stress-free polymer among pools of unreacted monomer. Next, during the flood cure stage, the entire system is illuminated to achieve a consistently high conversion throughout the coating. Shrinkage stress may develop during the flood cure step, especially in the regions that were previously masked; however, the total stress is greatly reduced since much of the polymerization took place during the stress-free structured illumination stage. The overall shrinkage stress that will develop depends upon a number of variables including the illumination pattern, the structured illumination time, flood cure time, the monomer mobility, and the polymerization rate.

In contrast to traditional approaches for shrinkage stress reduction, such as the development of specialty low-shrinkage monomers[59] or the use of fillers[40], the structured illumination approach is quite general and is applicable to all photopolymerization coating systems regardless of coating formulation or the reaction mechanism. However, for each reaction system the illumination pattern must be optimized to ensure that monomer migration will occur during the timescale of the polymerization over the characteristic length of the pattern. In this contribution, the structured illumination method for polymerization shrinkage stress reduction will be presented and a systematic study of variables contributing to stress relief will be discussed.

Structured Illumination for Polymerization Shrinkage Stress Reduction

The use of specially designed patterns to control the directions along which polymerization shrinkage occurs is extremely versatile with a multitude of possible illumination patterns and resulting stress profiles. Figure 5.1 helps to illustrate the general concept with a relatively simple structured illumination pattern.

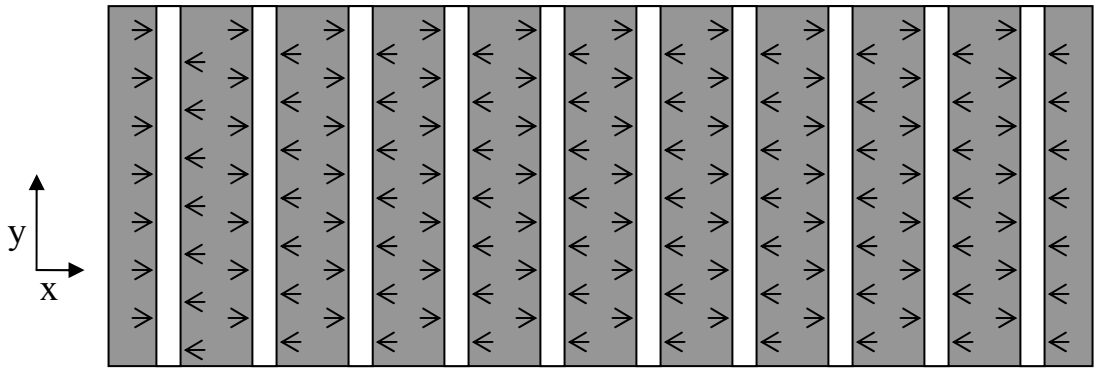

Figure 5.1: Schematic representation of a two-dimensional plane parallel to the film surface illustrating the pattern of monomer migration during structured illumination through a mask consisting of alternating zones of dark and light. Here the arrows represent monomer migration towards the photo-induced polymerizing regions.

This figure corresponds to a two-dimensional plane parallel to the film surface, and illustrates the general pattern of monomer flow during structured illumination through a mask consisting of alternating zones of dark and light. Upon illumination and subsequent polymerization, shrinkage will occur both in the x- and y-directions, however, stresses will be developed principally in the y-direction. The stresses in the x-direction will be largely alleviated by monomer migration, as indicated by the arrows in Figure 5.1. The final complete cure of the sample can be achieved by flood illumination of the entire sample, or by subsequent patterned illumination. Line pattern illuminations will lead to

differential stresses in the x- and y-directions and a higher stress relief in the direction perpendicular to the illuminated lines. Figure 5.2 shows an example of a pattern that is not continuous in either the x- or y-direction.

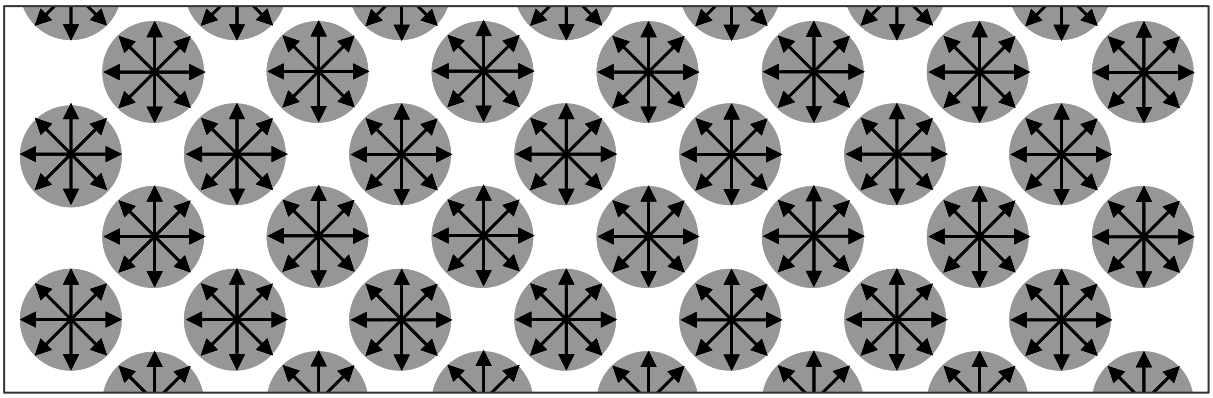

Figure 5.2: Schematic representation of a two-dimensional plane parallel to the film surface illustrating the pattern of monomer migration during structured illumination through a mask consisting of an array of illuminated circles. Here the arrows represent monomer migration towards the photo-induced polymerizing regions.

Here a high degree of stress relief is possible along both axes since monomer migration will not be limited to one axis. This approach to the relief of shrinkage stresses for all possible patterns depends upon the local, micro-scale migration of monomer from the masked regions to the polymerizing zones during the time of structured illumination. The driving forces for this monomer migration arise from the conversion of monomer to polymer in the illuminated regions, the resulting monomer chemical potential gradient provides a driving force for diffusion, and the local polymerization shrinkage itself provides a driving force for flow of the unreacted monomer into the illuminated region. Therefore, the factors that affect the ability of the monomer to migrate will determine the effectiveness of this method and a fundamental understanding of the system is necessary to optimize the structured illumination pattern and temporal sequence for each monomer

system under consideration. It is certainly clear that the viscous and diffusive properties of the monomer system will affect the monomer migration, and the reaction rate will dictate the timescale over which much of the migration must happen in order to relieve polymerization shrinkage stress.

As a general guideline, the structured illumination pattern and temporal sequence should be selected to maximize the low stress regions created by the monomer migration. Therefore, it is generally desired to maximize the illuminated regions before the final flood cure. However, the pattern must also allow sufficient monomer migration from the shaded regions (in the necessary timescale), thereby requiring a minimum shaded area for a given pattern. If the masked areas are too small there will not be enough volume of monomer to migrate. Even with enough monomer for stress relief, the length scale of the illuminated regions must not be so large that it prevents effective monomer migration during the timescale of the reaction.

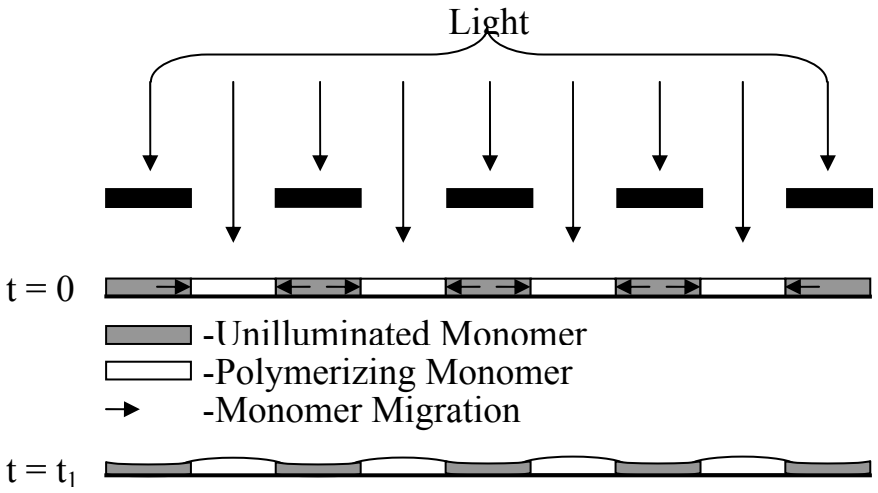

Figure 5.3: Schematic representation of the film cross-section during structured illumination. Immediately upon illumination (t=0) monomer migrates from the dark regions in response to polymerization in the illuminated regions. At subsequent times, $t_1>0$, the polymerizing region is raised relative to the dark regions. The raised patterned has been experimentally observed in the final flood-cured polymer.

These requirements must be properly balanced in the spatial and temporal structured illumination protocol. Figure 5.3 represents a well designed system in which there is both sufficient monomer for migration due to adequate spacing of illuminated regions and the size scale is such that monomer migration can affect the entire illuminated region. For systems in which the shrinkage stress is greatly reduced by structured illumination, it has been experimentally observed that the regions that are structurally illuminated prior to flood cure are raised in the final cured polymer. This observation verifies the occurrence of monomer migration during alleviation of shrinkage stress.

Experimental Methods

Materials

The monomer, 1,6 hexanedioldiacrylate (HDDA), was chosen because acrylate monomers are standard for a wide variety of photopolymerized coating applications, and the cured polymer has a substantial modulus of elasticity (~10000MPa). This monomer exhibits polymerization shrinkage on the order of 17% at full conversion. In addition, the vapor pressure of HDDA is low (0.015 mm of Hg); therefore no significant evaporation occurs at room temperature. An α-amino ketone (BDMP or Irgacure 369, CIBA Chemicals), was chosen as the photoinitiator because it is a commonly-used initiator tailored for emission from a mercury/xenon arc lamp.

Shrinkage Stress Measurements

The method presented in Chapter 4 based upon the deflection of a well-characterized cantilever beam was used to characterize the shrinkage stress reduction achieved using structured illumination. The method, which is briefly described below, is very similar to an ASTM standard[26].

The brass cantilevers were 5 centimeters long, 12.7 mm wide and 0.0508 mm thick (standard half inch, 2 mil precision brass foil). To ensure consistent adhesion of the cured coatings to the brass substrate, the cantilevers were washed in soap and water followed by a rinse with DI water and acetone before storage in acetone. Twenty microliters of HDDA monomer containing 1 wt% BDMP initiator was placed near the middle of the cantilever covering the 12.7 mm (1/2") width and measuring 9.525 mm (3/8") in length. Polymerization was initiated using light from a 1000W Hg/Xe Oriel arc lamp controlled by a shutter then passed through a water-cooled IR filter and directed onto the monomer pool with a beam turner. The UVA intensity was measured using a Uvicure Plus (EIT, Inc.) at 0.38 W/cm^2. This lamp system was used for both the structured illumination and the flood cure stages. The masks for the structured illuminate step were prepared by printing black lines onto acetate sheets using a Xerox 7300 D/N Phaser printer in the high resolution color setting. Line widths varied from 0.127 mm to 1.016 mm (5-40 mils) and line spacings ranged from 0.254 mm to 1.27 mm (10-50mils).

The described setup in Chapter 4 was allowed to illuminate the surface of all samples for 10 seconds during flood cure and additional illumination was done prior to flood cure during the structured illumination step. This allowed the samples that were structurally illuminated to see more light and therefore were given more time to polymerize than those samples which were simply flood cured. This ensures that reductions in stress are not related to a reduction in the degree of polymerization[24] and is proven by the use of a thin film calorimeter (TFC)[33] and Raman Spectroscopy techniques[60] which will be elaborated upon in Chapter 7.

For the cantilever beam experiments, the analysis of Corcoran *et al.* was used to estimate the percent reduction in shrinkage stress achieved using structured illumination. This modified relationship is shown in Equation 5.1. In this Equation 5.1: S represents the internal stress; h is the deflection of the cantilever; E_s *and* E_c correspond to the modulus of elasticity for the substrate and coating, respectively; γ_s and γ_c are Poisson's

ratio of the cantilever substrate and the coating, respectively; L_s denotes the length of the substrate between the edge point at which it is clamped and point at which deflection is measured; L_c is the length of the coating; t denotes the thickness of the cantilever substrate; and c represents the thickness of the coating.

$$S = \frac{hE_s t^3}{3L_s L_c c(t+c)(1-\gamma_s)} + \frac{hE_c(t+c)}{L_s L_c(1-\gamma_c)}$$

Eq 5.1: Stress related to bend height and physical properties

The second term in Equation 5.1 gives a value for the stresses removed as a result of the cantilever deformation while the first term gives a value for the stresses remaining in the coating[46]. Equation 5.1 is based on the assumption that the coated portion of the cantilever lies centered along the cantilever's length

Statistical Design of Experiments

A statistical design of experiments (DOE)[61] analysis was performed based upon the Box-Behnken method[62] for structured illumination of HDDA polymerization systems. This analysis, aided by Minitab® Statistical Software[63, 64], allows efficient characterization of how important process variables affect resulting stress reduction. The process variables chosen for this analysis are readily controllable, and include: line thickness (width of the dark lines during the structured illumination step); line spacing (distance between the mask lines thereby defining the illuminated regions during structured illumination); S.I. time (duration of the structured illumination step); and mask orientation (the convention for the angle of orientation is illustrated in Figure 5.4).

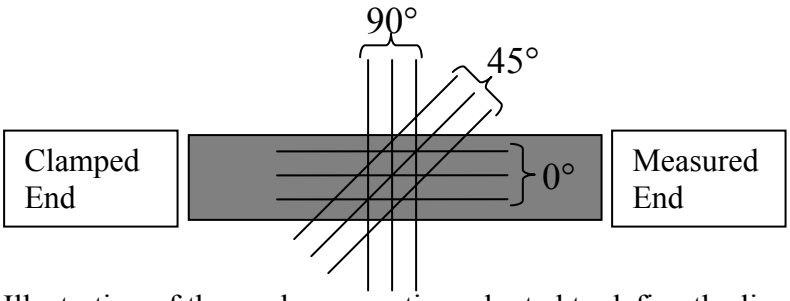

Figure 5.4: Illustration of the angle convention adopted to define the line mask orientation relative to the length of the brass cantilever.

Results

Figures 5.5 through 5.8 illustrate the effects of the process variables as characterized using the statistical design of experiments analysis described above. For each figure, the abscissa corresponds to the spacing between mask lines (illuminated area), the ordinate is the line width (masked area during structured illumination) and the shaded contours correspond to regions for which the normalized deflections lie within the indicated ranges. Since the deflections are normalized by the value obtained for a flood cured sample, the maximum value of the normalized deflection is unity. In all figures, the high stress regions are presented by light shades, while low-stress regions are represented by darker shades. The range of values for the abscissa and ordinate shown in the figures are determined by the range of values used in the experiments. Therefore, very little extrapolation beyond experimental conditions are shown.

A representative contour plot obtained from the design of experiments analysis is shown in Figure 5.5, which illustrates the dependence of normalized deflection on line mask variables (line spacing and line width) for a structured illumination time of 8 seconds at an orientation of 90°. Each dot in the figure corresponds to a point at which an experimental measurement was made as defined by two independent sets of modified Box-Behnken design experiments. Figure 5.5 illustrates that, for this case of 8 second

structured illumination, the maximum stress relief occurs in a finite region corresponding to normalized deflections between 0.1 and 0.2. The region of maximum stress relief assumes an elliptical shape due to the quadratic fit used to model the experimental data. The model effectively gives an idea of the best masks for efficiently eliminating polymerization shrinkage stress for the given system. Each successive contour representing a boundary to a region of increasing normalized deflection assumes a concentric ellipse of larger size with the same major axis slope. Note that the spacing between successive boundaries decreases as the normalized deflection increases.

Comparison of Figure 5.5-5.7 will illustrate the effect of the structured illumination time on the resulting stress relief (as characterized by the normalized deflection).

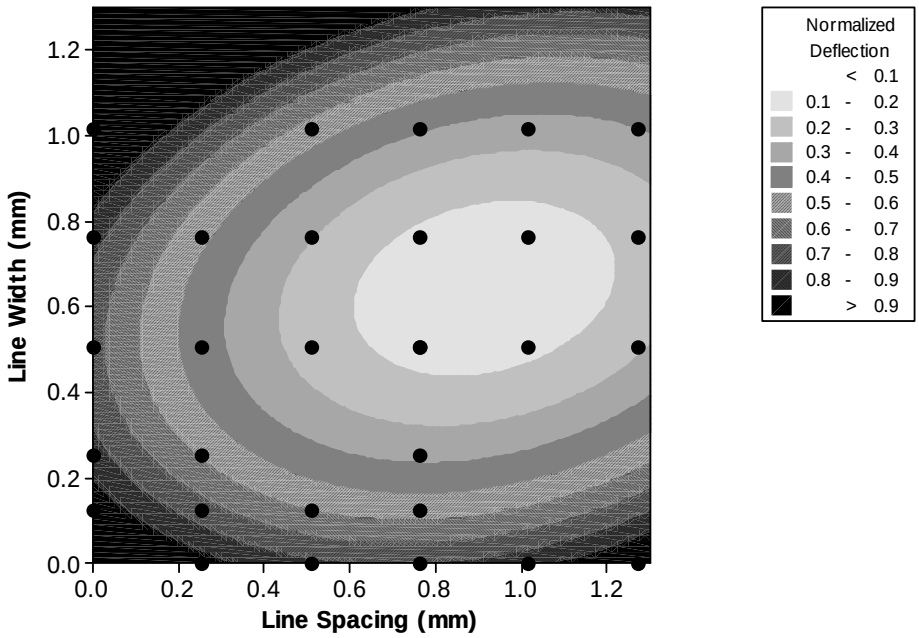

Figure 5.5: Contour plot illustrating the dependence of the observed stress reduction on the mask characteristics for an 8 second structured illumination through a line mask with a 90° orientation. The abscissa is the spacing between mask lines (the illuminated area), the ordinate is the line width (the masked area) and the shaded regions correspond to normalized deflections within the indicated ranges. High stress reduction corresponds to a low normalized deflection.

Values that can be used to characterize the normalized stress contours for different conditions: slope of the axis of the major axis (less than one may mean that illuminated area must be larger than masked region of optimize stress relief), minimum value of the normalized stress (some have a minimum value of 0 to 0.1), center of optimal region.

The illuminated area during structured illumination needs to be larger than the masked regions thereby allowing for larger regions of stress-free polymer, however, the size of these regions is limited by the available monomer from the masked regions. This slope defines the relationship between the concepts of available monomer and maximizing stress-free regions. The reason for the pattern not being continuous across the range of mask feature sizes is that as the illuminated and masked regions get larger the ability of monomer to migrate across the entire surface ceases. This ability is dependent on factors involved in reaction kinetics and viscosity. Also as the masked regions get smaller diffusion of light through the mask becomes a larger factor, as it is being held a finite distance above the monomer sample. Diffusion of light through a small enough mask pattern could actually lead to the entire sample being flood cured. Another reason for optimum stress relief not being attained at smaller mask feature sizes is the thickness of the system being studied. Thicker systems require larger amounts of monomer to migrate in response to polymerization shrinkage stress thereby creating larger variations in thickness. These larger variations in thickness can only be facilitated at certain larger periods of illuminated and masked regions due to factors involved in surface energy. In other words, the sharp curvatures necessary to facilitate the large volume differences over small lengths between the structurally illuminated areas and the masked areas may not be possible.

As is seen in Figure 5.6, stress relief is observed with even as little as 1 second of structured illumination. Stress relief here is not near as great as is seen with longer structured illumination times because substantial conversion and monomer migration

does not occur for this system within the 1 second of structured illumination. Full conversion in the structurally illuminated regions must be attained during structured illumination for maximal stress relief. Uncured monomer in the structurally illuminated regions will lead to a large continuous stress development during the flood cure stage. For faster reacting systems with little resistance to monomer migration, 1 second of structured illumination may suffice for obtaining optimal stress relief. This would be due to the ability of the monomer to migrate on that short of a time scale and also the reactivity of the system leading to a fully cured structurally illuminated region within the 1 second of structured illumination.

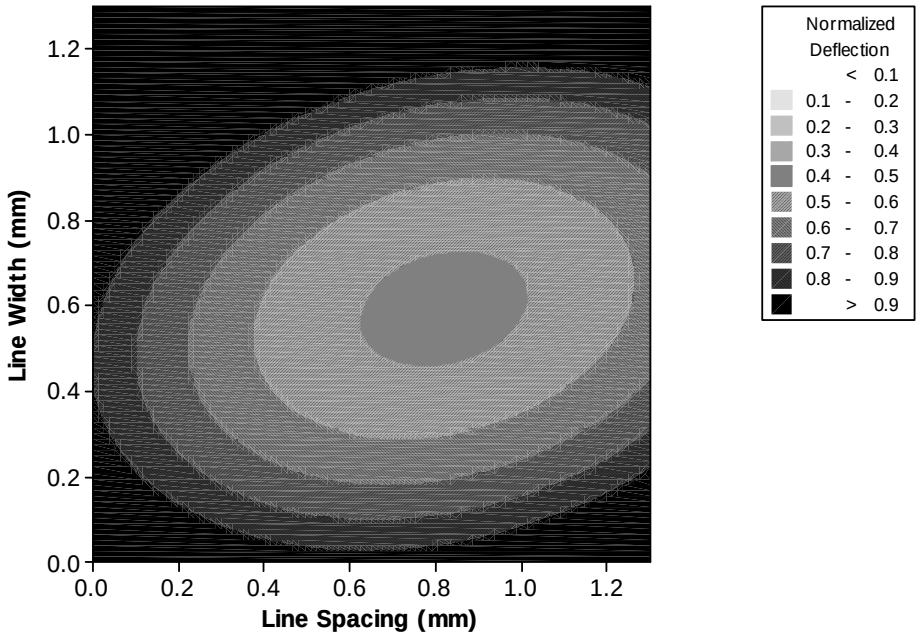

Figure 5.6: Contour plot illustrating the dependence of the observed stress reduction on the mask characteristics for a 1 second structured illumination through a line mask with a 90° orientation.

Figure 5.7 shows that with 15 seconds of structured illumination, smaller values of normalized deflection are observed indicating greater stress relief. Here virtually

complete conversion is attained in the structurally illuminated regions thereby not allowing stress to build in those regions during the flood cure step. As stated previously all samples were flood cured for 10 seconds following the structured illumination step leading one to surmise that despite those samples in Figure 5.7 having undergone longer total illumination times and hence more time for cure, the internal stress of the systems are greatly reduced as evident by the decrease in deflection. Figure 5.7 shows normalized deflection values of less than 0.1 which, in these experiments, corresponds to a net bend height of less than 2 mm. Compare that to systems which are simply flood cured having consistent net deflections of approximately 19 mm and it is easily apparent that structured illumination relieves polymerization shrinkage stress.

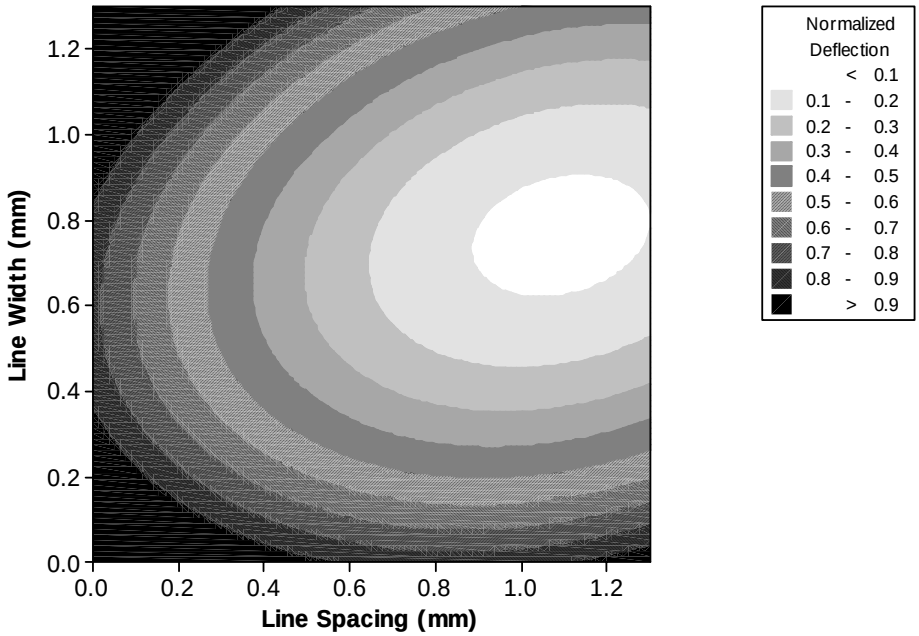

Figure 5.7: Contour plot illustrating the dependence of the observed stress reduction on the mask characteristics for a 15 second structured illumination through a line mask with a 90° orientation.

Despite the large change in net deflection between Figures 5.5, 5.6 and 5.7, comparing experiments show that the more important variable in stress relief using line patterns is the orientation of the mask lines to the direction of measure. When mask line orientation is held at 0°, meaning the lines run parallel to the cantilever beam, he best experimental results for this orientation at 8 seconds of structured illumination are in the 0.4-0.5 normalized deflection range corresponding to a far higher stress than seen when measuring the stress perpendicularly to the line mask. These results show the differential stresses realized when illuminating a line pattern during the structured illumination step and that although stress is relieved in all directions, the stress in the direction of monomer migration achieves maximal relief.

An orientation of 45° was also studied and again confirmed differential stress relief. In all samples illuminated using the 45° orientation the left edge of the cantilever deflected more than the right edge. Upon examination of Figure 5.4 this observation should be expected since it has been shown with the 0° and 90° orientations that maximal stress relief occurs in the direction perpendicular to the mask direction. Differences between the two edges of each sample were generally 0.1 for normalized deflection which in these experiments corresponds to approximately 2 mm.

Figure 5.8 shows the optimum values for the variables within the ranges studied in the aforementioned experiments, as depicted by the low and high values. There is an obvious diminishing return on the addition of structured illumination time which has also been seen in prior experiments. One can also deduce that if orientation was further studied past 90° on to 180° that, due to symmetry, the direction of the minimization curve would reverse and follow itself back upwards leaving 90° as the optimum. The best line spacing and thickness for this particular setup (including monomer/initiator system, illumination equipment and illumination protocol) was optimized at 38.2 and 26.9 mils respectively.

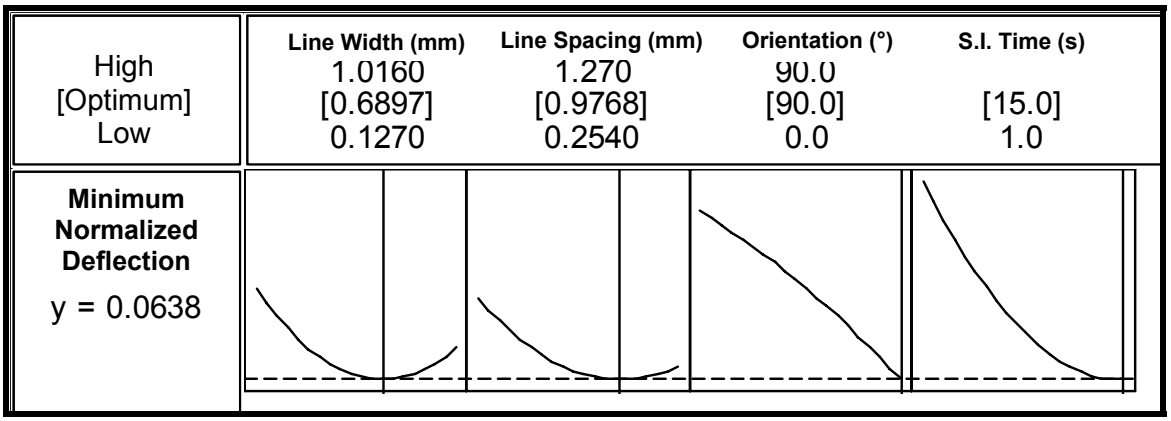

Figure 5.8: Predicted minimum of net deflection within the range, as indicated by the high and low values, of the experimental variables: line width, line spacing, orientation and structured illumination time.

These results pinpoint the best line patterned mask for the height of the mask over the substrate and the intensity and type of light used in the cantilever setup. It is also important to note that the minimization of stress is precisely applicable to this initiator/monomer system. A change in initiator concentration or a change in the initiator itself would affect the reaction rate and the time for monomer migration. A change in the monomer could change the reaction rate and the viscosity, which would change the rate of monomer migration.

Discussion

It is believed that certain general guidelines can be drawn in order to help choose the correct pattern for a particular application. In order to maximize stress relief, it is proposed that there be enough monomer migration to alleviate all of the stress in the structurally illuminated regions, and also that the fully stressed regions which only undergo illumination during the flood cure be as small as possible. It is currently thought that small, discontinuous regions of stressed polymer will cause less stress to be seen by the substrate. The length scale over which monomer migration will occur in order to relieve stress is determined by monomer viscosity, reaction kinetics and resultant

polymer viscosity and monomer/polymer diffusivity. If the area being illuminated is so large that monomer migration does not occur across the entire length of the sample then stress regions will build in the structurally illuminated regions thereby not maximally relieving stress. Also if there is not enough available monomer for migration in the masked regions either insufficient monomer migration will occur or there will be insufficient monomer left in the masked regions to provide a suitable coating.

With no limitations on migration, the minimum percent area masked that would still allow for maximum stress relief, would be equal to the percent shrinkage. This application would not suffice for a coating, because there would be no remaining monomer beneath the masked portions for subsequent flood cure. It is, however, a good place to start in our calculations to find the minimum masked and therefore stressed regions, for optimum stress relief. Still with no limitations on migration, the optimum percent masked area is a function of needed coating thickness and percent shrinkage of the given system. With the limitation to migration given by the uncured monomer viscosity and the change in diffusivity of the monomer into the curing polymer, the system becomes far more complex.

Conclusion

With no significant difference in degree of cure and very significant measures of reduction in polymerization shrinkage stress it has been shown that structured illumination is a viable method for improving the production of low stress photopolymerized coatings. The hope is that control of polymerization shrinkage stress will ultimately lead to better products.

CHAPTER 6: A NOVEL METHOD FOR CONTROL OF GLOSS IN PHOTOPOLYMERIZED COATINGS, FILMS AND SURFACES

Introduction

This chapter describes an invention of a method for controlling gloss in photopolymerized coatings over the entire range from high gloss to matte finishes. The method of structured illumination is generally applicable to photoinitiated systems and is independent of chemical composition of the resin or monomer. Wavelengths of light ranging from ultraviolet through infrared (including visible) can be used in this method. Photopolymerized (also referred to as photocured or light-induced) systems, with few exceptions[65, 66], tend to produce high gloss surfaces, however low gloss finishes are often more desirable. Common methods to reduce gloss involve the use of additives such as silica or micronized waxes which may reduce the gloss, but may also undermine other physical, optical or chemical properties of the system[67-69]. Other methods of gloss reduction involve either additional or complex processing steps. These steps may include but are not limited to embossing, chemical etching/dissolution, mechanical abrasion (sanding, blasting, etc.) and a wash step[70, 71]. This invention avoids extra processing steps to achieve the desired gloss reduction, thereby eliminating waste generation.

The structured illumination methods described in this invention disclosure makes use of the spatial and temporal control afforded by photopolymerization to produce a textured surface of specified gloss. Structured illumination involves the patterning of light on the surface of a photopolymerizable system. This patterning sets up alternating regions of light intensity which in turn initiates polymerizations at differential rates across the system. Areas not undergoing significant polymerization provide monomer for migration to those areas that are. This causes changes in the surface morphology which when illuminated correctly gives a micro-roughening of the surface; a common trait of low gloss systems. This structured illumination step is generally followed by a flood cure

step in which the entire system is illuminated at an intensity such that the final cured product is uniformly converted. This micro-rough surface gives a diffuse reflection of light and an apparent low gloss characteristic. This method can be used with any monomer system including but not limited to industrially important acrylate monomers which are typically high in gloss. The method which will be described will not require expensive light sources or intricately designed systems yet will be amendable to continuous processes and high through-put.

Background: Need for Gloss Control

Relative gloss is a characteristic of a polymer system that can have great impact on its function and appearance. For example, in the automotive industry high gloss finishes are desirable, while for applications involving the use of finished wood, such as cabinetry, flooring and furniture, a high gloss surface is often considered to undermine the apparent value of the product by making it look "plastic" or "unnatural." Display technology is another more technically advanced area where control of gloss is needed. Anti-reflective or low-gloss films are used for glare reduction for a wide variety of displays and optical systems or components[72, 73].

Smooth shiny surfaces reflect light in a specular manner which gives an appearance of a high gloss, mirror-like finish while low gloss surfaces tend to be micro-rough which diffusely reflect light. This concept is portrayed in Figure 6.1.

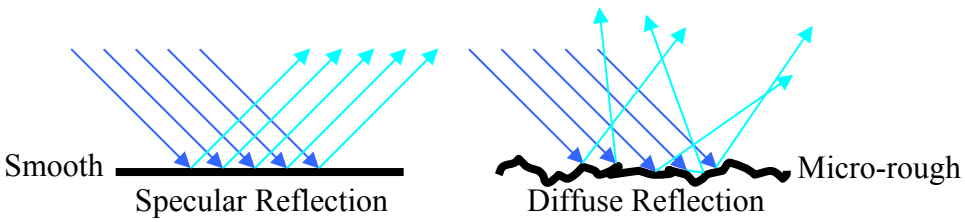

Figure 6.1: Pictorial representation of specular and diffuse reflection from a smooth and micro-rough surface, respectively.

A gloss meter measures the specular reflection of directly illuminated light at an angle dependent on the type of surface being measured. Measurement angles are recorded as their deviation from normal to the surface of interest. High gloss is measured at an angle 20° from normal while semi-gloss and matte finishes are measured at 60° and 85° respectively. High gloss numbers in the 20° geometry represent very glossy systems where as low gloss numbers in the 85° geometry are from low gloss systems.

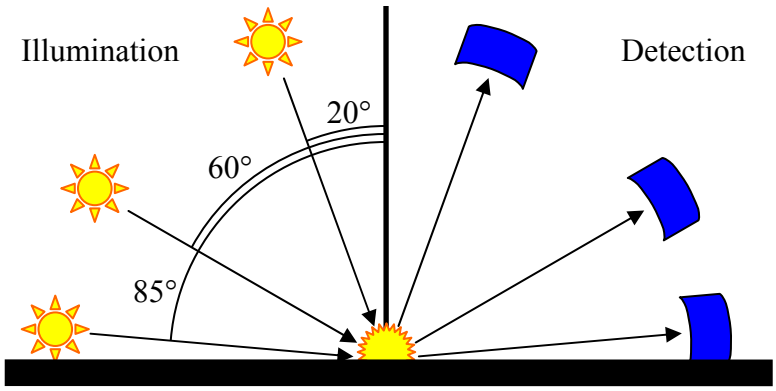

Figure 6.2: Illumination and detection scheme carried out when using a glossmeter. Direct illumination and detection of reflected light are done at specified angles depending on the level of gloss for the surface.

A common method to reduce gloss by producing a micro-rough surface is the addition of silica fillers[67-69]. This micro-roughening causes a more diffuse reflection of incident light providing a decrease in the apparent gloss. One drawback may be absorption of light by the filler, depending on the loading, thereby altering the curing characteristics. Figure 6.3 portrays the micro-roughening obtained by the use of silica in a polymerized coating or film.

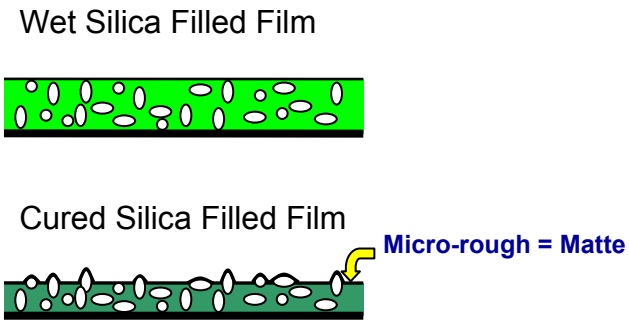

Figure 6.3: Pictorial representation of silica fillers micro-roughening the surface of a polymer system giving matte finish.

Structured Illumination as a Novel Method for Gloss Control

Structured illumination provides a means of producing a micro-roughened surface without the use of additives. The micro-roughening obtained using structured illumination is due to the monomer migration from areas which are masked during the structured illumination step to those which are illuminated. This concept is portrayed in Figure 6.4. After structured illumination has taken place a flood cure step is generally needed to uniformly cure the entire coating giving raised areas where structured illumination first occurred.

By using structured illumination there is no need for the use of additives and therefore no drastic change in the curing kinetics of the system. The texture or roughness obtained using structured illumination is affected by the pattern of the light incident on the surface of the monomer, the intensity of the light, the thickness of the coating and the concentration of initiator. Shown in Figure 6.5 is a simple diagram portraying the concept of how structured illumination can mimic the surface modifications achieved with additives, resulting in gloss reduction.

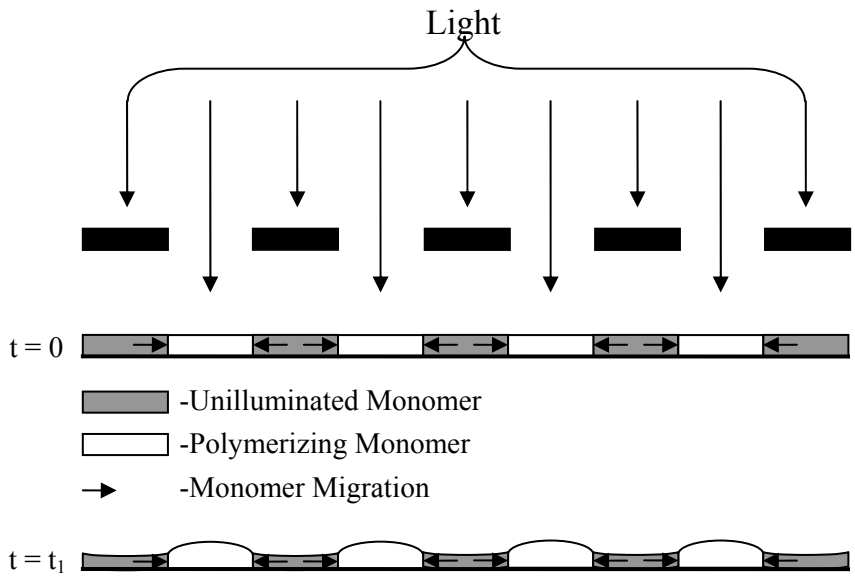

Figure 6.4: Illustration representing structured illumination of a film of monomer where the light is turned on at time zero and subsequent monomer migration occurs before time t_1.

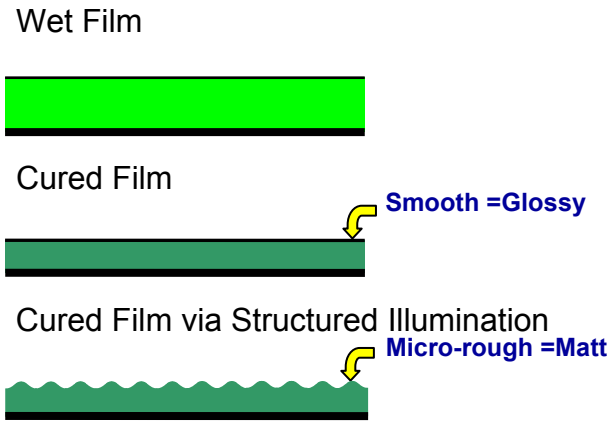

Figure 6.5: Illustrative cross-section comparison of standard flood cured system and a structurally illuminated system showing the potential of structured illumination as a method to reduce gloss in photopolymerized coatings.

Selection of Spatial Patterning for Structured Illumination

For effective gloss control by structured illumination, the spatial illumination pattern (a variation in light intensity as a function of location in a two-dimensional plane) plays an important role in determining the surface morphology, texture, or roughness in the final cured product. The pattern may be most easily generated by illumination through a mask, however it could also be produced by projection or by an interference pattern from two or more light sources. There are many key variables in the design and selection of the illumination pattern. Some of the variables include feature size and feature shape, which are indicative of each individual pattern. The optimize size and shape may depend upon the specific polymerization system, monomer formulation, comonomers, additives, dyes or pigments. Also the spatial relationship between the dark and light regions and whether or not there is a clearly defined difference or if there is an intensity gradient between the two. There are essentially an unlimited number of illumination patterns (including mask designs) available for use with this invention. With that comes a high degree of flexibility in the final characteristics of the system. A wide range of apparent gloss can be obtained on the surface of the system. Differential gloss, depending on viewing angle, which will be discussed further in the following section, can be obtained. Also different gloss values depending on spatial location due to different patterning on various sections of the system can be produced.

Anisotropic Gloss Reduction

We have shown that line masks give not only less gloss reduction than a multi-axis pattern, but a differential gloss reduction depending on the angle of measure. This idea is shown in Figure 6.6, below. Higher gloss is seen when making a measurement parallel to the direction of the patterned lines while rotating the sample 90° in order to measure at an axis perpendicularly to the patterned lines gives a lower apparent gloss.

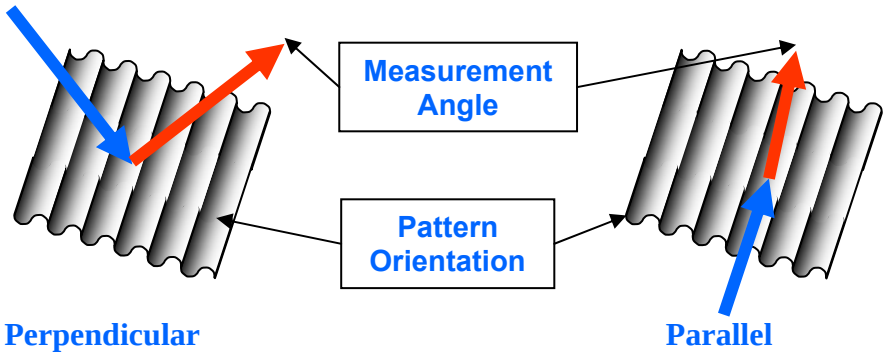

Figure 6.6: Schematic showing measurement angles with respect to the line-patterned polymer surface whereby higher gloss readings are measured in the parallel axis when compared to the perpendicular axis of measure.

Multi-directional texturing of the surface, which will give a more diffuse reflection of light, can be obtained by mask patterns such as cross-hatch and camouflage patterns. Such patterns have shown greater ability than line patterns to reduce gloss with far less of a dependence on viewing axis. Examples of gloss reduction using a cross-hatched mask pattern will be discussed further in the Demonstration of Invention section.

Illumination System

For effective gloss reduction using structured illumination, the light source must be such that significant cure takes place during the time in which structure illumination takes place. For a given photopolymerization system, the illumination variables include the intensity or irradiance, illumination time, and wavelength. If the wavelength of light being emitted does not match that of light which is absorbed by photoinitiation system then sufficient cure will not take place. Even if the light is of the correct wavelength the length of the structured illumination and the intensity of the light must be sufficient in order to cause enough polymerization to take place in the illuminated regions to set up a concentration gradient for diffusion or cause enough shrinkage for monomer microflow. There is a possibility that even in the masked regions there is sufficient light for

polymerization to take place however if there is enough of a cure differential then surface distortions could appear that reduce gloss. This would lead to negating the next criteria which is that the mask must be removable or that the mask must end so that a subsequent flood cure can take place.

Structured Illumination using Masks in Continuous (Web) Processes

Some processes call for continuous production in which case a web process is desired. In the simplest case, masks for such processes, unless they are line masks running parallel to the axis of production, cannot be stationary. They must move along with the product in order to give the proper illumination pattern which best reduces gloss. Processes which are stationary in application are far less involved, but do share some of the same concerns as web processes. In both cases the distance of the mask from the coated surface is important. Faithful representation of the mask on the surface of the coating is best achieved by placing the mask as close to the coating as possible. Touching the coating is not a likely option in that this may hinder monomer migration unless the mask is a non-wetting substance in which case one can imagine it aiding the movement of monomer to the illuminated regions.

A more involved process could incorporate a stationary mask in a continuous process if a flash lamp is used. The pulsed illumination from this lamp would need to be synchronized to the speed of the belt in order to illuminate a well defined pattern on the surface of the system. Again considerations for degree of cure during structured illumination would have to be taken into account for each short pulse and the total pulsed illumination time.

Specific Example Using HDDA and BisA Epoxy Acrylate

Studies were carried out on formulations involving two widely used monomers in industrial coatings. Hexane Diol DiAcrylate (HDDA) and BisA Epoxy Acrylate (EA)

were used in a one to one ratio by weight and initiated with a BisAcylPhosphineOxide (BAPO) added to the mixture at 1% by weight. These monomers and initiator are shown in Figures 6.7-6.9.

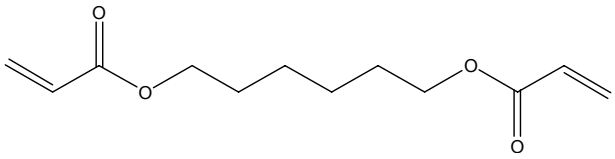

Figure 6.7: Molecular structure of Hexane Diol DiAcrylate (HDDA), a widely used industrial standard in coating applications.

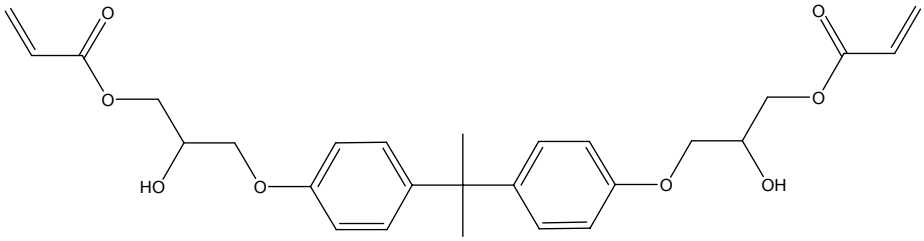

Figure 6.8: Molecular structure of BisA Epoxy Acrylate (EA), a widely used industrial standard in coating applications.

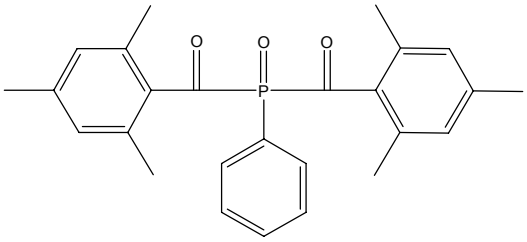

Figure 6.9: Molecular structure of Bis(2,4,6-trimethylbenzoyl)-phenylphosphineoxide (BAPO), a commercially available photoinitiator with absorbance peaks at 295 and 370nm.

Both monomers are difunctional acrylates which undergo cross-linking providing a very tough, mar resistant, yet somewhat brittle coating. Coatings made from these acrylates via a conventional photopolymerization process tend to give high gloss finishes. By adding matting agents one can reduce the gloss; however this may create problems in the mixing stage or during application in that the system is no longer a homogenous liquid mixture.

BAPO is a commercially available initiator made by Ciba under the brand name IrgaCure 819. It undergoes alpha cleavage at the phosphor and initiates a free radical polymerization when near UV illuminates the system.

Experimental Setup and Procedure

Experiments were completed on 3 in. by 6 in. stainless steel Q-panels (Q-Lab, Cleveland, OH). The panels were coated with red epoxy spray paint to reduce the gloss of the panel and eliminate the interference in measurement as a result of reflection from the bare metal substrate. 500 μL of our system was applied in a thin line near the top of the Q-panel using a P-1000 precision pipette. Care was taken to ensure that the line covered approximately the same width on the panel during each trial to ensure a consistent coating thickness and coverage.

A #80 wire wound applicator rod was then used to distribute the monomer across the panel in a thin, evenly distributed layer. The Q-panel was then placed in a sealed inerting chamber beneath a Hybrid Technologies Corp. model 63-10 ultraviolet light source. The UVA intensity of the light source was measured at 160 mW/cm^2 and the panels were placed at a distance of approximately 10 inches from the light source optic, centered under the 6in. quartz window which makes up the top of the inerting chamber. This distance was chosen due to the height of the brass sieves being used as masks. The coated Q-panel was placed as close to the sieve as possible (<1 mm spacing) using spacer blocks. Figure 6.10 illustrates the experimental setup that was used.

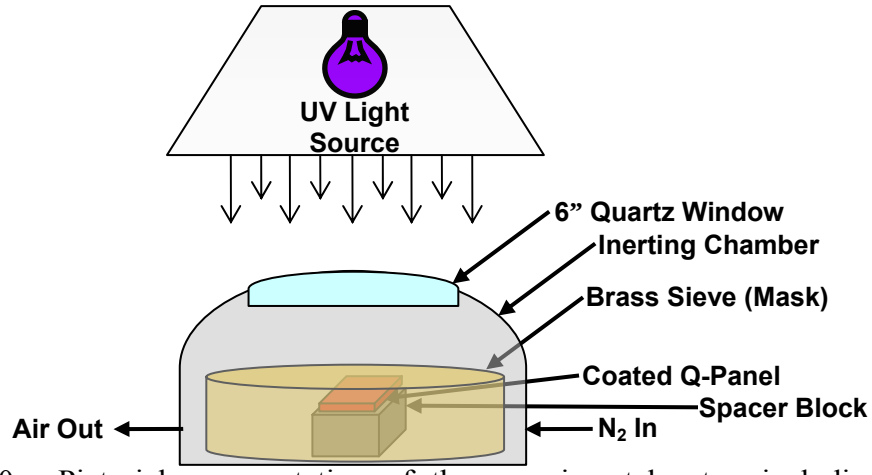

Figure 6.10: Pictorial representation of the experimental setup including the light source, inerting chamber, brass sieve (mask openings not portrayed in drawing) and coated Q-panel.

For structured illumination ASTM standard brass sieves, of which the dimensions are well established, were used. The wire thicknesses and mesh openings for the various mesh numbered sieves used in our gloss reduction experiments are shown in Table 6.1.

Table 6.1: ASTM standard sieve dimensions of mesh opening and wire diameter.

U.S. Sieve # Wire Mesh Size	MESH OPENING		WIRE DIAMETER	
	inches	mm	inches	mm
80	0.007	0.18	0.0052	0.131
100	0.0059	0.15	0.0043	0.11
120	0.0049	0.125	0.0036	0.091
140	0.0041	0.106	0.003	0.076
170	0.0035	0.09	0.0025	0.064
200	0.0029	0.075	0.0021	0.053
230	0.0025	0.063	0.0017	0.044
270	0.0021	0.053	0.0015	0.037
325	0.0017	0.045	0.0012	0.03

A cover was placed over the inerting chamber to prevent any light from reaching the coating while the panel was being inerted by nitrogen for approximately 5 minutes to eliminate the effects of oxygen inhibition on the photopolymerization process. This is an important step because our interest is in a surface property and oxygen inhibition affects surface cure[74]. After completing the inerting step, the cover was removed and the coated panel structurally illuminated (with mask) for 60 seconds. The brass sieve was then removed and the system underwent a 60 second flood cure (no mask) in order to complete the polymerization.

Gloss measurements were made by using a Byk Gardner micro-tri-gloss meter which also has the capability to measure thickness on both ferrous and nonferrous metal substrates. This meter measures, within seconds, gloss readings at the 20°, 60°, and 85° geometries and gives a thickness measurement. The 20° geometry is used for high gloss finishes, while the 60° geometry is used for semi gloss and the 85° geometry for matt finishes (see Figure 6.2). Each sample was measured a total of six times; three times perpendicularly to the length of the coated panel and three times parallel to its length.

Results

Upon structurally illuminating, for 60 seconds, the inerted samples through the various sieves, followed by a 60 second flood cure in the aforementioned setup, six gloss measurements were taken on three samples for each of the sieves. The average results are shown in the Table 6.2 along with average coating thicknesses which have a standard deviation of 6 μm.

Clearly one can see the dramatic gloss reduction achieved upon structured illumination of the samples shown in Table 6.2. By simply flood illuminating the HDDA/EA system, an extremely high gloss surface is produced. Structured illumination followed by flood cure gives a range of apparent gloss readings with the lowest being well within the range thought of as low gloss finishes.

Table 6.2: Gloss measurements for the three common measurement angles and thickness readings taken for HDDA/EA samples structurally illuminated beneath various sieves.

U.S. Sieve # Wire Mesh Size	20° (High Gloss)	60° (Semi-Gloss)	85° (Low Gloss)	Thickness (um)
none	91.4	95.9	97.6	143
80	4.9	26.6	32.0	141
100	4.7	26.7	30.3	147
120	4.5	24.5	25.1	143
140	4.6	23.8	22.9	138
170	5.6	32.2	38.4	145
200	4.1	23.3	32.0	140
230	7.4	41.7	57.9	137
270	7.0	46.7	68.3	139
325	72.6	94.8	94.6	142

Summary of Invention

The above discussion illustrates that utilizing structured illumination as a method to prepare photopolymerized surfaces one can achieve different values of gloss ranging from high gloss to matte finishes. Our experimental results demonstrate that we were able to achieve low gloss finishes for an acrylate system which otherwise would produce a very glossy surface. In addition, we were able to describe straightforward implementation to a continuous process. And finally, the method and understanding of why gloss control is achievable is unique but fairly simple.

Current methods for reducing gloss in polymer coatings, films and surfaces generally involve additives or secondary mechanincal or chemical processing steps. Additives are commonly present in the form of inert matting agents such as silica or micronized waxes. Besides reducing gloss, additives may also undermine other important properties of the system. Secondary processing steps used to reduce gloss

include sanding, grinding, blasting, machining and other mechanical abrasion techniques in which a micro-roughened surface is achieved. This type of gloss reduction is capable of producing waste material in varying quantities. Embossing or transfer molding is also a common technique to micro-roughen a surface in order to reduce gloss. Here cleaning of the embossing tool or mold can be an issue along with the capital expense of the embossing or molding system. Chemical methods can also be used to reduce gloss such as chemical etching and dissolution. These methods will almost certainly generate chemical waste. Structured illumination as a method to reduce gloss eliminates waste generation and can be a simple, inexpensive method to reduce gloss without adversely affecting other properties of the polymer system.

Structured illumination, which is the patterning of incident light on the surface of a photopolymerizable system, has not been taught in prior art. Its important aspects include feature sizes of both the illuminated and dark areas and the time of structured illumination. Choosing the correct spatial and temporal patterning parameters will allow for variable gloss reduction in the finished product.

The idea of structuring the illumination of a photopolymerizable system for gloss control is unconventional. Generally, the composition of a photopolymerized system is changed in order to change the appearance of gloss. This method focuses on the processing, not the components of the system, in order to obtain desired characteristics of gloss. This method, however, is not a mechanical processing such as embossing, sanding, blasting, etc., which also may be used to create a low gloss surface. Structured illumination is in general a non-contact chemically driven processing method for reducing gloss in photopolymerizable coatings that does not involve a wash step or chemical etching/dissolution. Masks used in this process can be very inexpensive and because of the non-contact nature may never need cleaning. Structured illumination by its nature of being a photopolymerization process caries along with it the many

advantages of photopolymer processing in that it is generally quick, inexpensive, and can be considered in some applications as a green chemistry.

Conclusion

Applying structure illumination is straight forward in most applications as described in the *Structured Illumination using Masks in Continuous (Web) Processes* section of this work. It can be used in continuous and batch configurations with high production rates. Because of the ease of application, areas where this method may be used include most photopolymerization processes. Key areas have been mentioned which include display technologies involving films which reduce glare and wood coatings industries where low gloss may be preferred over higher gloss coatings. This method is not limited to but may be included in areas of paint and clear coats to provide a variety of finishes, printing to produce textured images, optical films such as light diffusers, anti-reflective and directionally reflective films, packaging and any film or coating industry where an aesthetically pleasing look or feel may be desired.

At the onset of this writing all samples used for gloss reduction experiments were acrylate formulations. Studies have been carried out on different substrates including coated and uncoated metals, wood of different varieties and plastics. With the exception of one experiment which was carried out to simulate a web process, all others were done under the setup described in the *Experimental Setup and Procedure* section of this work. Future studies should concentrate on simulating a web process and industrially applicable formulations for display films and wood coatings.

CHAPTER 7: CHARACTERIZATION OF STRUCTURALLY ILLUMINATED THIN AND THICK FILM PHOTOPOLYMERS

Photo Differential Scanning Calorimetry

A long time standard for measuring the conversion of monomer to polymer during a photopolymerization process has been the use of a photo differential scanning calorimeter (photo-DSC)[75-77]. With its ease of use and its principles based in the fundamentals of chemistry, photo-DSC has been used reliably for many years. It is an adaptation of a standard DSC[78] where the main difference is that an illumination source is mounted atop the unit with a shutter controller and a quartz window placed over the sample tray so as to allow light to enter while preventing convective cooling of the sample. Photo-DSC reaction rates and conversion measurements can be acquired at any initial temperature required within the range of an ordinary DSC due to reactions being induced by light energy and not thermal energy. Reaction rates and overall conversion of monomer to polymer are calculated from the heat evolved during the reaction.

Possible problems with the current photo-DSC setup are that it gives a bulk measurement and the geometry of the measured sample may cause differences in reaction rate and conversion measured when compared to the sample it is representing. Bulk measurements give an average conversion and reaction rate which may be all that is required. For those applications where there may be a sizable difference in properties due to differences in the conversion throughout the sample thickness or other dimension, a DSC will not suffice. Raman Spectroscopy gives an adequate alternative when properties such as conversion of a small region of a larger sample are required.

Comparing the reaction rate and overall conversion of a DSC sample to that of a process may bring about discrepancies. Thin films will not evolve a large change in temperature analogous to an isothermal measurement attainable with the use of a DSC; however, larger geometries with a sizable exotherm may cause a substantial increase in

temperature, thereby changing the kinetics of the reaction. This is not easily measurable in a DSC where the size of the sample is small. Even with the correlation between thin films and the isothermal measurement of the DSC, there may be differences in how the reaction is initiated. Photopolymerizations give the ability to initiate specific portions of the sample at different rates by varying the intensity across the surface of the monomer. To measure an overall conversion of the sample with these variations, such as in structurally illuminated coating samples, a larger surface geometry is needed than is provided by the photo-DSC. Here a Thin Film Calorimeter is useful and will be discussed further in a following section.

Raman Spectroscopy

Short Raman Study of Conversion

It is well known that photons of light interact with molecules causing a transition between energy states. When the photon induced excited state molecule transitions back to the initial state, a photon of light equal in energy to the original photon which caused excitation, is released thereby creating Rayleigh scattered light. In a less common phenomenon, energy is either absorbed or released by the molecule (i.e. transitioning from the excited state to a state other than the initial state) and Stokes and Anti-Stokes scattering is observed, respectively. In Stokes scattering a lower energy, higher wavelength photon is emitted. From a polarizable molecule this scattered light occurs due to a change in vibrational energy and that change in energy is equal to the diminished energy in the photon which is emitted.

The Stokes band, as it is referred to, is larger than the Anti-Stokes band and therefore is generally measured in Raman Spectroscopy. A very intense monochromatic light source must be used in order to obtain a detectable signal from the Stokes scattering. This is due to the fact that a very small fraction of light undergoes Stokes scattering and the difference in energy between the excitation light and the Stokes scattered light is

small. Detection is done with a device called a photomultiplier tube which allows for the transformation of light into an electric signal. A photon of light incident to the photomultiplier tube creates a shower of electrons which is captured as the digital signal of a photonic event. A monochromator or spectrograph and multichannel detector can be used to distinguish light of varying energies.

Some of the advantages of Raman Spectroscopy are that sampling is inherently small and, because it is a scattering process, it does not require a certain size or transparency of the sample. Also any place a laser light can be directed and collection of scattered light can be obtained, a Raman Spectrograph can be produced. This includes remote sensing through the objective of a microscope with confocal abilities giving rise to Confocal Raman Spectroscopy. This is obtained through the use of fiber optics. Also, Raman Spectroscopy in larger areas can be done. One such example is the sensing of emissions from a smoke stack by directing a laser at the plume rising above it[20, 60, 79]. For structurally illuminated samples Raman Spectroscopy allowed for facile acquisition of data due to the ease or lack of sample preparation. Both composition and conversion of the monomer to polymer were examined.

Initial studies using the Raman to look at conversion differences of masked samples were done on glass slides. This was unsuccessful due to the fluorescence of the glass and as a result brass slides were used. Brass allowed for the different characteristic peaks of the polymer to be seen.

A short Raman study was done on two samples illuminated with differing mask types. The first was a simple line mask and the second was a dot mask both made from acetate paper. Each sample consisted of 75 μL of a solution of HDDA and 1% by weight of IrgaCure 369 spread over an area of approximately 0.75”x1.5” on a 1”x3”x0.015” brass slide. These samples were put on a sled that was placed on a lab jack set up to be 13 cm from the 200W medium pressure Hg/Xe arc lamp. The samples were structurally illuminated through one of the two masks for 240 seconds and then passed through the

Fusion System at a belt speed of three feet per minute for flood illumination. After correction of the baselines (Figure 7.1B) and doing a peak ratio to compensate for signal intensity differences due to the difference in thickness of the peak and valley (Figure 7.1C), the signals of the two measurements were nearly identical. This leads one to believe that the conversion is the same in both the structurally illuminated and flood cured areas of the sample after it has been passed through the Fusion. The light intensity is so great that conversion must be nearly complete and any small differences are not ascertainable within the capabilities of the Raman.

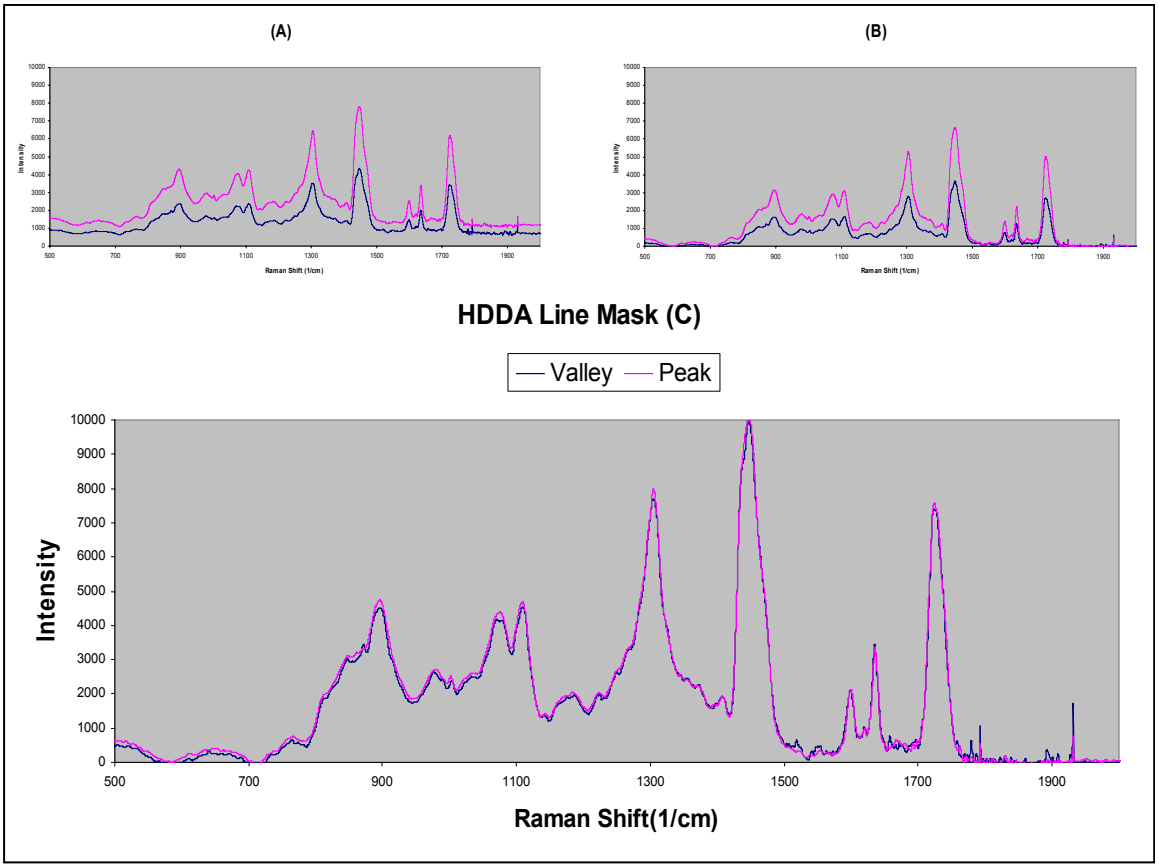

Figure. 7.1**:** Three graphs showing the steps of correcting Raman data taken of an HDDA sample which was first mask illuminated followed by a full illumination done using the Fusion to show the similarities between the two spectra taken at both the peak and the valley of the illuminated sample.

Here the Fusion was used to ensure that the samples were solid for use in other analytical measurements such as profilometry which will be discussed later in this chapter. When illuminating with the arc lamp only, the samples retain a greasiness that is attributed to short chained molecules. This lack of consistent chain length is due to oxygen inhibition. During the Raman studies the surface of the polymer could be easily seen on the computer screen. It was observed that under a dot illumination the surface of the polymer seemed to have risen, collapsed and then risen once more. This left the surface looking like a dome within a donut-like annulus. This could be attributed to varying light intensities as light is shown through a small aperture and diffraction occurs.

Involved Mapping Study of Conversion

A more involved conversion study was carried out using samples that were first measured for total conversion using a thin film calorimeter, discussed later in this chapter. The samples, which were prepared on sheets of aluminum, were mounted on glass slides and a mapping technique was carried out to determine conversion across the surface of a structurally illuminated sample. As with all samples studied the structured illumination was followed by a standard flood cure period. For the study line masks were used and were illuminated in the same manor as was done for stress studies mentioned in Chapter 5. A structurally illuminated sample with masked lines 762 μm wide and illuminated lines 1016 μm wide was mapped for conversion. Essentailly five line scans running parallel to one another and spaced 25 μm apart were done perpendicularly to the direction of the mask lines. The scans were set to be 3600 μm so as to encompassed two full on-off cycles for the structurally illuminated sample.

Peaks representative of the double bond and the cyclical structure in the photoinitiator were determined to be present at approximately 1630 and 1600, respectively. The cyclical structure in the photoinitiator remains unchanged throughout the reaction and therefore makes a good reference peak. To find the ratios of the peak

areas a Sav-Golay second derivative method[80, 81] was used to reduce the noise in the raw signal so that the peaks areas can be correctly determined. The double bond conversion was then determined using Equation 7.1.

$$\%\text{Double Bond Conversion} = \left(1 - \frac{DB^p / R^p}{DB^m / R^m}\right) \times 100\%$$

Eq 7.1: Double bond conversion calculated using Raman Spectroscopy.

Here DB^p and DB^m represent the areas of the double bond peaks in the polymer and monomer, respectively. R^p and R^m are the areas of the reference peaks. The averages of the five points are shown as one line scan in Figure 7.2 providing insight into the variation of conversion across the bumpy surface of two full cycles of masked and illuminated areas.

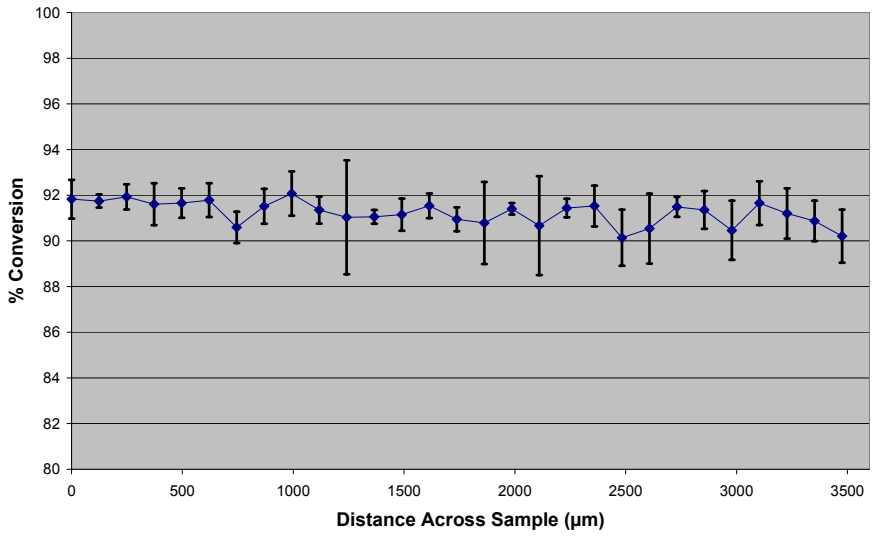

Figure 7.2: Double bond conversion across a structurally illuminated sample of HDDA.

The scan across the surface of the sample varies by less than ±1% and there is no noticeable pattern indicating a difference in conversion between the structurally illuminated portion of the sample and that which simply undergoes flood illumination. It is also interesting to note that measurements taken from a sample which was simply flood cured shows that within the error of measurement there is no difference in conversion. The flood illuminated sample had a conversion that fell within the range of 90-92%.

Raman Studies of Monomer Migration

In order to understand the migration of monomer which is taking place and causing distortions in the surface of the polymer coating, a study using Raman Microscopy to track the concentrations of the two species shown in Figures 7.3 and 7.4 was attempted.

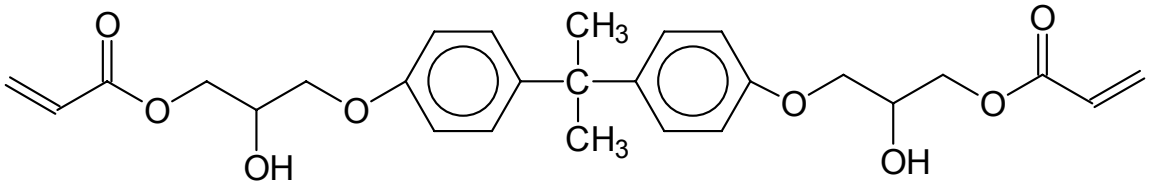

Figure. 7.3: Bis-A Epoxy Acrylate used in migration of monomer studies not only for its industrial significance but also for its large molecular weight.

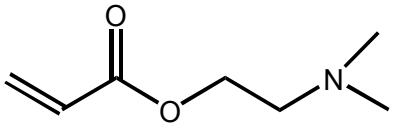

Figure. 7.4: 2-(DiMethylAmino) Ethyl Acrylate (DMAEA) used in migration of monomer studies because of its small molecular weight and its distinctive Raman peaks when compared to Bis-A Epoxy Acrylate.

Both species are acrylates and are photopolymerizable when mixed with Irgacure 369 (done at 1% by weight), however the Bis-A Epoxy Acrylate is a far larger molecule and therefore much more viscous than the 2-(DiMethylAmino) Ethyl Acrylate (DMAEA). This inhibits both the viscous flow and diffusional flow of the epoxy acrylate during the structured illumination step. After structurally illuminating the surface of the coating, thereby inducing monomer migration, and flood curing the samples, studies were done on the photopolymerized sample. The cross-section of a coating subject to a simple line pattern appears much like the following figure, with peaks where structured illumination took place and valleys where monomer was depleted in order to combat polymerization shrinkage stress. Scanned profiles of this phenomenon will be shown in the profilometry section of this chapter.

The idea was to first take measurements at both the peak and valley to compare areas which received structured illumination followed by flood cure to those which only underwent flood illumination. This, in practice, was easy to do once reference points were scribed onto the polymer sample in order to discern peak from valley when viewing through either the 10X or 50X objectives. The comparison of the Raman data retrieved from these points showed no distinguishing differences so a point scan across the sample from the masked region to the structurally illuminated region was done to capture data closer to the boundary between the illuminated and unilluminated regions during structured illumination. This scan is depicted in Figure 7.5. In order to study the workup of the data acquired using Raman spectroscopy, a peak representing the amino peak in the DMAEA was compared to the peak representing the ring structures in the epoxy acrylate. By setting one of these peaks for every point in the scan to 1000 and comparing the height ratio of it and the other peak any concentration difference should be seen. Below are graphs of such a workup showing the raw data and a blow up of the important peaks for a mixture of DMAEA and epoxy acrylate at a weight ratio of 1/1.

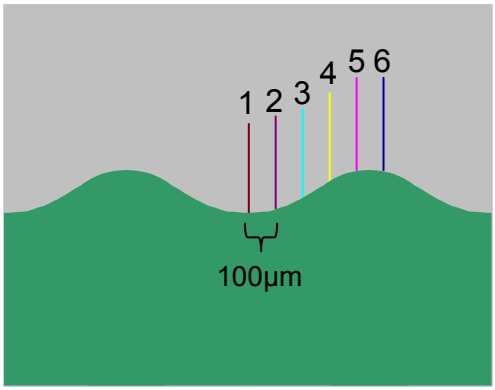

Figure. 7.5: Pictorial representation of the cross-section of a patterned surface with six Raman scan points as marked.

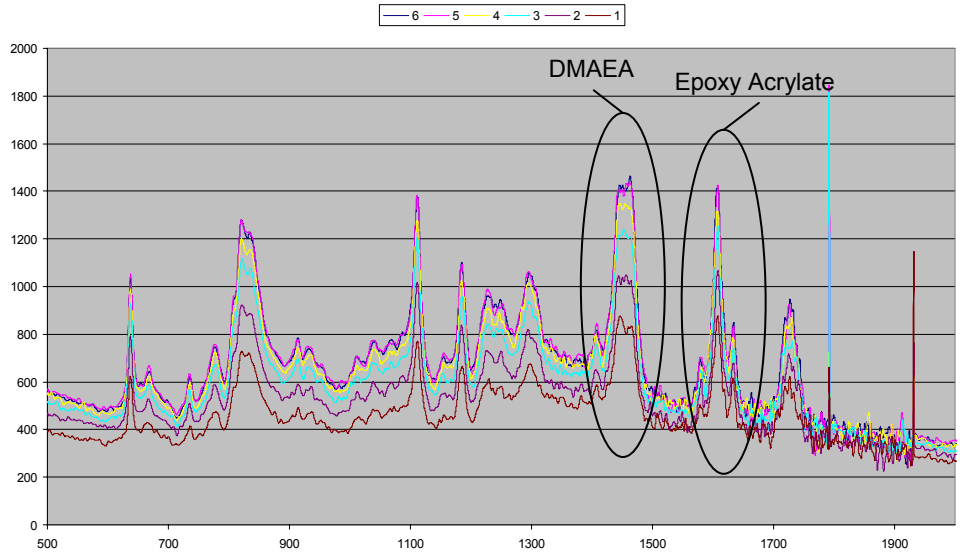

Figure. 7.6: Raman Spectrum of 1/1 weight ratio of DMAEA and Epoxy Acrylate scanned from valley to peak on a structurally illuminated sample.

After correcting the data for thickness differences by setting the peak height of the epoxy acrylate to 1000 and zooming in on the area between 1400 and 1700 one can clearly see that the only difference in height of the DMAEA peak falls within the noise of the Raman scan.

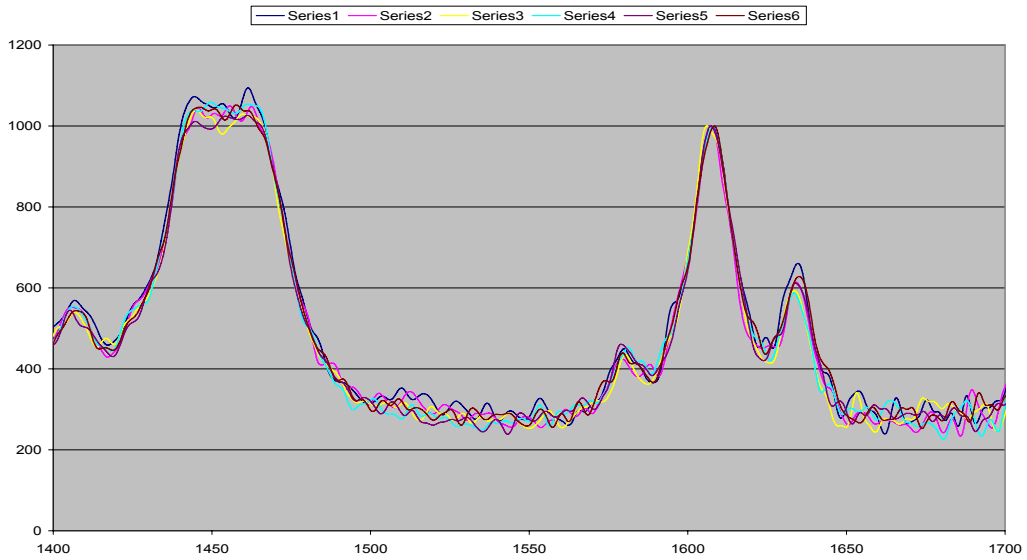

Figure 7.7: Raman scan showing no measurable difference in molecular composition in a scan from valley to peak on a structurally illuminated polymer sample.

The implications of these results point to the possibility of accidentally matching the differences between the viscous and diffusive properties of the two monomers with their differences in reactivity. The higher reactivity due to multiple double bonds in the epoxy acrylate may have led to a higher concentration difference during structured illumination and therefore a higher chemical potential between the illuminated and unilluminated portions of the coating. This may have counter acted the slower mobility of the epoxy acrylate monomer.

Another possibility is that diffusion plays far less of a role than does microflow and the 100 μm spacing of the scan was not sufficiently small to pick up any differences in microflow between the two monomers occurring only at the boundary of the structurally illuminated areas and the masked areas.

Thin Film Calorimetry

Following the lead of Todd Roper a thin film calorimeter was constructed for the measurement of heat flow from photopolymerizations[33]. At the heart of the device is a

heat flux sensor obtained from Omega (HFS-4). It produces 6.5μV/BTU/Ft^{2}Hr and has a type K thermal couple on its surface. It is a flexible flat device measuring 0.007" X 1.38" X 1.12", with a response time of 0.6 seconds. It also has a low thermal capacitance and resistance of 0.02 BTU/Ft^{2}Hr and 0.01°F/BTU/Ft^{2}Hr respectively, which makes it ideal for the application of measuring even very small amounts of heat flow from a thin layer of polymerizing monomer. Placing this device on an aluminum heat sink and recording an amplified output signal is the basis for the results that follow.

Figure 7.8 is an overhead representation of the heat flux sensor nested in the aluminum heat sink. An aluminum mask has been added over top of the sensor to reflect any excess light not necessary for the polymerization and the unwanted heat from that light so as to make the device more sensitive. The four small black circles represent alignment posts to ensure consistent placement of the mask. This mask is used to eliminate unnecessary light from affecting the very sensitive heat flux measurement. The wires are routed through a signal amplifier and voltmeter before going to an analog to digital converter and entering the computer for recording.

In order to save the heat flux sensor for multiple measurements the polymerization takes place atop a thin foil of aluminum which is thermally coupled to the heat flux sensor via a thermally conductive paste (OT-201 from Omega). This device can be placed beneath most light sources for quick and easy comparison measurements of the heat generated by a photopolymerization. The following results will show a comparison of the heat generated from photopolymerizing samples of 1% IrgaCure 369 in HDDA applied to the foil in a geometry similar to that of the stress measurements in order to show the extent of cure for both flood cured samples and ones which were first structurally illuminated.

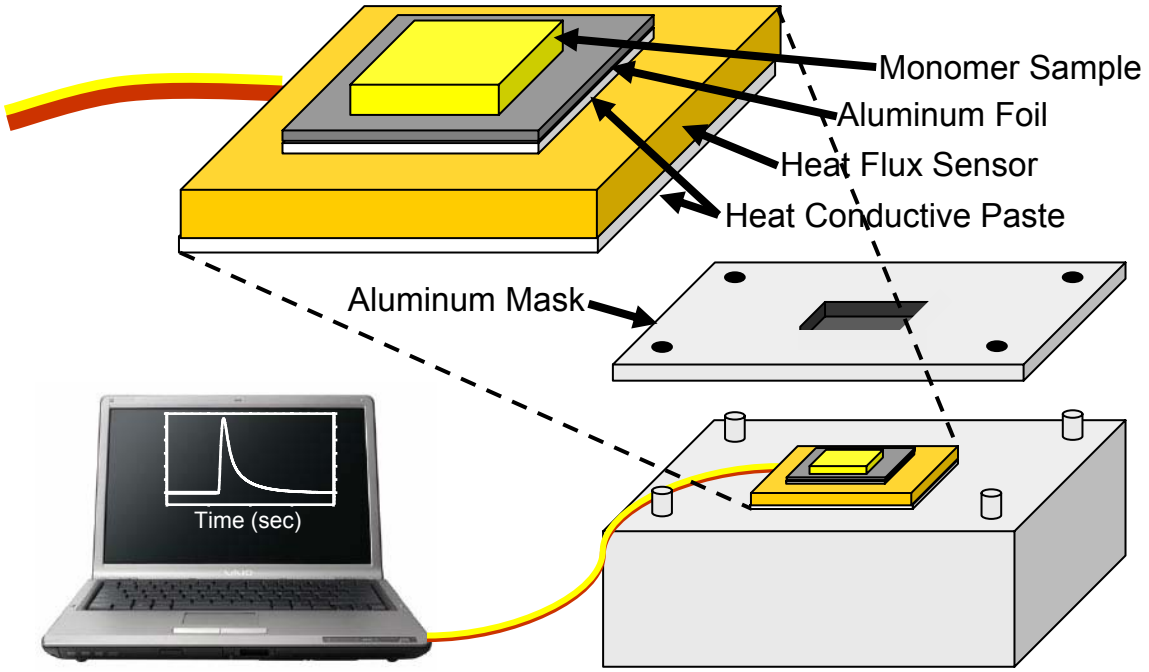

Figure. 7.8: Thin Film Calorimetry diagram showing the heat flux sensor thermally coupled to an aluminum heat sink being masked by an aluminum plate. All data is acquired through the use of a computer.

Comparison Study of the Structured Illuminated Process to the Standard Flood Cure Method

Figure 7.9 shows three experiments where the monomer was spread on the TFC and the heat evolution during illumination with the same kilowatt arc lamp used in the stress experiments is recorded. An illumination time of 10 seconds was used to mimic the stress experiments. As can be seen by the output data in Figure 7.9 the polymerization is virtually complete during the 10 second duration. This substantiates the choice of flood curing for 10 seconds during the stress experiments. The overlap of the three runs is quite good considering they were the first three runs done with little to no optimization done to the measurement process.

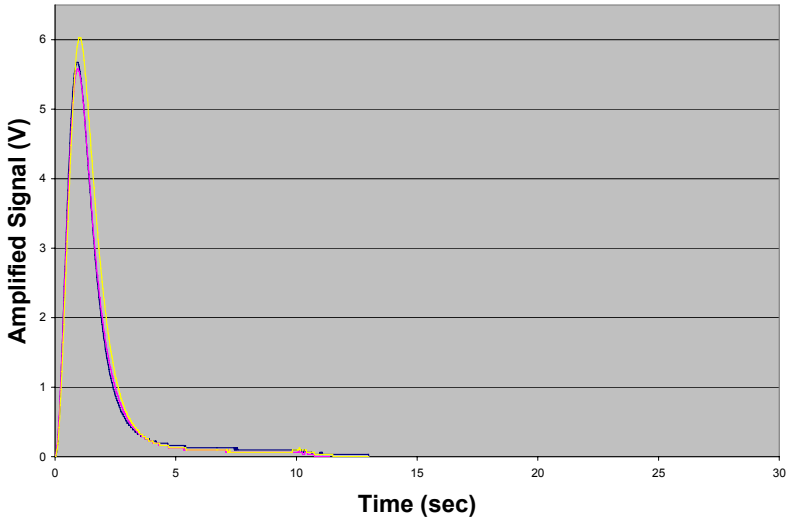

Figure. 7.9: Amplified signal from a heat flux sensor, representing the heat given off by reacting monomer during a 10 second flood cure of a sample containing 1% IC369 in HDDA.

Figure 7.10 shows the heat evolution during structured illumination followed with a flood cure. As is clearly shown, the illumination protocol includes 10 seconds of structural illumination followed by 5 seconds of no illumination so that the mask can be removed. Then there is a 10 second flood cure where most if not all the observable stress takes place, depending on the pattern of the structured illumination. It is obvious that much of the actual polymerization takes place during the structured illumination step for this experiment. This is a function of the illuminated area during the structured illumination step. In this experiment the area of the illuminated region when compared to the area of the masked region is approximately 150% larger. Add to that the diffraction of the light as it passes through the mask and it is easy to understand why most of the polymerization takes place in the first step. Again the exotherms of the three experiments track rather well with one another.

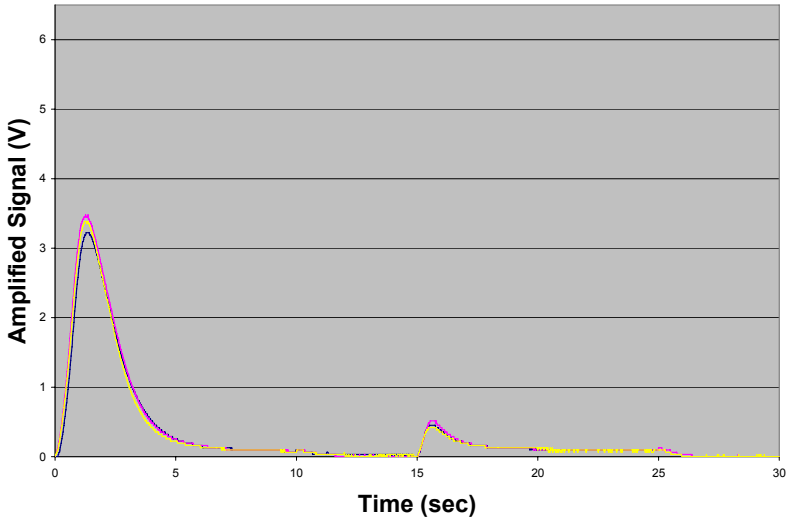

Figure. 7.10: Amplified signal from a heat flux sensor, representing the heat given off by reacting monomer during a 10 second masked illumination followed by a 10 second flood cure of a sample containing 1% IC369 in HDDA.

In order to understand how simply flood curing a sample differs from structured illumination followed by flood cure, the signals for the two illuminations in the second protocol are added together and the following graph was produced. Here it is clearly shown that the initial intensity of heat and therefore the initial rate of polymerization is somewhat smaller than that of the simply flood cured samples. However, the breath of the polymerization peak is larger and appears to diminish less rapidly giving an overall area under the curve, representing conversion, of equal value to that of the flood cured samples. The areas under the curves of Figures 7.9 and 7.11 are shown in Table 7.1 immediately following Figure 7.11. Statistically the areas are equal meaning the conversion of the various samples are equal, thereby showing that stress relief is possible without compromising conversion.

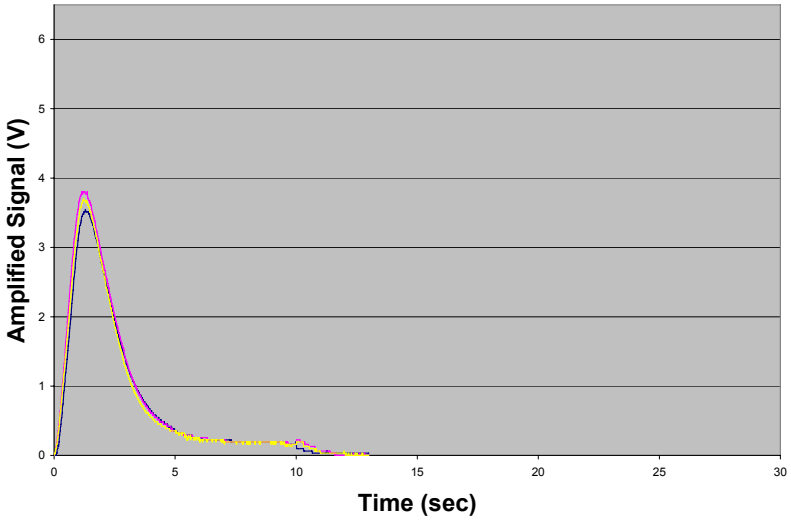

Figure. 7.11: The summation of amplified signals from a heat flux sensor for a 10 second masked illumination and a 10 second flood cure, representing the heat given off by reacting monomer of a sample containing 1% IC369 in HDDA.

Table 7.1: Areas under amplified signal curves representing conversion of monomer during the 10 second photopolymerizations.

Illumination Protocol	**Average Area Under Curve**	**Standard Deviation**
Flood Cured	9.11	0.45
Structurally Illuminated followed by Flood Cured	9.34	0.38

In all the aforementioned results involving the use of a TFC, the heat evolution due to simply illuminating the surface of the aluminum foil is subtracted from the data taken during polymerization by first doing an illumination without monomer for every run, both structured and flood, depending on the illumination protocol. The timing of these illuminations is where much of the error is likely produced. The shutter timing was done manually and will need to be changed to a more consistent automated system in order to reduce error. This should eliminate the intermittent rise in heat sometimes

shown immediately following the 10 second mark when the light is shuttered off after subtracting the light energy. In this way, true polymerization decay may be realized.

TFC Comparison Study of Different Line Masks Used in the Structured Illumination Process

Using the general method of analysis just described two different line patterns were studied. Both had the same mask line width (masked region), but the line spacing was varied thereby varying the structurally illuminated region. This gave rise to two masks, one which masked 75% of the light and the other which masked only 43%.

Table 7.2: Data showing dependences of stress deflection on when conversion took place during the structured illumination process.

	75% Masked		43% Masked	
Structured Illumination Time (sec)	8	15	8	15
% of Total Conversion During Structured Illumination	68.7%	73.6%	82.8%	88.2%
% of Total Conversion During Flood Cure	31.3%	26.4%	17.2%	11.8%
Normalized Deflection	0.58	0.3-0.4*	0.19	0.06
*As determined by a cubic model fit				

As can be determined intuitively and proven by the values in the table, the longer one structurally illuminates the more conversion takes place during the structured illumination step. Also the less masked region again, the greater the percent conversion taking place during the structured illumination step. The interesting results represented by the data is that for these two masks the more conversion that takes place during the structured illumination step, the less stress is measured as evident by the lower values for normalized deflection. This is exciting evidence leading to a conclusion that as long as

there is sufficient monomer for migration, polymer formed during structured illumination is virtually stress free.

Profilometry

Curious as to how much the surface of the polymer is distorted during masked illuminations; methods to measure the surface profile were explored. Since structurally illuminated samples are in the macro range for bumps on a surface a profilometer was found to be ideal[82]. Profilometry measurements were taken to characterize the surface of the polymer coatings prepared when both stress and gloss experiments were being carried out. Studies were done using a Sloan DEKTAK 3030 profilometer within the Microscopy Lab at the University of Iowa.

In order to obtain a profile of a coated surface some considerations were made in the preparation of the sample. Ideally the coating needed to be applied to a smooth level substrate. Stress experiments resulted in bent cantilevers so their profiles were not directly measured. Experiments mimicking their reaction parameters and coating preparation were done on thicker non-deforming brass substrates prior to profilometry experiments. Gloss experiment samples were done on flat, level Q-panels and were very easily measured by the profilometer when the thickness of the coating was relatively consistent.

Consistent coating application was done using a wire-wound applicator rod. As illustrated in Figure 7.12 this device consists of a wire, tightly wrapped around a stainless steel rod. The coating is created by monomer passing through the grooves or spaces left between the round wire coils as the rod is dragged across a pool of monomer. The monomer subsequently congeals on the other side to form a smooth, uniformly thick coating. The thickness of the coating depends on the diameter of the wire, the speed of draw and the viscosity of the solution.

Profilometry studies gave an idea of the relative bump heights attained with structured illumination depending on the thickness of the coating and the feature sizes of the mask being used in the structured illumination process.

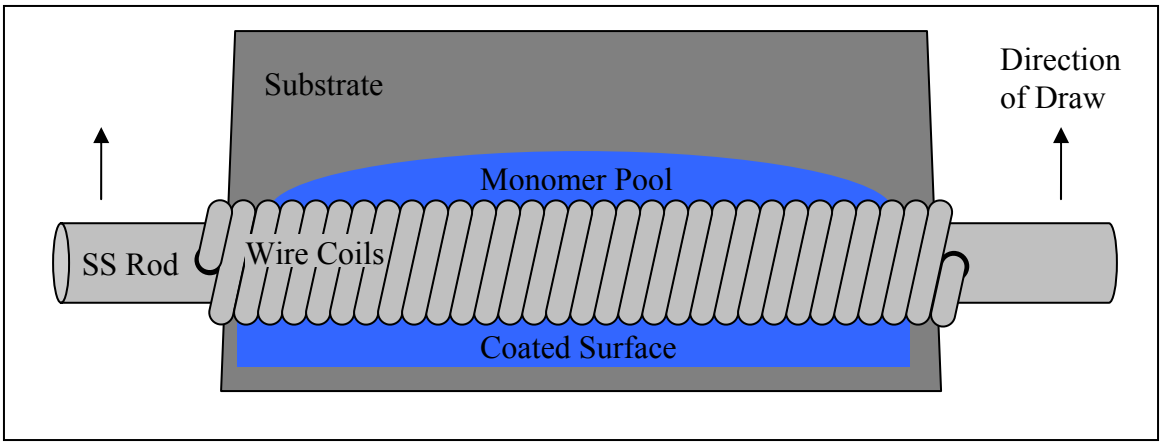

Figure 7.12: Illustration of a wire-wound applicator rod coating a substrate with a thin layer of monomer.

Figure 7.13 shows one of the relatively thick polymer samples which were done to replicate stress relief studies. One can easily see the curvature of the sample because of its thick geometry and relatively small surface area (approx. 1/2" X 3/8"). The size of the mask repeat pattern can be seen to be approximately 1mm by looking at the x-axis with an amplitude of 200,000 angstroms or 0.02 mm.

Figure 7.14 shows a sample in which the thickness was lessened and the monomer spread out over a larger area. This resulted in a smaller amplitude, and the mask used here had too large of a structured illumination area thereby not allowing for monomer migration across the entire illumination area, resulting in a double humped profile within each structurally illuminated region.

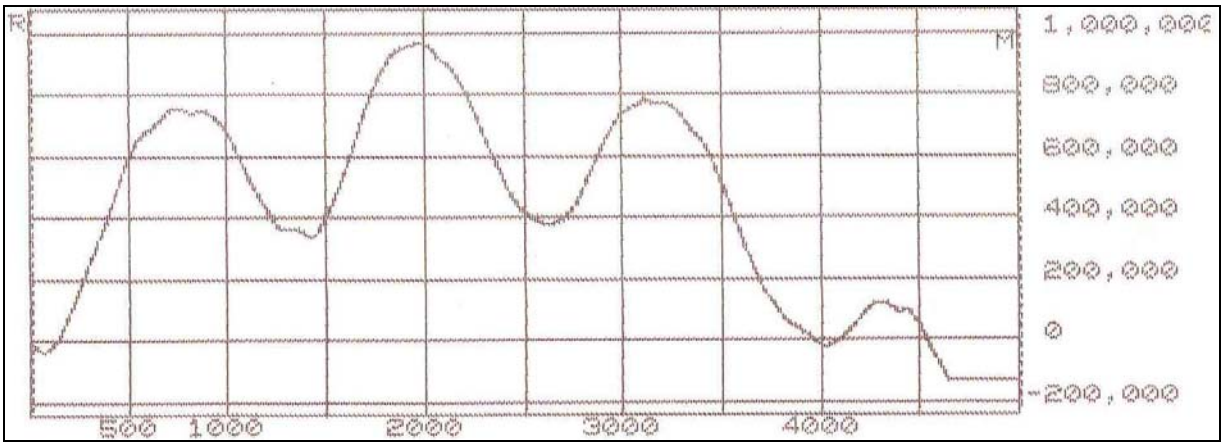

Figure 7.13: Profilometry scan of a sample meant to simulate stress reduction experiments via structured illumination. The x-axis is in micrometers and the y-axis is in angstroms.

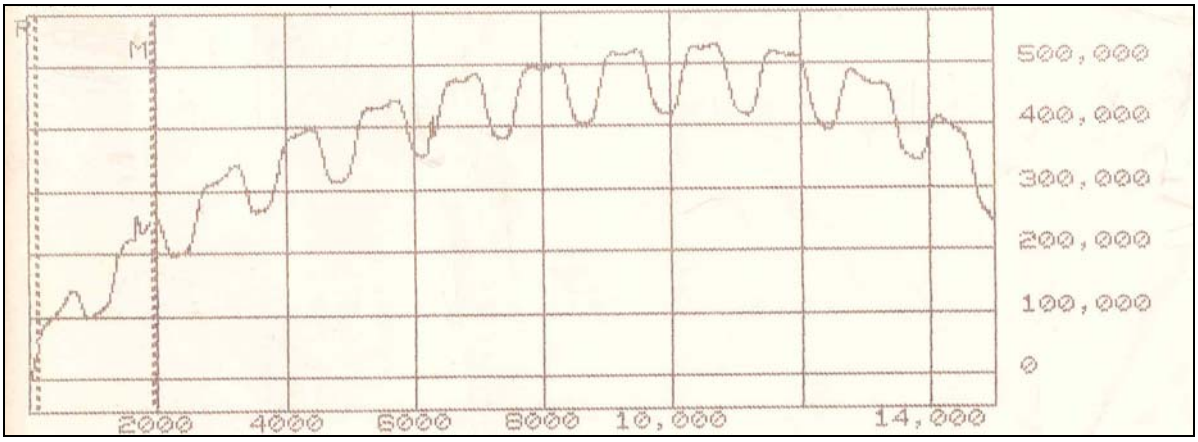

Figure 7.14: Profilometry scan of a sample with a structurally illuminated area that was too large to allow for optimal stress relief. The x-axis is in micrometers and the y-axis is in angstroms.

Still other scans were done on thinner coating samples in order to study the variations in bump amplitude with respect to structured illumination time. These thinner coatings led to flatter, more uniform profiles. Times were set to 1, 2, 5, 10, 20, and 60 seconds. With the exception of the 2 second structured illumination run all bump

amplitudes fell within the range of 35,000±3000. This leads us to believe that with as little as 1 second of structured illumination reduced gloss can be obtained.

Conclusion

Characterizing a product is an important part of any commercial application and is also extremely helpful in determining the fundamentals of a process. This chapter has shown that the conversion of a structurally illuminated sample has not been compromised in order to reduce stress or control gloss. It has also shown that properties can be changed with as little as 1 second of structured illumination.

CHAPTER 8: MATHEMATICAL MODELING OF POLYMERIZATION SHRINKAGE, STRESS AND MONOMER MIGRATION

Motivation for Mathematical Modeling

Mathematical modeling used in conjunction with today's ever expanding computer technology is a powerful tool for obtaining an excellent understanding of complex processes. The interactions of many facets of a process can be computed and deciphered at a much higher rate than is possible with even the most exquisitely planned experiments. Some of the best and easily obtainable software for use of understanding structured illumination and its applications in stress relief and gloss control include FlexPDE, FemLab and MatLab. Each program had a part in adding to the knowledge base of not only the structured illumination process, but also to understanding modeling in general. The knowledge gained and the shortcomings of each of these software programs will be discussed further in this chapter.

FlexPDE Modeling of Shrinking Polymer and Subsequent Deformation of a Cantilever Substrate

FlexPDE is a user defined, finite element model builder and numerical solver. Its advantages over other software is that the user may input any partial differential equation (PDE) system into the software and the PDE system will be converted into a finite element model, solved, and the results presented in a graphical and tabular output[9].

Realizing the similarities between polymerization shrinkage and thermal expansion we attempted to demonstrate the effects of polymerization shrinkage of an acrylate coating on a brass cantilever beam by use of a thermal expansion model. We adapted to our system, a model designed for showing the deformation of a bimetallic part during a change in temperature. By setting the thermal expansion coefficient of the brass cantilever substrate to zero and that of the acrylate coating to a negative number, a

shrinking polymer is realized. During the modeling of a temperature rise the polymer portion shrinks and forces determined using the Young's Modulus of the polymer act upon the substrate causing a deflection. In this model, the cantilever is allowed to move freely in space; however a Young's Modulus is defined for the cantilever to resist deformation. Other important variables include the geometry of the system, including both the cantilever and the polymer coating. Also the temperature rise and thermal expansion coefficient are important to be set such that a specified shrinkage is obtained.

Changing the value of the negative thermal expansion coefficient for the polymer coating for a given temperature rise to match the percent shrinkage seen during polymerization gives this model facile control of an imperative parameter. Modeling the free polymer and calculating the percent shrinkage allows matching to a real world experiment. When coupled to a brass cantilever substrate a deflection is then realized.

It is interesting to note that even though the geometry of both the shrinking polymer and the substrate are rectilinear, the resulting X-displacement profile shows a radial pattern. This is shown in Figure 8.1 with the color scale ranging from purple to red showing both positive and negative displacement since the geometry is not constrained and is allowed to freely move about in space. Laboratory experiments do not support the radial pattern of displacement seen here, but it does seem to be an excellent concept for modeling shrinkage.

Figure 8.2 is a 3D rendering of the previous displacement model given by FlexPDE. Again, a radial displacement, not substantiated by experimental observations is shown.

Experimentally the short axis of the cantilever (z-axis in the case of Figure 8.2) has been observed as the easiest axis around which to bend and little or no deformation manifests itself around the long axis (y-axis).

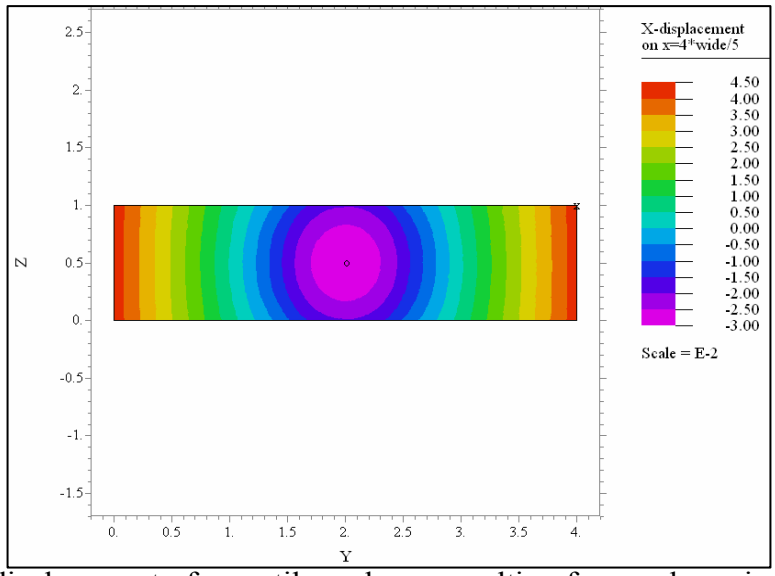

Figure 8.1: X-displacement of a cantilever beam resulting from polymerization shrinkage being modeled similarly to thermal expansion.

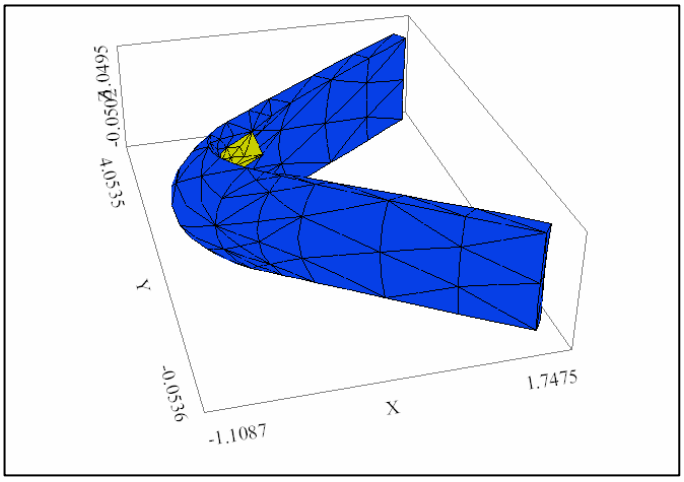

Figure 8.2: Output from FlexPDE showing a representation of displacement in three dimensions.

The software is only limited by the input from the user. Our input, although quite adept at simulating the shrinkage, does not adequately represent the deformation of a cantilever beam from our experiments. This could be due to the experimental cantilever

beam being held in place on one end (at y = 2.5 or -2.5), thereby keeping it flat about the y-axis not allowing for displacement in the x-direction.

FemLab Modeling of Stresses in Cantilever Beam Experiments

The intention of this study, using FemLab Multiphysics Modeling[83, 84], was to develop a correlation between bend height deflection of a cantilever beam induced by a shrinking photopolymer coating, and the resulting stress imparted on the cantilever beam by the shrinking polymer. While a standardized ASTM test (D6991) exists for this type of experiment, the laboratory experiments were completed over a year before the publication of this standard. As discussed in prior chapters, the experiments completed did not exactly match the criterion specified by the ASTM standard[26].

Developing the Structure

In order to accurately model the cantilever beam experiments done within the lab, the exact geometries and mechanical properties of the system needed to be entered into the software package. The first step in building a model for the bending cantilever beam was to draw the structure in FEMLAB drawing mode. FEMLAB contains built-in features that allow for the construction models without the use of an outside CAD program, such as ProEngineer or AutoCAD. The substrate (cantilever beam) was drawn first as shown in Figure 8.3.

The polymer was then added to the substrate previously built for the model (Figure 8.4). The polymer was modeled as a solid permanently fixed to the top side of the substrate, centered across its length as was done during experimentation. Since 20μL of monomer was used, the proper height of the polymer was calculated from the known length and width of the monomer pool. This calculated height, not taking into account curvature due to surface tension, is 0.0165cm.

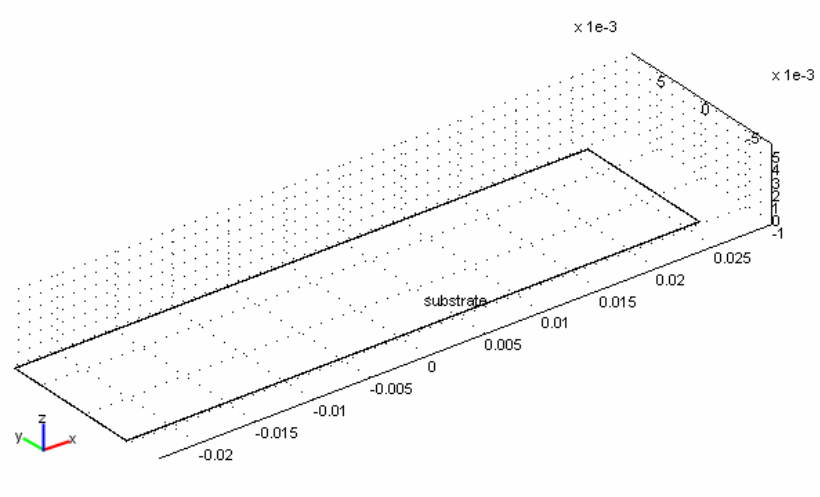

Figure 8.3: 3D substrate geometry as drawn within the drawing program of FemLab.

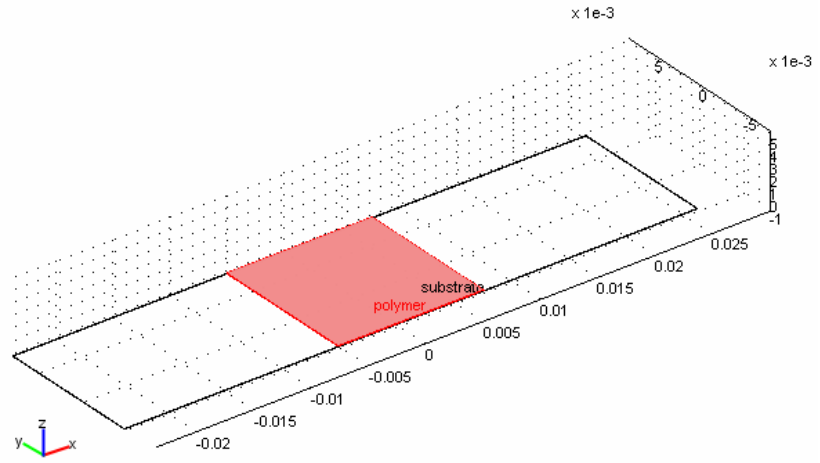

Figure 8.4: 3D substrate/polymer geometry where the substrate and polymer are affixed to one another at their interface.

Figure 8.4 shows the completed drawing of the cantilever beam and polymer coating, but not without some inaccuracies. First, the cantilever is depicted as a flat, rectangular polyhedron, which is not exactly the case in the lab. The actual cantilever beams used are slightly arced upward because they are cut to length from a roll of brass

foil. Second, the coating is not a rectangular polyhedron. In the lab, the monomer (before illumination) and polymer surface (after illumination) is curved due to surface tension. While these inaccuracies are known beforehand, their effects are likely secondary and are ignored for the purpose of creating a model from first principles.

After the geometry was entered, constraints were applied in order for the system to behave according to experimental observations. The leftmost edge of the substrate in Figure 8.4 was held in place, which served to hold the left end of the cantilever down, while the right end was allowed to move freely in 3 dimensions. Constraining the left edge simulated the condition in the lab where one end of the cantilever was fixed in place using a clamp.

Before the geometry could be solved, the model was meshed. Meshed model geometry is depicted in Figure 8.5.

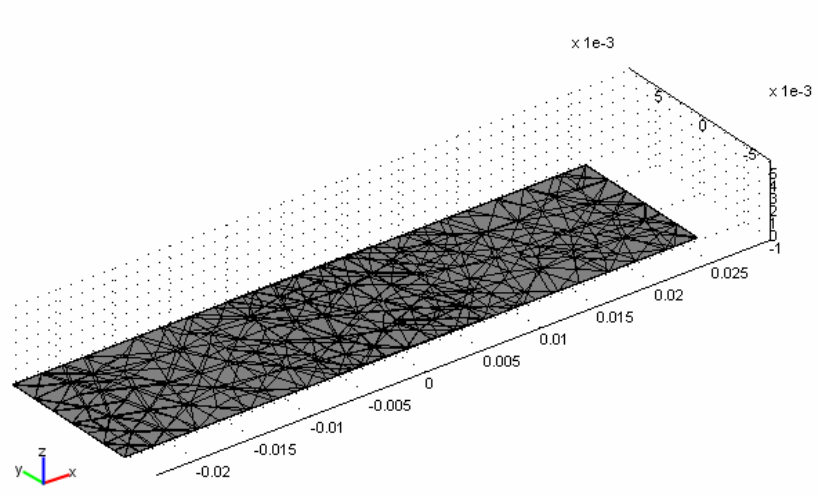

Figure 8.5: Manually meshed 3D cantilever beam structure taking into account the vast difference in the relative size of the z axis with the other two.

FEMLAB assigns a standard mesh size to all portions of a model geometry based on the smallest dimension, which in this case is the z-direction. Because the z-direction

thickness is approximately 1000 times smaller than the x-dimension length, the default mesh number exceeded the maximum allowable number of meshes. Therefore, the meshes in the z-direction were manually altered to be smaller than those in the x and y-directions so that the system of equations could be solved.

After meshing the geometry, the modeling environment was implemented. First, the Structural Mechanics module was loaded into FEMLAB, utilizing a solid, stress-strain transient analysis environment described by Equations 8.1-8.15 Note that a 2D model can similarly be built. The difference between the 2D and 3D models is that there is no y-direction in the model geometry depicted in Figures 8.3, 8.4 and 8.5 for a 2D analysis and that Equations 3—17 simplify into two dimensions.

Figure 8.6: 2D substrate geometry drawn in the drawing package included in the FemLab software.

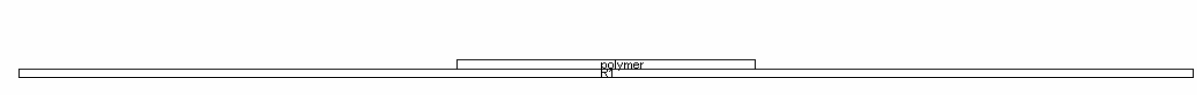

Figure 8.7: 2D substrate/polymer geometry again affixed to one another at their interfacial boundry.

Figure 8.8: Meshed 2D cantilever beam structure. Here there is no need to manually change the mesh size in the two axes.

Structural Mechanics Module

A structural mechanics module was used within the FemLab software in order to realize a deflection and stress in the cantilever substrate. The module solves partial differential equations for strain tensors in order to determine the strain development. The relationship between displacement and strain for the x, y, and z directions are given in the following equations:

$$\varepsilon_x = \frac{\partial u}{\partial x}$$

Eq 8.1:

$$\varepsilon_y = \frac{\partial v}{\partial x}$$

Eq 8.2:

$$\varepsilon_z = \frac{\partial w}{\partial x}$$

Eq 8.3:

$$\varepsilon_{xy} = \frac{\gamma_{xy}}{2} = \frac{1}{2}\left(\frac{\partial u}{\partial y} + \frac{\partial v}{\partial x}\right)$$

Eq 8.4:

$$\varepsilon_{yz} = \frac{\gamma_{yz}}{2} = \frac{1}{2}\left(\frac{\partial v}{\partial z} + \frac{\partial w}{\partial y}\right)$$

Eq 8.5:

$$\varepsilon_{xz} = \frac{\gamma_{xz}}{2} = \frac{1}{2}\left(\frac{\partial u}{\partial z} + \frac{\partial w}{\partial x}\right)$$

Eq 8.6:

Here, *u*, *v* and *w* signify the x, y and z-direction displacement, respectively. ε_x, ε_y and ε_z are the shear strains in the x, y and z-directions. ε_{xy} represents the x-y shear strain tensor, ε_{yz} the y-z shear strain tensor and ε_{xz} the x-z shear strain tensor. γ_{xy} corresponds to the x-y shear strain tensor in engineering form, γ_{yz} the y-z shear strain tensor in engineering form and γ_{xz} the x-z shear strain tensor also in engineering form. Equations 8.1-8.6 form the symmetric strain tensor matrix, ε, which contains the shear stresses in the x, y, and z directions, as well as the strain tensors, xy, yz, and xz.

$$\varepsilon = \begin{bmatrix} \varepsilon_x & \varepsilon_{xy} & \varepsilon_{xz} \\ \varepsilon_{xy} & \varepsilon_y & \varepsilon_{yz} \\ \varepsilon_{xz} & \varepsilon_{yz} & \varepsilon_z \end{bmatrix}$$

Eq 8.7:

The symmetric stress tensor, σ, is defined in Equation 8.8 where, $\tau_{xy} = \tau_{yx}$, $\tau_{xz} = \tau_{zx}$ and $\tau_{yz} = \tau_{zy}$ all via symmetry. σ_x, σ_y and σ_z correspond to the x, y, and z direction normal stress, respectively. τ_{xy} signifies the x-y shear stress while τ_{xz} is the x-z

shear stress and τ_{yz} the y-z shear stress. The stress-strain relationship is then determined as is shown in Equation 8.9 from the cross product of the elasticity matrix, D, and the vector forms of the strain tensor, ε, and the stress tensor, σ, in their respective vector forms.

$$\sigma = \begin{bmatrix} \sigma_x & \tau_{xy} & \tau_{xz} \\ \tau_{xy} & \sigma_y & \tau_{yz} \\ \tau_{xz} & \tau_{yz} & \sigma_z \end{bmatrix}$$

Eq 8.8:

$$\sigma = D \times \varepsilon$$

Eq 8.9:

$$D = \frac{E}{(1+\nu)(1-2\nu)} \begin{bmatrix} 1-\nu & \nu & \nu & 0 & 0 & 0 \\ \nu & 1-\nu & \nu & 0 & 0 & 0 \\ \nu & \nu & 1-\nu & 0 & 0 & 0 \\ 0 & 0 & 0 & \frac{1-2\nu}{2} & 0 & 0 \\ 0 & 0 & 0 & 0 & \frac{1-2\nu}{2} & 0 \\ 0 & 0 & 0 & 0 & 0 & \frac{1-2\nu}{2} \end{bmatrix}$$

Eq 8.10:

ν and E symbolize Poisson's ratio and Young's modulus, respectively in Equation 8.10.

$$\sigma = \begin{bmatrix} \sigma_x \\ \sigma_y \\ \sigma_z \\ \tau_{xy} \\ \tau_{yz} \\ \tau_{xz} \end{bmatrix}$$

Eq 8.11:

$$\varepsilon = \begin{bmatrix} \varepsilon_x \\ \varepsilon_y \\ \varepsilon_z \\ \gamma_{xy} \\ \gamma_{yz} \\ \gamma_{xz} \end{bmatrix}$$

Eq 8.12:

At equilibrium, the 3D forces are determined from Equations 8.13, 8.14 and 8.15.

$$-\frac{\partial \sigma_x}{\partial x} - \frac{\partial \tau_{xy}}{\partial y} - \frac{\partial \tau_{xz}}{\partial z} = F_x$$

Eq 8.13:

$$-\frac{\partial \tau_{xy}}{\partial x} - \frac{\partial \sigma_y}{\partial y} - \frac{\partial \tau_{yz}}{\partial z} = F_y$$

Eq 8.14:

$$-\frac{\partial \tau_{xz}}{\partial x}-\frac{\partial \tau_{yz}}{\partial y}-\frac{\partial \sigma_z}{\partial z}=F_z$$

Eq 8.15:

Here F_x stands for the x-direction volume force, F_y the y-direction volume force and F_z the z-direction volume force. For a two-dimensional model, the governing equations for the Structural Mechanics module in 2-dimensional space are similar to those for a 3D analysis (Equations 8.1-8.15). A 2D model only considers the x and y directions; therefore, the width of the sample is negated for a 2D model and the equations simplify accordingly. Due to symmetry, little error is incurred by using a 2D model to simulate a 3D process, however large gains in computing time due to fewer equations are obtained. Reductions in an order of magnitude are common when simulating a 2D model as opposed to a 3D one.

Structural Mechanics Simulations

The first attempt made to simulate the bending cantilever beam was made by applying forces to the polymer film. By applying these forces, stress was induced in the cantilever beam, which bent in order to accommodate the induced stresses. The forces applied are depicted in Figures 8.9 and 8.10. For the 3D model depicted in Figure 8.9 forces were applied to all sides of the polymer coating while in the 2D model (Figure 8.10) the only sides available to apply forces to were the ends. Effects of this fact were only seen if different forces were applied in the x and y directions in the 3D model.

It turns out that simulating shrinkage stress in this way, although easy, is actually quite representative of actual shrinkage stresses. All forces are transferred from the coating to the substrate in a realistic manner. The physical properties of the system determine the amount of stress in the system.

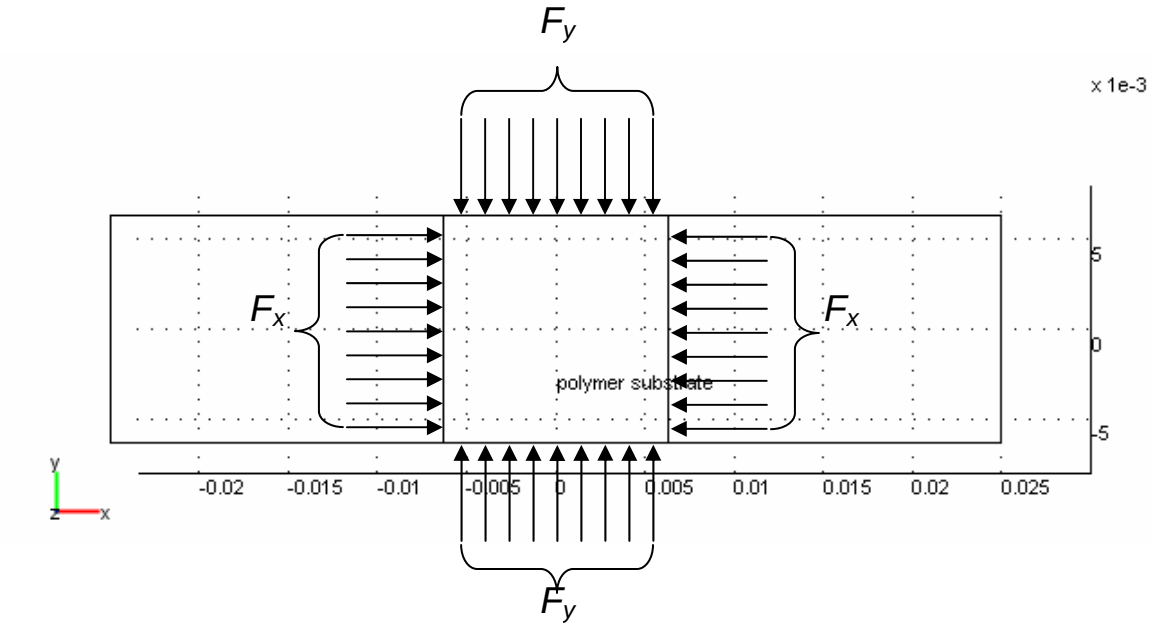

Figure 8.9: Schematic of forces acting on the 3D cantilever beam structure.

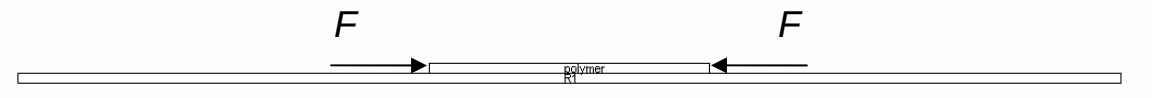

Figure 8.10: Schematic of forces acting on the 2D cantilever beam structure.

As previously stated, the forces acting on the polymer caused the unrestrained side of cantilever beam to deflect vertically. Figures 8.11 and 8.12 show the deflection of the cantilever beam after the model has been solved.

Results and Discussion

Figures 8.11 and 8.12 show what typical model results were and the deformation of the geometry. As expected, the cantilever beam deflects upward as an increasing load

is applied. Figure 8.12 shows a surface plot where the color scheme correlates to the y-direction displacement of the end of the cantilever beam with red being the largest deflection and blue being the least. Figure 8.11 is analogous to Figure 8.12 with the exception that it is an edge displacement plot of the 2D model.

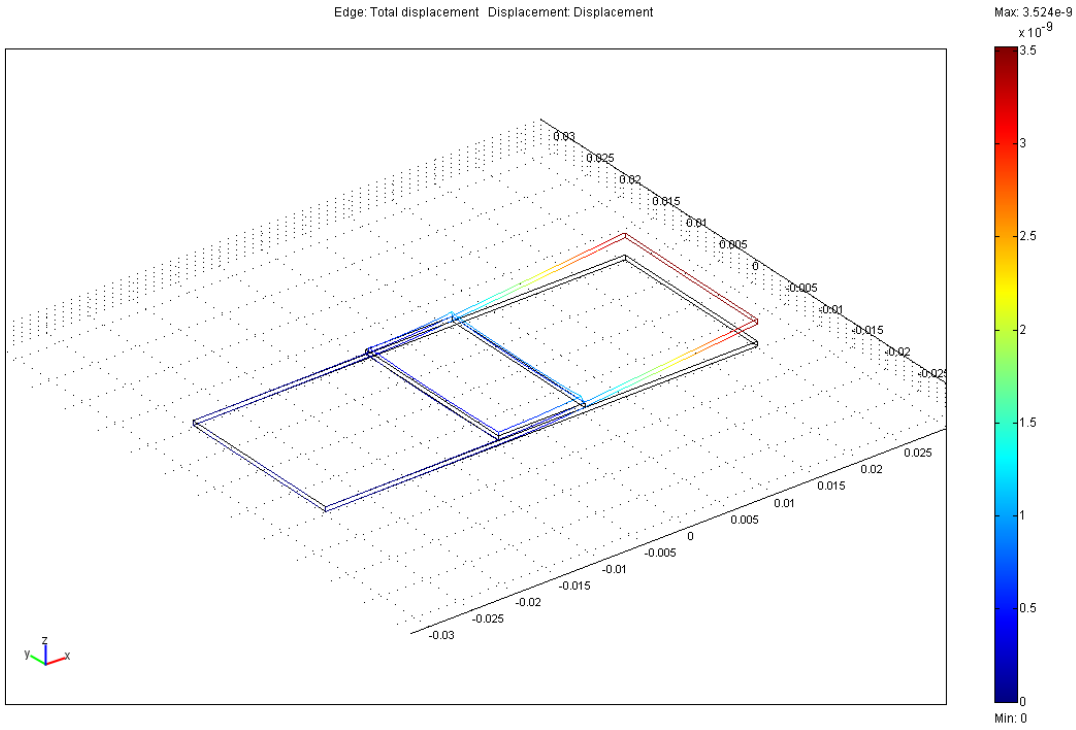

Figure 8.11: Solved 3D cantilever beam model: edge deflection.

Here Equal forces were applied to all sides of the polymer coating acting in the positive and negative directions in the x and y axes. For the 2D model equal forces were applied in the positive and negative direction parallel to the plane of the non-deformed cantilever. In both cases the left most edge of the cantilever had to be restricted from movement in order to correctly model the actual experimental setup used in the laboratory.

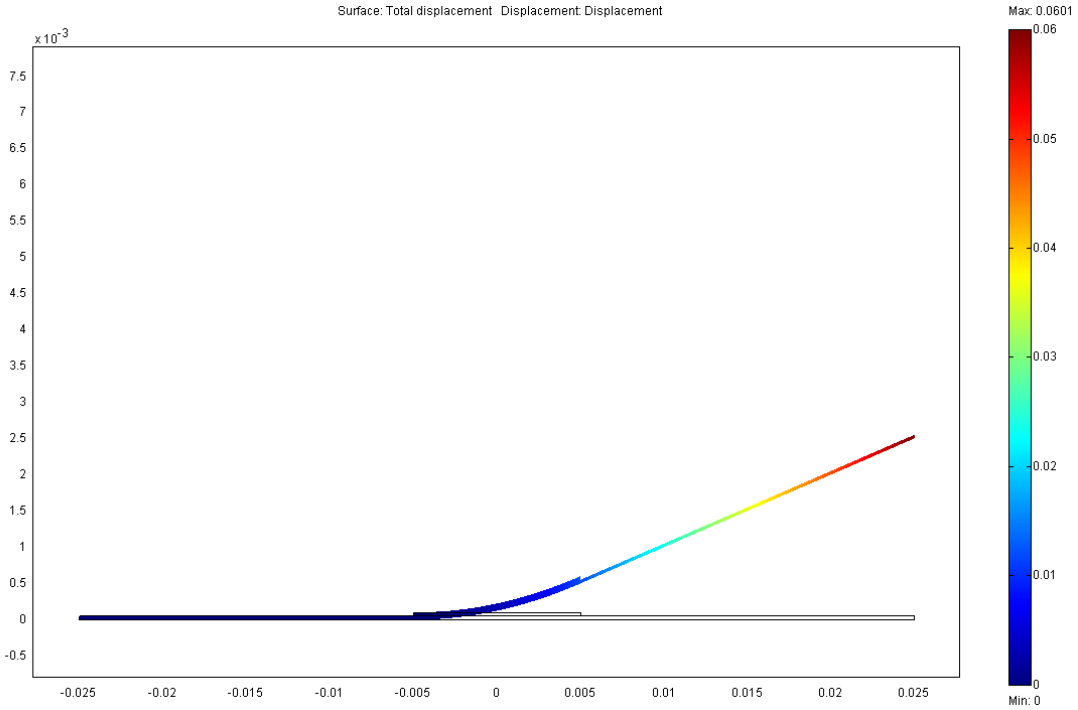

Figure 8.12: Solved 2D cantilever beam model: Displacement.

Figures 8.11 and 8.12 show how the cantilever beam structure deforms as forces are applied to the polymer coating. By varying the forces acting on the polymer, a trend between stress and bend height deflection was determined. The color maps of these figures show the deflection of the cantilever beam, with red and blue representing the highest and lowest deflection, respectively.

Two-Dimensional Structural Mechanics Analysis

In order to develop a correlation between stress and deflection height, a series of increasing forces acting on the polymer was simulated within the Structural Mechanics Module. For two dimensions, the force F, increased following a pattern of $F_i = 1/2\,F,..., F, 2F, 3F,..., 8F$ to produce nine data points. This amount of increase was chosen so that the range of deflections modeled encompassed the entire range of deflections observed in the laboratory of 1.5mm-18mm.

The resulting models shown in Figure 8.13 were obtained.

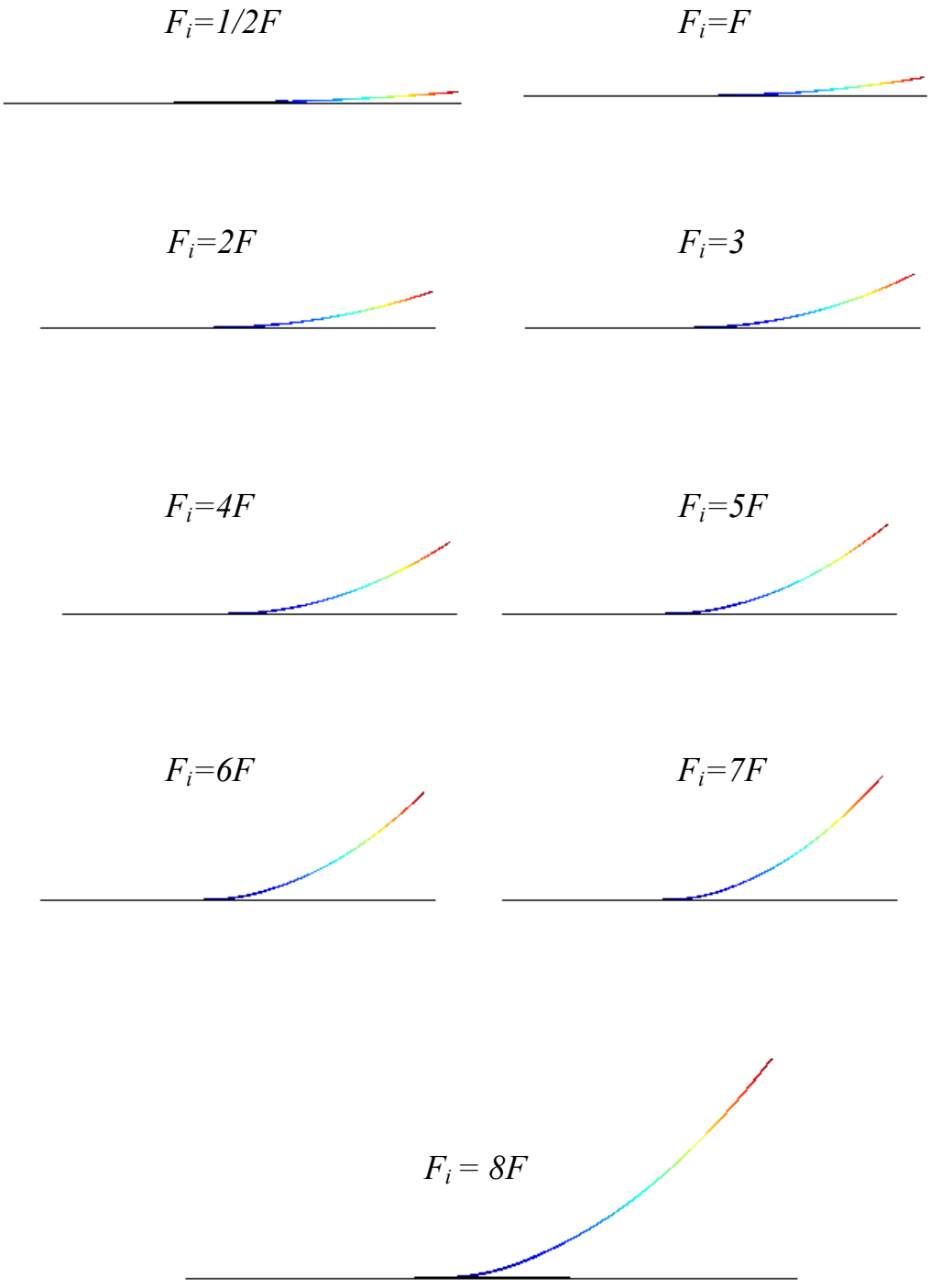

Figure 8.13: 2D varying force simulation results.

Figure 8.13 shows a combination plot of boundary deflection and surface von Mises stress, however the stress is not able to be seen in Figure 8.13. An enlarged plot makes the stress visible to the eye. The colors on the edges correspond to deflection (the right color code) and the colors of the surfaces correspond to the von Mises stress (the left color code).

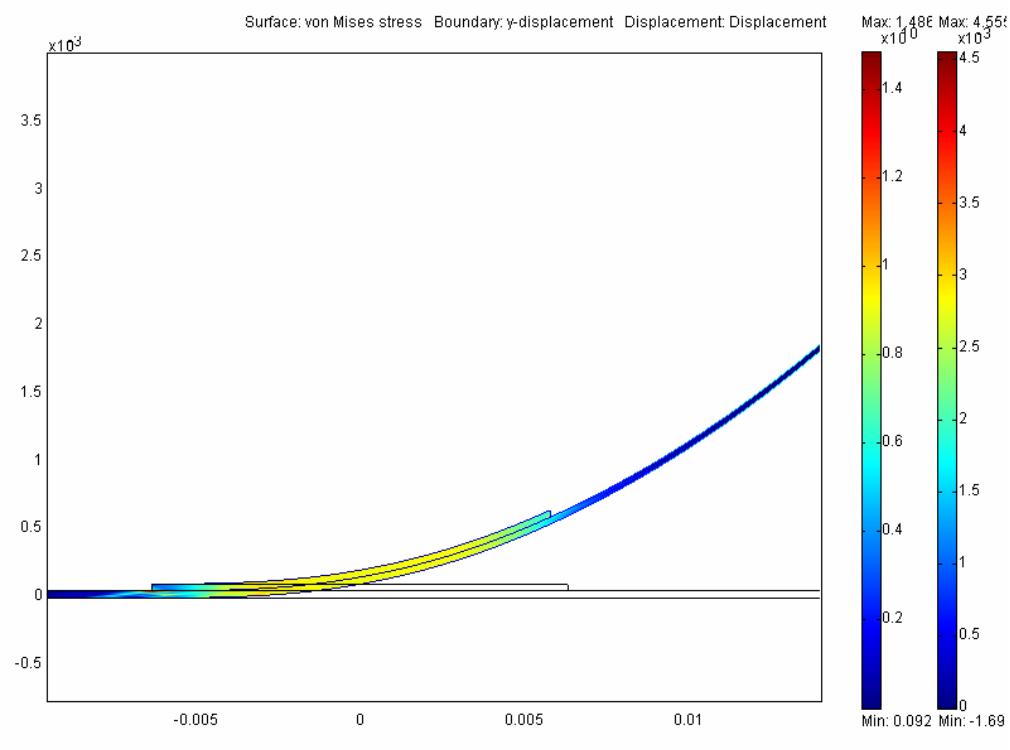

Figure 8.14: 2D solved model enlargement.

A similar plot can also be developed in three dimensions for the 2D model; the y-axis shows the deflection and the z-axis (upwards) shows the von Mises stress which can also be determined using the color scale.

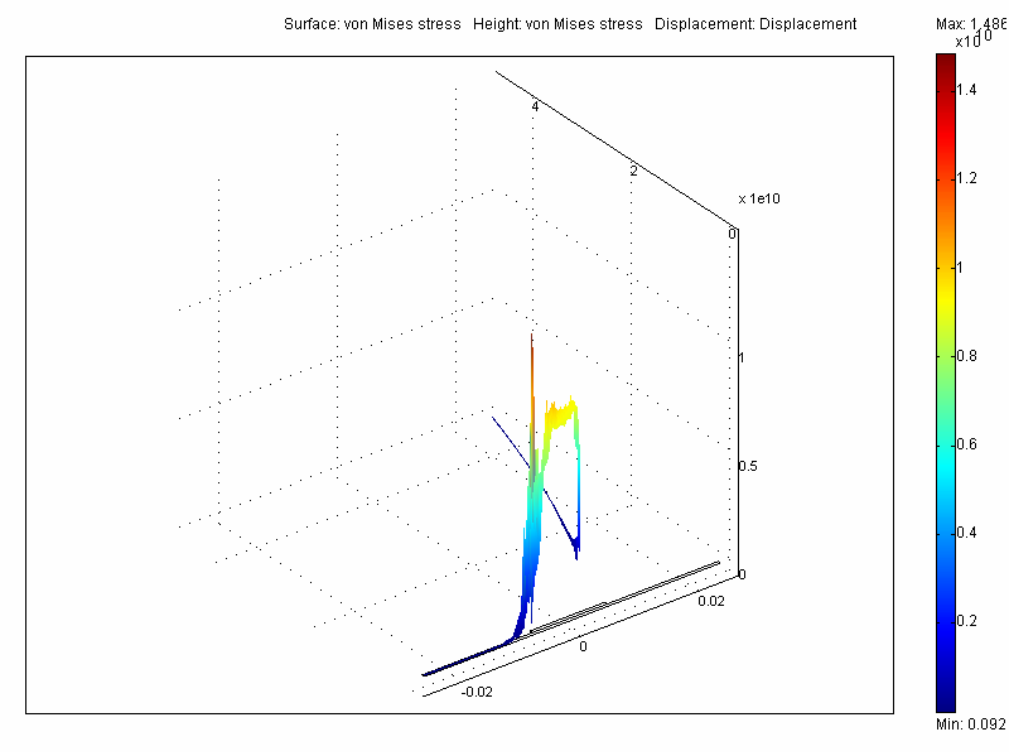

Fig 8.15: 3D contour plot of displacement and von Mises stress for 2D model.

As Figures 8.14 and 8.15 show that the most significant stress buildup on the substrate is the region where the polymer and brass meet. Inspection of Figure 8.15 shows that the maximum stress occurs at the left edge of the polymer. This is expected as the left end of the substrate is constrained from freely deforming, the most stress should occur at the boundary of the polymer nearest the constraint.

With the data from Figure 8.13, a plot of stress versus deflection height was constructed in order to determine the correlation between the height of deflection and the stress imparted on the substrate. Here normalized stress was used which was determined by dividing the stress value for each force applied by the modeled stress value for the maximum deflection seen in a particular set of laboratory experiments.

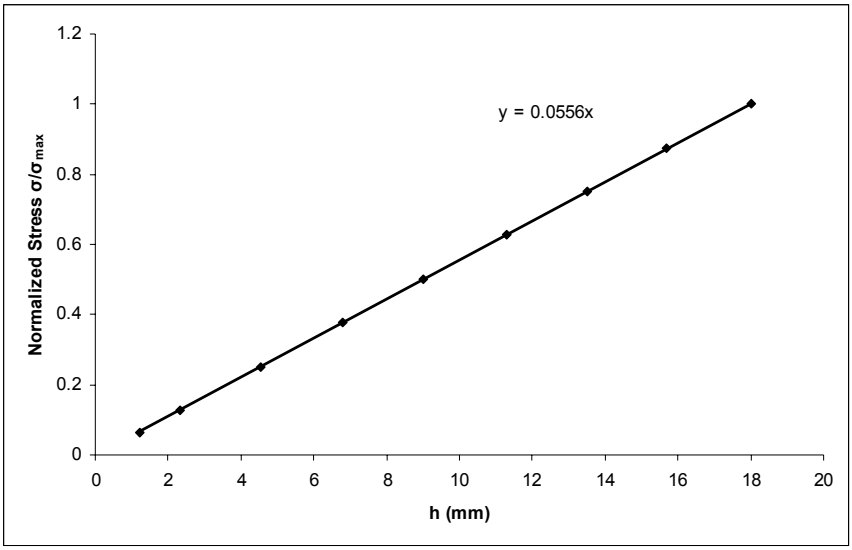

Figure 8.16: Normalized stress versus deflection height, 2D model.

Because the key concept in our experiments is reducing the stress of an otherwise highly stressed and unusable system, normalized stress is plotted to show the percent decrease in stress as the system bends the substrate to a lesser degree due to structured illumination.

Figure 8.16 shows that there is a linear relationship between deflection height of the cantilever beam and the stress induced on the substrate. The relationship is now expressed as:

$$\sigma_{2D} \propto \omega \cdot h$$

Eq 8.16: Stress relationship where ω is 0.0556, σ_{2D} is the induced stress and h is the deflection height.

Three-Dimensional Structural Mechanics Analysis

Similar to the simulations completed for 2D geometries, forces acting on the polymer were varied so that a correlation between stress and cantilever deflection could be constructed. An example of the output, which has von Mises stress plotted on the surface and deflection height plotted on the edges of the geometry, is as follows.

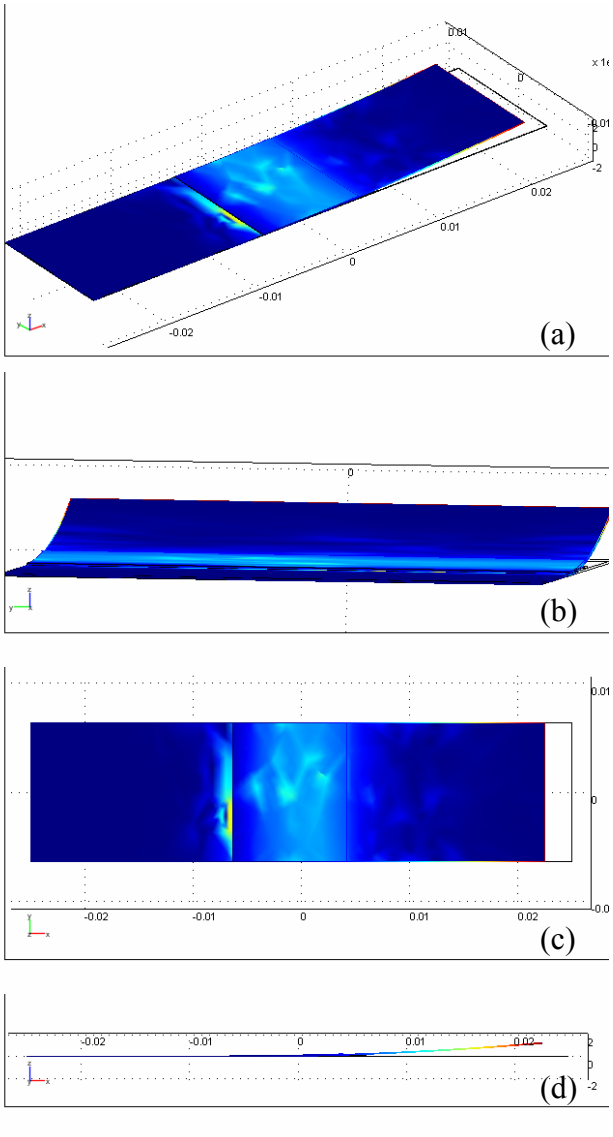

Figure 8.17: 3D solved model showing stress on surfaces and displacement on edges, (a)xyz-plot, (b)yz-projection, (c)xy-projection, (d)xz-projection.

Like the simulations completed in two dimensions, the maximum stress on the substrate occurs at the left edge of the polymer where it meets the substrate. It is not understood why the stress seems to randomly vary across the width (y-direction) of the sample, since the forces are symmetric and opposite. This could likely be due to an error in the meshing of the system.

Due to the highly linear relationship of the 2D model and the first few points of the 3D relationship, only a few simulations were run. The resulting correlation plot showed approximately the same slope as Figure 8.16.

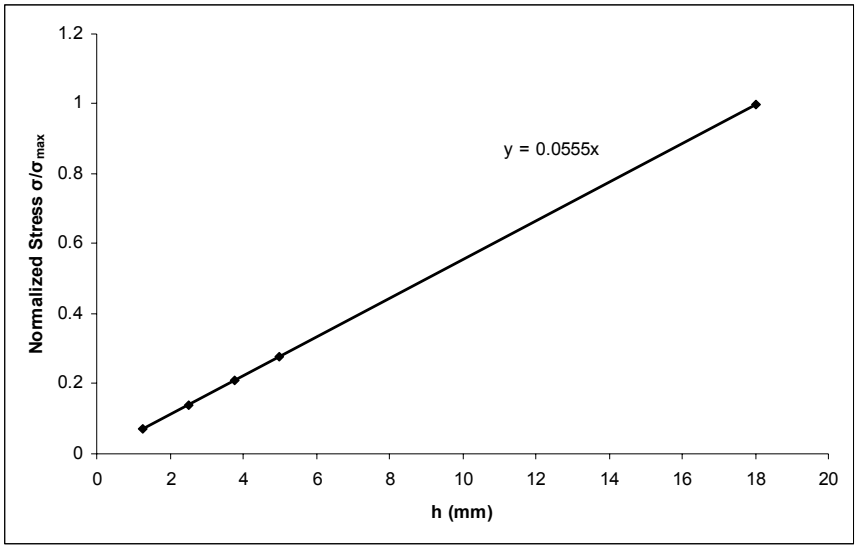

Figure 8.18: Normalized stress versus deflection height, 3D model.

Like the 2D plot, normalized stress is plotted rather than actual stress. Figure 8.18 clearly shows that there is a linear relationship between deflection height of the cantilever beam and the stress induced on the substrate. The relationship is now expressed as is in Equation 8.17.

$$\sigma_{3D} \propto \omega \cdot h$$

Eq 8.17: Stress relationship where ω is 0.0555, σ_{3D} is induced stress, and h is the height of deflection.

Heat Transfer Module

The Heat Transfer module of FEMLAB provided a means for analyzing shrinkage stress as was done with the FlexPDE model by modeling thermal shrinkage of the polymer. When this module is coupled with the Structural Mechanics module, stress due to thermal shrinkage can be determined. The Heat Transfer module can solve for thermal effects due to conductive, convective, as well irradiative thermal effects. For the model being considered, the transient conduction environment was used. In this module, the governing equation for thermal effects is the heat equation:

$$\delta_{ts} \rho C \frac{\partial T}{\partial t} - \nabla \cdot (k \nabla T) = Q$$

Eq 8.18:

Where T denotes the temperature, ρ the density, C the heat capacity, k symbolizes thermal conductivity, Q characterizes a heat source or heat sink and δ_{ts} represents a time-scaling coefficient. If the thermal conductivity is anisotropic (not the same in all directions), then k becomes the thermal conductivity tensor k, which is represented by the matrix in Equation 8.19. k_{xx} represents the x-direction thermal conductivity tensor, k_{yy} represents the y-direction thermal conductivity tensor, k_{zz} represents the z-direction thermal conductivity tensor, k_{xy} represents the x-y thermal

conductivity tenso,r k_{xz} represents the x-z thermal conductivity tensor and k_{yz} represents the y-z thermal conductivity tensor.

$$k = \begin{bmatrix} k_{xx} & k_{xy} & k_{xz} \\ k_{xy} & k_{yy} & k_{yz} \\ k_{xz} & k_{yz} & k_{zz} \end{bmatrix}$$

Eq 8.19:

For a two-dimensional model, the governing equations for the Heat Transfer module in 2-dimensional space are similar to those for a 3D analysis (Equations 18 & 19). A 2D model only considers the x and y directions, therefore the width of the sample is negated for a 2D model and the equations simplify accordingly.

Multiphysics Coupling

In order to use the Structural Mechanics module and the Heat Transfer module simultaneously (i.e. multiphysics), the two environments were coupled. Navier's equation including the thermal effects is:

$$-\nabla \cdot \left(c\nabla u - \alpha T\right) = K$$

Eq 8.20:

Here α is the thermal expansion matrix and K is the volume force while c is the matrix for Young's modulus and Poisson's ratio. The default settings for FEMLAB set the α-matrix set to zero, therefore the two environments are not automatically coupled. By manually adding expressions for the α-matrix, the thermal effect from the Heat

Transfer module was determined in the Structural Mechanics module. The stress, including the effect of heat is:

$$\sigma = \begin{bmatrix} \sigma_x \\ \sigma_y \\ \sigma_z \\ \tau_{xy} \end{bmatrix} - D\left(- \begin{bmatrix} \alpha \\ \alpha \\ \alpha \\ 0 \end{bmatrix} \left(T - T_{ref}\right) \right)$$

Eq 8.21:

In this equation D represents the elasticity matrix. When the reference temperature was then set equal to zero, Equation 21 became:

$$\sigma = \begin{bmatrix} -E\dfrac{\alpha}{(1-2\nu)} \\ -E\dfrac{\alpha}{(1-2\nu)} \\ -E\dfrac{\alpha}{(1-2\nu)} \\ 0 \end{bmatrix} T$$

Eq 8.22:

From the Subdomain Settings in FEMLAB, the above expressions can be entered so that the model incorporates the thermal stress in the structural analysis.

Multiphysics Simulations

The Multiphysics simulations are analogous to the structural simulations previously discussed. In this case, however, a heat is applied to the entire surface of the

polymer, which is assigned a negative thermal expansion coefficient (or, effectively a thermal contraction coefficient). Applying a heat will cause the polymer to shrink while the cantilever beam substrate deforms, and therefore deflects, due to the stresses induced on the substrate. Figures 8.19 and 8.20 depict this for 3D and 2D models, respectively.

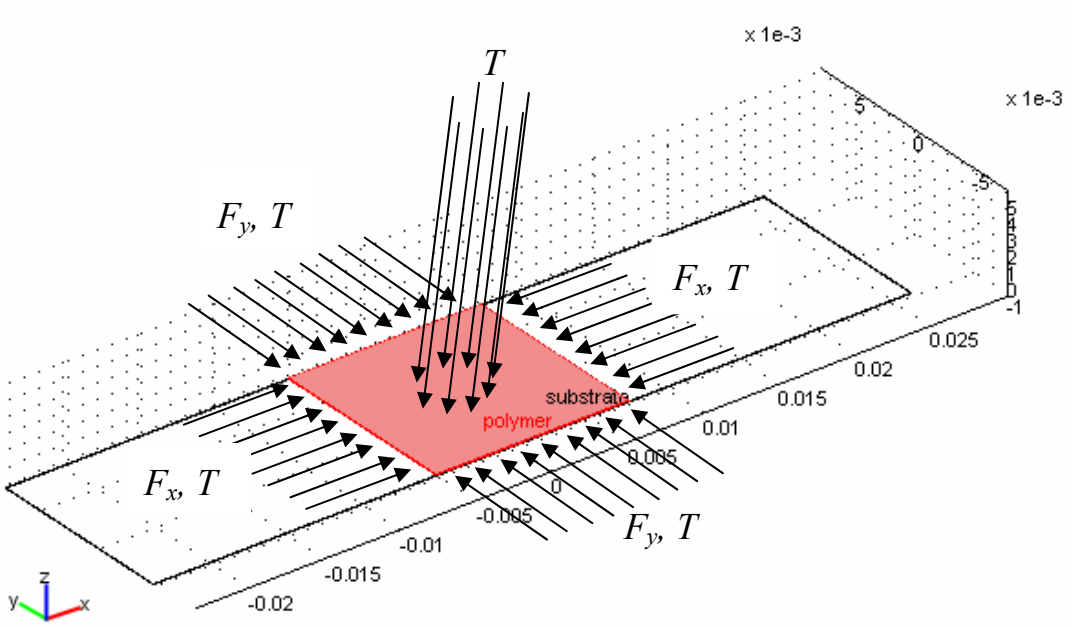

Figure 8.19: Schematic of forces and temperature acting on the 3D cantilever beam structure.

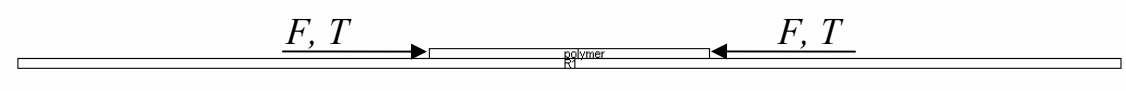

Figure 8.20: Schematic of forces and temperature acting on the 2D cantilever beam structure.

Multiphysics Analysis

Using both the Structural Mechanics Module and Heat Transfer Module, multiphysics analysis was attempted. Simulation times in 3D were inconsistent, varying from one or two minutes to thirty or more minutes. The 2D simulation times were consistent and the results interesting. The multiphysics analysis produced the same results as the Structural Mechanics Module alone. Therefore it was assumed that the application of forces to the edges of the polymer section of the model would suffice in determining stress in the cantilever substrate. Figure 8.21 shows a typical plot obtained for the 2D multiphysics analysis and Figure 8.22 shows a contour plot of displacement.

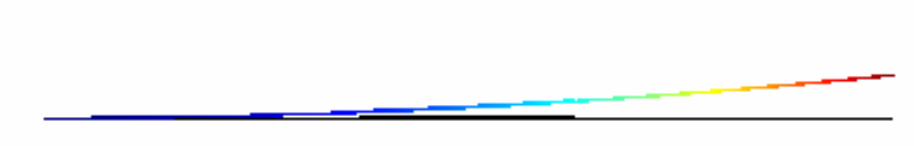

Figure 8.21: 2D model solved with multiphysics.

Comparing Figures 8.21 and 8.22 to Figures 8.13, 8.14, and 8.15, it is apparent that the graphs contain the same information. Figure 8.22 shows that the maximum stress imparted on the substrate occurs at the left edge of the polymer, as does Figure 8.15. From close inspection of Figure 8.21, it appears that the polymer did not shrink when the heat was applied to it. It seems that the multiphysics coupling instead converted the thermal stress into a force acting on a boundary, which is exactly the procedure used in the 2D Structural Mechanics analysis. Although this method of modeling did not work as expected, it proved that at this level of analysis, the coupling of the two environments is not necessary.

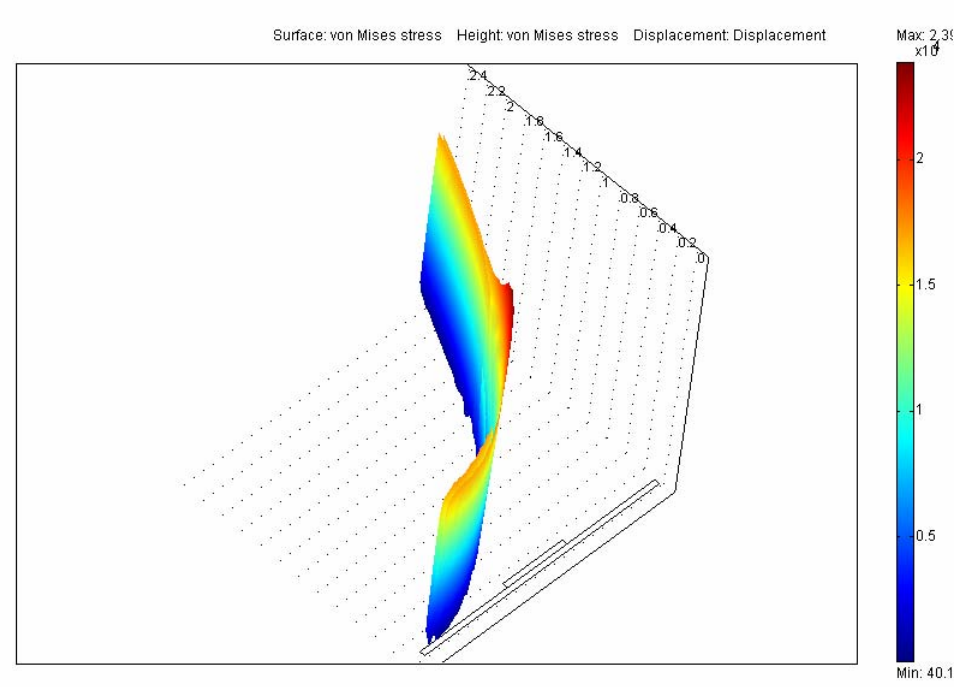

Figure 8.22: 3D contour plot of displacement and von Mises stress for 2D multiphysics model.

MatLab Modeling of Monomer Migration

One-Dimensional Diffusion Model

Monomer/monomer and monomer/polymer diffusion were first determined using a simple one-dimensional diffusion equation given by Fick's second law within MatLab software[85]. In Equation 8.23 D_{AB} is the diffusion coefficient of A into B and c_A is the concentration of component A.

$$\frac{\partial c_A}{\partial t} = D_{AB} \frac{\partial^2 c_A}{\partial x^2}$$

Eq 8.23: One-dimensional diffusion equation

Upon polymerization the diffusion coefficient (D_{AB}) changes dramatically from that of monomer/monomer diffusion shown here to almost no diffusion at all during the time frame of structured illumination as is represented by modeling monomer/polymer diffusion or polymer swelling. The following figure illustrates the best possible scenario attainable with a specified monomer because it is known that the diffusion rate will decrease with conversion of monomer and also here is modeled the diffusion of differing species; meaning monomer A is diffusing to a region completely void of other monomer A.

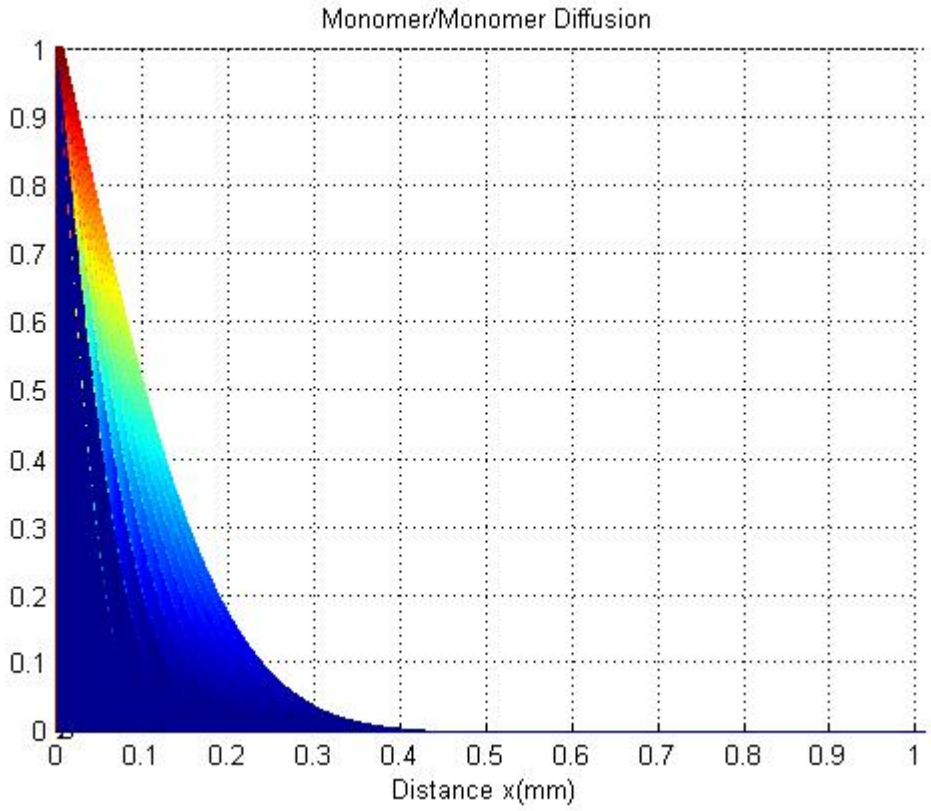

Figure 8.23: Plot showing concentration of one monomer diffusing into another monomer over a period of 10 seconds. Every variation in shade represents 1 second of diffusion.

Because of the vast difference in the diffusion coefficient (D_{AB}) for the case of monomer/monomer diffusion and monomer/polymer diffusion, and the fact that monomer is diffusing to a region with both a combination of like monomer and polymer from that monomer in the structurally illuminated samples, a far more complex model needed to be developed that incorporated a change in the diffusion rate as the polymerization reaction occurred[86].

Dynamic Reaction Diffusion Model

Introduction

In order to better understand the fundamental reasoning for migration of monomer as a result of structured illumination a mathematical model was prepared. This model was adapted from the work done by C.M. Leewis[6, 87, 88]. His work focused on monomer diffusion essential in making polymer gratings for use as optical devices. By modeling our laboratory work, knowledge of the relative importance of key variables in the structured illumination process was established[89]. This fundamental understanding helped in the application of structured illumination for not only stress reduction but also as a method of gloss control

For our system of HDDA and initiator the components which must be tracked and calculated are the concentrations of both the monomer and polymer in the structurally illuminated regions and those masked off in darkness. During subsequent flood cure the model assumes no additional monomer migration occurs. In order to track the changes in monomer and polymer concentrations Flory-Huggins theory is employed. This theory was developed to describe mixtures of polymer and/or solvents. In our case the solvent is the monomer of the polymer that is being formed. It takes into account degree of crosslinking for the polymer system, concentrations of components and swelling to reveal chemical potentials giving rise to migration of monomer. The model assumes constant ambient pressure and constant temperature which are fair assumptions when working

with thin films on metal substrates which will quickly dissipate any heat caused by the exothermic reaction of the system. Also the reactions are being carried out at atmospheric conditions resulting in virtually no change in ambient pressure over the time scale of reaction. The model also assumes a constant total volume of the system which is not the case in a high shrinking monomer such as HDDA. In trying to deal with this shortcoming all attempts yielded little improvement in the model. Despite this fact, the model is very enlightening and helps to portray the important factors in designing a structured illumination system that will either reduce stress or control gloss or both.

Background

With the prior assumptions made the chemical potentials for a time (t) during a reaction in both the structurally illuminated and masked regions are shown in the following two equations.

$$\mu_m^{SI} - \mu_m^0 = kT\left[\ln\left(1-\varphi_p^{SI}\right)+\varphi_p^{SI} - \frac{v_m}{v_p}\varphi_p^{SI} + \chi_{mp}\left(\varphi_p^{SI}\right)^2 v_1 + v_1\frac{n_e}{N_p}\left(\frac{1}{\varphi_p^{SI}} - \frac{\varphi_p^{SI}}{2}\right)\right]$$

Eq 8.24: Equation showing the change in chemical potential in the structurally illuminated region for a step in time.

$$\mu_m^{mask} - \mu_m^0 = 0$$

Eq 8.25: Equation showing the change in chemical potential is equatl to zero for those regions masked off in darkness.

Within these equations μ represents the chemical potential with subscripts m and p signifying a property of the monomer and polymer phases, respectively and

superscripts SI, mask and 0 representing structured illumination region, masked region and initial conditions, respectively for all characters within these equations. φ_p is the volume fraction of polymer while v symbolizes the number of monomer or polymer segments depending on the subscripted character.

$$\mu_m^{SI} - \mu_m^0 = kT\left[\ln\left(1-\varphi_p^{SI}\right)+\varphi_p^{SI}+v_1\frac{n_e}{N_p}\left(\frac{1}{\varphi_p^{SI}}-\frac{\varphi_p^{SI}}{2}\right)\right]$$

Eq 8.26: Chemical potential equation after eliminating terms associated with the ratio of monomer segments to polymer segments and the χ parameter.

$$\frac{n_e}{N_p}=\frac{1}{v_m}\frac{-\ln\left(1-\varphi_p^{SI}\right)-\varphi_p^{SI}}{\left(\frac{1}{\varphi_p^{SI}}-\frac{\varphi_p^{SI}}{2}\right)}$$

Eq 8.27:

For a dynamic reaction diffusion model a more general form of Fick's second law was used and is seen in Equation 8.28

$$\frac{\partial c}{\partial t}=\frac{\partial}{\partial x}\left(\frac{Dc}{kT}\frac{\partial \mu}{\partial x}\right)$$

Eq 8.28: General form of Fick's second law.

Here D symbolizes the diffusion coefficient, k is the Boltzmann's constant, c is the concentration, T the temperature and μ the chemical potential. The diffusion

coefficient was determined as a function of the degree of polymerization as shown in Equation 8.29.

$$\left(\ln\frac{D(\varphi_m)}{D_p}\right)^{-1} = K_1\left(\frac{1}{\varphi_m} + K_2\right)$$

Eq 8.29: Diffusion as a function of degree of polymerization

Here, D_p represents the monomer diffusion coefficient in pure polymer and φ_m the monomer volume fraction, while K_1 and K_2 are positive constants described in free volume theory.

Surface energy was also taken into account with the following relationship. After being relieved of some of the monomer in the masked regions the remaining monomer will redistribute itself in a manor that depends on surface tension. This redistribution will have effects on how much monomer will be available for migration to the structurally illuminated regions.

$$\mu_s = -\kappa\gamma v = -\gamma v\frac{\frac{\partial^2 h}{\partial x^2}}{\left(1+\left(\frac{\partial h}{\partial x}\right)^2\right)^{3/2}}$$

Eq 8.30: Chemical potential due to surface energy

The surface energy is symbolized by γ, while molecular volume of the migrating species is v, the surface curvature is κ and h represents the height.

Modeling Procedure

Using the aforementioned equations, the procedure for a dynamic reaction diffusion model starts with determining conversion of monomer to polymer in the structurally illuminated regions, considering the reaction rates, and then determining the new volumes of the monomer and polymer in the structurally illuminated regions during a time (Δt) by the following equations.

$$V_m(x,t+\Delta t) = V_m(x,t) - RV_m(x,t)\Delta t$$

Eq 8.31:

$$V_p(x,t+\Delta t) = V_p(x,t) + RV_m(x,t)\Delta t$$

Eq 8.32:

Next the cross-linking density is calculated in the structurally illuminated regions.

$$n_e(x,t) = \varphi_p(x,t)V(x,t)\frac{1}{v_m v_{segment}}\frac{-\ln\left(1-\varphi_p^*(x,t)\right)-\varphi_p^*(x,t)}{\left(\frac{1}{\varphi_p^*(x,t)}-\frac{\varphi_p^*(x,t)}{2}\right)}$$

Eq 8.33:

Where $\varphi_p^*(x,t)$ is defined in Equation 8.34.

$$\varphi_p^*(x,t) = \varphi_p(x,t)\frac{V(x,t)}{V_{initial}}$$

Eq 8.34:

Then the chemical potential is determined in both the structurally illuminated regions (Eq. 8.35) and the masked regions (Eq. 8.36).

$$\mu_m(x,t) - \mu_m^0 = kT\left[\ln\varphi_m(x,t) + 1 - \varphi_m(x,t) + v_m\frac{n_e(x,t)v_{segment}}{V(x,t)\varphi_p(x,t)}\left(\frac{1}{\varphi_p(x,t)} - \frac{\varphi_p(x,t)}{2}\right)\right]$$

Eq 8.35:

$$\mu_m(x,t) - \mu_m^0 = kT\left[\ln\varphi_m(x,t) + 1 - \varphi_m(x,t)\right]$$

Eq 8.36:

Next the diffusion coefficient is determined using the volume fraction of polymer produced by the reaction.

$$D(x,t) = D(0)\exp\left(-\frac{1}{K_1(1+K_2)}\right)\exp\left(\frac{1}{K_1\left(\frac{1}{1-\varphi_p(x,t)} + K_2\right)}\right)$$

Eq 8.37:

Knowing the diffusion coefficient and chemical potentials the new volumes of monomer and polymer in all regions are then calculated with the following equation

$$V_m(x,t+\Delta t)=\left\{V_m(x,t)+\Delta t\left(\begin{array}{l}\dfrac{D(x,t)V_m(x,t)}{kT(\Delta x)^2}\left[\mu(x-1,t)-2\mu(x,t)+\mu(x+1,t)\right]+\\ +\dfrac{1}{2}\dfrac{D(x-1,t)V_m(x-1,t)}{kT\Delta x}\left[\mu(x-1,t)-\mu(x,t)\right]+\\ +\dfrac{1}{2}\dfrac{D(x+1,t)V_m(x+1,t)}{kT\Delta x}\left[\mu(x+1,t)-\mu(x,t)\right]\end{array}\right)\right\}$$

Eq 8.38:

The surface chemical potential is then calculated with Equation 8.39 and used in determining a volume change associated with diffusion due to surface chemical potential as illustrated in Equation 8.40.

$$\mu_s(x,t)=-\gamma v_{segment}\left[\frac{\dfrac{1}{(\Delta x)^2}\left[h(x-1,t)-2h(x,t)+h(x+1,t)\right]}{\left(1+\left(\dfrac{1}{\Delta x}\left[h(x+1,t)-h(x-1,t)\right]\right)^2\right)^{3/2}}\right]$$

Eq 8.39:

The volume change leads to the surface deformations seen as bumps on the final cured polymer coating. This process is then repeated by again initiating a reaction for a time Δt and recalculating all the parameters and new volumes associated with the change due to reaction[6].

$$V_m(x,t+\Delta t)=\left\{V_m(x,t)+\Delta t\left(\begin{array}{l}\dfrac{D(x,t)V_m(x,t)}{kT(\Delta x)^2}\left[\mu_s(x-1,t)-2\mu_s(x,t)+\mu_s(x+1,t)\right]+\\ +\dfrac{1}{2}\dfrac{D(x-1,t)V_m(x-1,t)}{kT\Delta x}\left[\mu_s(x-1,t)-\mu_s(x,t)\right]+\\ +\dfrac{1}{2}\dfrac{D(x+1,t)V_m(x+1,t)}{kT\Delta x}\left[\mu_s(x+1,t)-\mu_s(x,t)\right]\end{array}\right)\right\}$$

Eq 8.40:

Modeling Results and Discussion

By inputting parameters for the structural illumination experiments into the model results were obtained and will be studied here. Some of the parameters which are system specific include: reaction rate, diffusion coefficient, sample thickness, mask feature size, surface energy and system specific constants[3, 89, 90]. By specifying constants and parameters indicative to the HDDA system results were obtained and varying those parameters gave a general idea of the relative importance of each.

As the thickness of the system was increased so to did the vertical size of the surface features for a constant mask feature size. However, the ratio of vertical size of the feature to thickness of the system decreased slightly. This is shown in the following figure. Within the graphs in Figure 8.24 the abscissa is the position, in μm, with respect to the mask features and the ordinate is the ratio of the height after polymerization to the original height before any reaction took place. These results are all associated with the same illumination protocol including line width (10μm) and spacing (μm). All other factors and input parameters such as reaction rate, diffusivity and surface tension forces are also held constant.

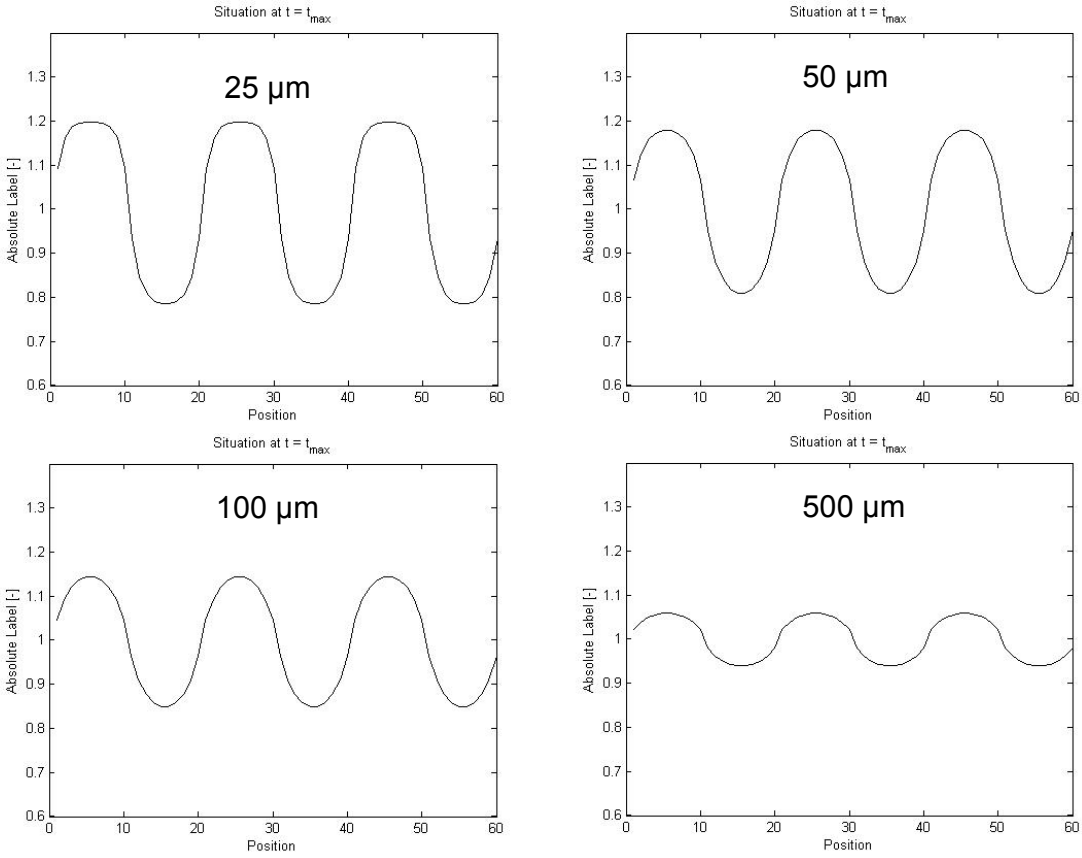

Figure 8.24: Model output showing the relative vertical size of the feature with respect to the overall thickness of the sample to be decreasing.

The increase in vertical surface feature size with an increase in thickness is expected because there is more available monomer for migration. The decrease in ratio of feature height to sample thickness is likely due to surface energy causing a tendency to reduce curvature.

Also studied was the effect of diffusion on the surface characteristics. In Figure 8.25 the y-axis is the height of the polymer surface in meters$X10^{-5}$ giving an average thickness of 50 µm. As is evident in Figure 8.25 the lower the diffusivity the less monomer will migrate thereby affecting the surface to a lesser extent.

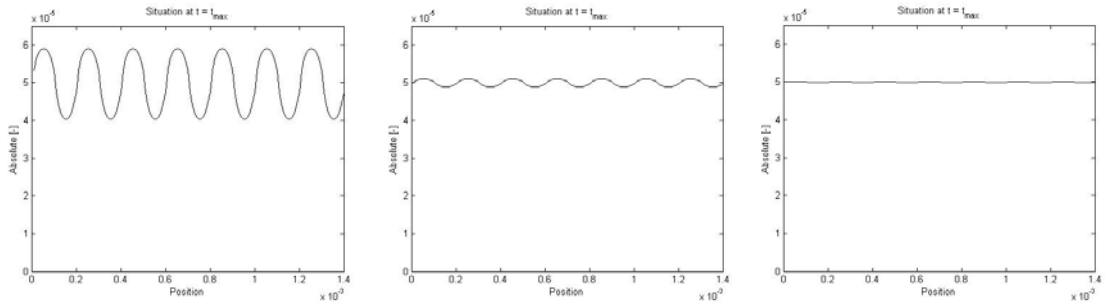

Figure 8.25: Decreasing monomer diffusivity from left to right (2 orders of magnitude) and the resulting profile for a 50µm initial sample thickness.

One important consideration for stress relief was the idea of a mask feature being too large for monomer migration to occur across the feature therefore giving less shrinkage stress reduction. This idea of a feature being too large is represented in the following figure where an increase in mask feature is shown with a resulting profile. The central regions for both the structurally illuminated and masked regions show little change in height. We know that in the masked regions flow would occur much more readily than has been simulated, leaving a meniscus shape showing that the model is somewhat inaccurate, however we have seen this "devil horn-shaped" profile in the structurally illuminated region in profilometry experiments.

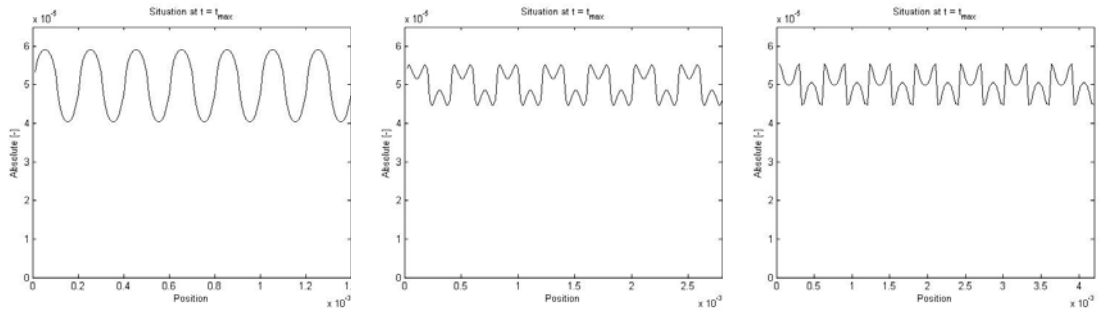

Figure 8.26: Increasing mask line and spacing thickness from 0.2 – 0.6 mm from left to right for the simulated system and the resulting profile.

Another key concept in both relieving shrinkage stress and reducing gloss is the idea of monomer migrating in the time of the reaction. Below is shown how increasing the reaction rate by an order of magnitude decreases the time available for migration to occur and ultimately leaves a flattened surface profile.

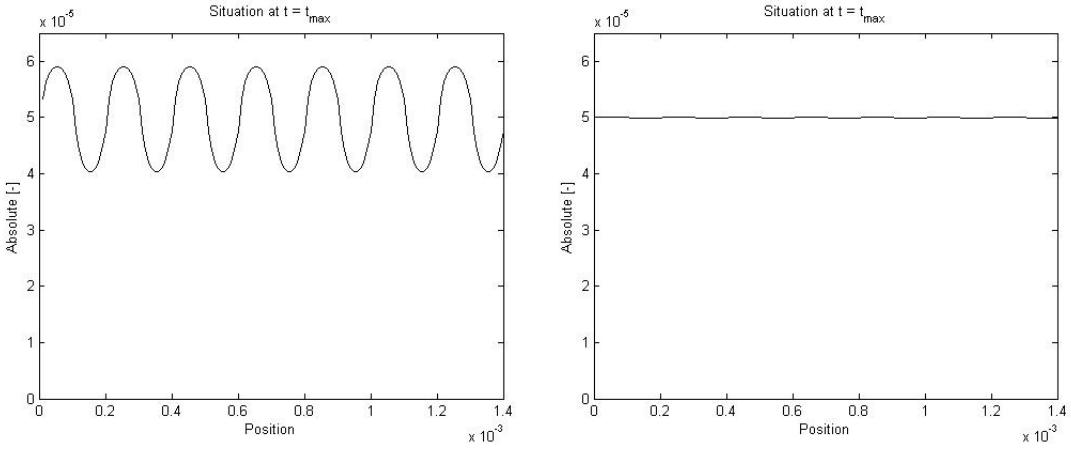

Figure 8.27: Increase in reaction rate by an order of magnitude resulting in a flattened profile.

All previous results are those of a non-cross-linking system because one substantial shortcoming of the model was that when a cross-linking system was modeled all migration ceased. This would only occur in reality if the system cross-linked so fast that diffusion could not occur before an impenetrable network was set up. In all likelyhood this is not the case and considerations for cross-linking had to be incorporated into the model. A cross-linking factor was introduced in order to initiate cross-linking immediately, thereby quickly cutting off diffusion, or simulate cross-linking occurring at a later time in the reaction. Figure 8.27 shows how changing the cross-linking factor effects the percent of cross-linking that occurs. The value of one on the cross-linking axis represents a system which is completely cross-linked and no longer allows for

monomer diffusion. A value of zero does not impede the migration of monomer above and beyond what is already modeled due to viscosity, surface tension and diffusional factors.

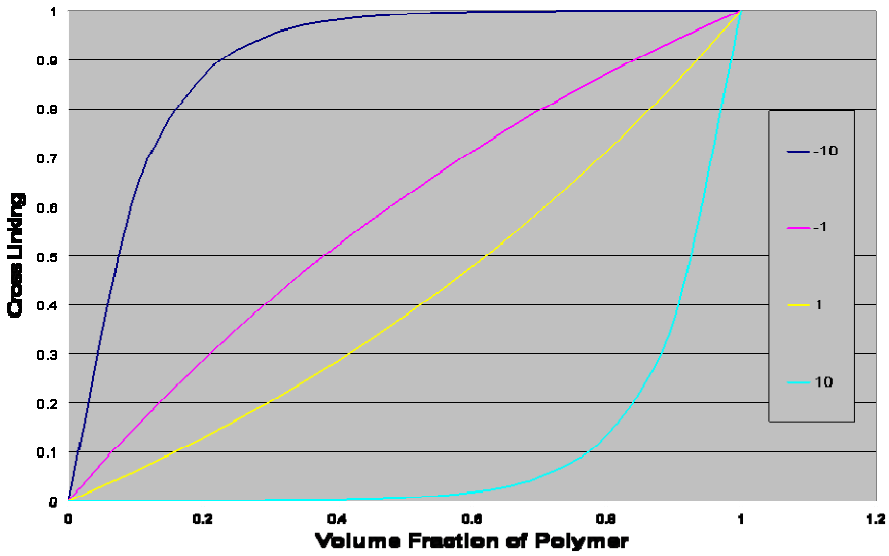

Figure 8.28: Plot showing the Cross-Linking variable as a function of volume fraction of polymer for different Cross-Linking Factors (CLF).

Figure 8.28 shows that by changing the CLF from -10 to +10 a system can be modeled that cross-links quickly or one that cross-links only when the polymerization reaction is nearly complete. By varying the CLF expected changes in the surface profile are modeled. The more rapidly cross-linking occurs, the less monomer migration occurs thereby creating a flatter surface profile as seen in Figure 8.29. This fact along with the other process variables may be used to tailor systems which have a relatively smooth surface or ones that are micro-rough leading to reduction in gloss of an otherwise shiny surface when flood illuminating the system as is standard practice.

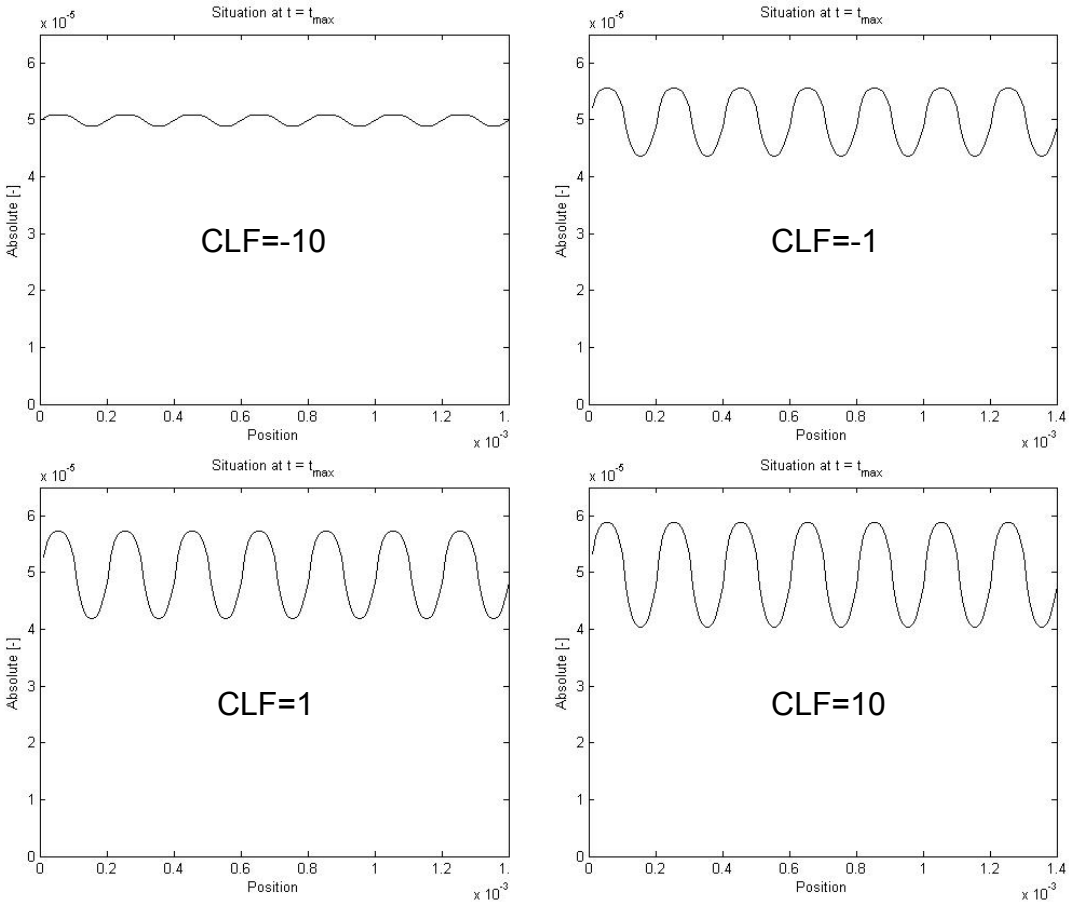

Figure 8.29: Variations in the Cross-Linking Factor (CLF) and the resulting surface profile of the simulation showing that delaying the decrease in monomer diffusion due to cross-linking gives larger surface features.

Another shortcoming of the model, which is not apparent when looking at the output profiles, is that the reaction rate was input as a constant. Photopolymer reaction rates generally increase sharply to a maximum then decrease and tail off towards final cure. This inaccuracy was dealt with by using DSC plots of reaction rate over time and fitting them with a high order polynomial in order to more exactly represent reaction diffusion.

This model only represents the monomer migration due to reaction setting up a concentration gradient leading to a difference in chemical potential across the system. It

does not address the fact that shrinkage is occurring and the possibility of stress playing an important role in flow of monomer.

Conclusion

With all the modeling that was done within the timeframe of this contribution a far better understanding of deformation, stress and monomer migration was developed. Although much more work could be done on modeling polymerization shrinkage stress and structurally illuminated systems, what was done contributed greatly to the understanding of most every facet of this work.

CHAPTER 9: CONCLUSIONS AND RECOMMENDATIONS

Obtained Research Objectives

Within this contribution the concept of combating the common problem of polymerization shrinkage stress, through the use of a processing method termed structured illumination, has been addressed. In the example system, structured illumination was shown to be effective in eliminating over 90% of the polymerization shrinkage stress seen the conventionally cured system without compromising conversion. The understanding of stress relief was pursued and conclusions of which are to follow. Structured illumination was also studied as a method to reduce or control gloss in otherwise high gloss coating systems. Again common acrylate coatings were studied including HDDA and a Di-epoxy Acrylate. Results showed that by using masks with various feature sizes, structured illumination could be used to create a coating with gloss ranging from extremely high gloss systems, obtained via conventional photopolymerization methods to low gloss systems generally only attainable through the use of additives. This method was shown not to rely on the use of additives or a change in the chemical makeup of the system. Finally, mathematical modeling was effectively used to assist in the understanding of monomer migration and its role in both stress relief and gloss control for structurally illuminated samples.

Conclusions and Recommendations Supported by Research Experience

Monomer migration is believed to be the reason for both stress relief and gloss control in structurally illuminated photopolymerizable coatings. It is brought about from both diffusion, setup by a concentration gradient and a change in chemical potential across the volume of the coating, and monomer microflow in response to the shrinking polymer. Each is likely to play a varying role depending on the system being studied.

For structured illumination as a method of stress relief the pattern chosen has a great impact on the directionality of stress relief. Feature size of the pattern also plays an important role in determining the extent of stress relief. A pattern that relieves stress in two dimensions is often preferred; however obtaining stress reduction in one dimension is far simpler. The ratio of feature sizes of structurally illuminated to masked regions is important in that there must be enough monomer present in the masked regions to maximally relieve stress. Also the masked regions should not be so large that during the flood cure step a significant amount of stress is realized. The size scale of these features is also important. The size must be such that monomer migration can occur to an extent that the entire volume is impacted. For fast reacting, very immobile monomers this size scale is smaller than for slower reacting more mobile monomers.

Many variables affect the outcome of stress relief when using structured illumination. The ability of the monomer to migrate in response to the polymerization shrinkage stress is a key concept. Factors which affect this ability ultimately affect stress relief. The viscosity of the system both before and during reaction is important to monomer migration. Viscosity is a function of many factors including the size of the monomer molecules and any non-covalent bonding which may occur between molecules. Molecular entanglement can also play a role. Also, light intensity can change the reaction rate which affects the migration of monomer leading to differences in measured stress. Reaction rate determines not only the change in viscosity of the system but also affects the time scale from migration to occur.

For structured illumination as a method to control gloss, the monomer migration and subsequent distortion of the surface must be on a size scale such that light is diffusely reflected. This means that sufficient deformation must occur in a short length across the surface of the sample. Again, reactivity, mobility (diffusivity, viscosity), light intensity, surface energy, thickness and cross-linking ability all play important roles in the migration of monomer.

The research presented within this contribution is not intended to encompass all possibilities for structured illumination as a processing technique to control photopolymerized coating characteristics. In fact it is recommended that further studies be done with industrially significant systems. Although structured illumination as a method to control gloss has been studied and proven successful, further implementation into a continuous process would verify industrial significance.

Application to other less common photopolymerized systems may also prove beneficial. Cationic systems, with long lived active centers, may provide a means of structurally illuminating a photopolymerized system to enhance physical properties without the need for a flood cure step. This would provide unique processing advantages, requiring but one illumination step to see changes in properties depending upon the pattern of illumination.

Various types of illumination sources could be studies which include light emitting diodes (LEDs), Lasers and flash lamps. The use of LEDs has become an important topic in the photopolymerization industry due to their low energy input. Using an array of LEDs may prove cost effective in both production costs and initial capital investments. The array of LEDs could be designed to impart varying light intensities across the surface of a coating negating the uses of conventional masks. Lasers could also be used to mimic line patterns on the surface of a web process. This would allow for all the light energy to be used instead of masking it off and potentially wasting the light. Flash lamps in conjunction with stationary masks could be used to provide two dimensional patterning on the surface of a continuous process. Timing of the flashes with the speed of the process would be critical.

More specific properties of coated products could be addressed such as the coating of a fiber to allow for lower friction during bundling[91] or the micro-roughening the surface of a plastic sheet for reduced glare in display applications. Also wear and

weathering characteristics of various coatings using structured illumination as a processing method could be examined.

REFERENCES

1. Roth JD, *United States Patent 5,889,084*. 1999.

2. Cox L, *Ultraviolet and Electron Beam (UV/EB) Cured Coatings, Inks and Adhesives*. 2001, Clean Air Technology Center, EPA.

3. van der Zande BMI, Steenbakkers J, Lub J, Leewis CM, and Broer DJ, *Mass transport phenomena during lithographic polymerization of nematic monomers monitored with interferometry.* Journal of Applied Physics, 2005. **97**(12): p. 123519-8.

4. Trout TJ, Schmieg JJ, Gambogi WJ, and Weber AM, *Optical Photopolymers: Design and Applications.* Advanced Materials, 1998. **10**(15): p. 1219-1224.

5. Gambogi Jr WJ, Weber AM, and Trout TJ. *Advances and applications of DuPont holographic photopolymers*. in *Holographic Imaging and Materials*. 1994. Quebec City, Canada: SPIE.

6. Leewis CM, *Formation of Mesoscopic Polymer Structures for Optical Devices: A Nuclear Microprobe Study*. 2003, Technical University Eindhoven: Eindhoven, The Netherlands. p. 166.

7. Stansbury JW and Ge J, *Photopolymerization Shrinkage and Stress in Resins and Composites.* RadTech Report, 2003. **May/June 2003**: p. 56-62.

8. Dauvillier BS, Aarnts MP, and Feilzer AJ, *Modeling of the viscoelastic behavior of dental light-activated resin composites during curing.* Dental Materials, 2003. **19**(4): p. 277-285.

9. Inc. PS, *FlexPDE User Guide: Version 4.2*. 2004: Fremont, CA.

10. Kenning NL, *Spatial and Temporal Evolution of the Photoinitiation Rate in Thick Polymer Systems*, in *Chemical and Biochemical Engineering*. 2006, University of Iowa: Iowa City. p. 147.

11. Baran R, *Nail Cosmetics: Allergies and Irritations.* American Journal of Clinical Dermatology, 2002. **3**: p. 547-555.

12. Rich P, *Nail cosmetics and camouflaging techniques.* Dermatologic Therapy, 2001. **14**(3): p. 228-236.

13. NICHIMA YUKITOMO US, *Japan Patent 2005-068280*. 2005.

14. TOSHIO M, *Japan Patent 11-172178*. 1999.

15. TOSHIO M, *Japan Patent 11-172179*. 1999.

16. Wiedemann B, Dusel KH, and Eschl J, *Investigation into the Influence of Material and Process on Part Distortion.* Rapid Prototyping Journal, 1995. **1**(3): p. 17-22.

17. Luan B, Liu XY, Nagata J, and Cheong W-J, *Residual stress analysis--an important consideration for coating of stereolithography polymers.* Surface and Coatings Technology, 2005. **192**(2-3): p. 323-330.

18. Perry AJ, Sue JA, and Martin PJ, *Practical measurement of the residual stress in coatings.* Surface and Coatings Technology, 1996. **81**(1): p. 17-28.

19. Tyler D, *Mechanistic Aspects of the Effects of Stress on the Rates of Photochemical Degradation Reactions in Polymers.* Journal of Macromolecular Science, Part C: Polymer Reviews, 2004. **44**(4): p. 351-388.

20. Lewis LN and Katsamberis D, *Ultraviolet-curable, abrasion-resistant, and weatherable coatings with improved adhesion.* Journal of Applied Polymer Science, 1991. **42**(6): p. 1551-1556.

21. de Gee AJ, Davidson CL, Smith A, *A modified dilatometer for continuous recording of volumetric polymerization shrinkage of composite restorative materials.* J Dent., 1981. **9**(1): p. 36-42.

22. de Gee AJ, Feilzer AJ, Davidson CL, *True linear polymerization shrinkage of unfilled resins and composites determined with a linometer.* Dent Mater., 1993. **9**(1): p. 11-4.

23. Feilzer AJ, Dooren LH, de Gee AJ, Davidson CL, *Influence of light intensity on polymerization shrinkage and integrity of restoration-cavity interface.* Eur J Oral Sci., 1995. **103**(5): p. 322-6.

24. Lim BS, Ferracane JL, Sakaguchi RL, and Condon JR, *Reduction of polymerization contraction stress for dental composites by two-step light-activation.* Dental Materials, 2002. **18**(6): p. 436-444.

25. Stansbury J, Trujillo L, Lu, Ding, Lin, and Ge, *Conversion-dependent shrinkage stress and strain in dental resins and composites.* Dental Materials, 2005. **21**(1): p. 56-67.

26. D6991-05, *Standard Test Method for Measurement of Internal Stresses in Organic Coatings by Cantilever (Beam) Method.* ASTM International.

27. Hwang DK, Moon JH, Shul YG, Jung KT, Kim DH, and Lee DW, *Scratch Resistant and Transparent UV-Protective Coating on Polycarbonate.* Journal of Sol-Gel Science and Technology, 2003. **V26**(1): p. 783-787.

28. Bongiovanni R, Montefusco F, Priola A, Macchioni N, Lazzeri S, Sozzi L, and Ameduri B, *High performance UV-cured coatings for wood protection.* Progress in Organic Coatings, 2002. **45**: p. 359-363.

29. Ha C-S, Jung S-J, Kim E-S, Kim W-S, Lee S-J, Cho W-J, *Properties of UV-curable polyurethane acrylates using nonyellowing polyisocyanate for floor coating.* Journal of Applied Polymer Science, 1996. **62**(7): p. 1011-1021.

30. Fried JR, *Polymer Science and Technology*. 1995, Upper Saddle River, NJ: Prentice Hall PTR.

31. Pappas SP, *UV Curing: Science & Technology*. Vol. Two. 1985, Norwalk, CT: Technology Marketing Corporation.

32. Belfield KD and Crivello JV, *Photoinitiated Polymerization*. ACS Symposium Series 847, ed. ACS. 2003, Washington, DC: American Chemical Society. 565.

33. Roper TM, Lee TY, Guymon CA, and Hoyle CE, *In Situ Characterization of Photopolymerizable Systems Using a Thin-Film Calorimeter.* Macromolecules, 2005. **38**(24): p. 10109-10116.

34. Kaur M and Srivastava AK, *PHOTOPOLYMERIZATION: A REVIEW.* Journal of Macromolecular Science, Part C: Polymer Reviews, 2002. **42**(4): p. 481-512.

35. Morgan VA and Fewings JM, *1,6-Hexanediol diacrylate: A rapid and potent sensitizer in the printing industry.* Australasian Journal of Dermatology, 2000. **41**(3): p. 190-192.

36. Lin-Gibson S, Landis FA, and Stafford CM, *Polymerization Shrinkage Measurements of Photocross-Linked Dimethacrylate Films.* Polymer Preprints, 2006. **47**(1): p. 500-501.

37. Schaeffer WR, *New Radiation Curable Polyester Acrylate Oligomers Exhibiting Superior Abrasion Resistant Properties While Offering a Cost Effective Alternative to Urethane Acrylate Oligomers*. 2006, Sartomer Company, Inc.: Exton, PA. p. 8.

38. Acham N, Crisp J, Holman R, Kakkar S, and Kennedy R. *Shrinkage: Its Measurement and Consequences*. in *RadTech Europe*. 1995. Fribourg, Switz.

39. Neo WK and Chan-Park MB, *A New Model and Measurement Technique for Dynamic Shrinkage during Photopolymerization of Multi-Acrylates.* Macromolecular Rapid Communications, 2005. **26**(12): p. 1008-1013.

40. Braga, Ballester, and Ferracane, *Factors involved in the development of polymerization shrinkage stress in resin-composites: A systematic review.* Dental Materials, 2005. **21**(10): p. 962-970.

41. Francis LF, McCormick AV, Vaessen DM, and Payne JA, *Development and measurement of stress in polymer coatings.* Journal of Materials Science, 2002. **37**: p. 4717-4731.

42. Stolov AA, Xie T, Penelle J, and Hsu SL, *Simultaneous Measurement of Polymerization Kinetics and Stress Development in Radiation-Cured Coatings: A New Experimental Approach and Relationship between the Degree of Conversion and Stress.* Macromolecules, 2000. **33**(19): p. 6970-6976.

43. Watts DC, Marouf AS, and Al-Hindi AM, *Photo-polymerization shrinkage-stress kinetics in resin-composites: methods development.* Dental Materials, 2003. **19**(1): p. 1-11.

44. ASTM, *Standard Test Method for Measurements of Internal Stresses in Organic Coatings by Cantilever (Beam) Method.* ASTM International, D6991-05.

45. Stoney G, *The Tension of Metallic Films Deposited by Electrolysis*. Proceedings of the Royal Society of London. Series A, 1909. **82**(553): p. 172-175.

46. Corcoran EM, *Determining Stresses In Organic Coatings Using Plate Beam Deflection.* Journal of Paint Technology, 1969. **41**: p. 635-640.

47. Oxman JD, Jacobs DW, Trom MC, Sipani V, Ficek B, and Scranton AB, *Evaluation of initiator systems for controlled and sequentially curable free-radical/cationic hybrid photopolymerizations.* Journal of Polymer Science Part A: Polymer Chemistry, 2005. **43**(9): p. 1747-1756.

48. Fouassier J, *Photochemistry and UV Curing: New Trends*. First ed. 2006, Kerala, India: Research Signpost. 475.

49. Stephenson N, Kriks D, El-Maazawi M, and Scranton A, *Spatial and temporal evolution of the photo initiation rate for thick polymer systems illuminated on both sides.* Polymer International, 2005. **54**(10): p. 1429-1439.

50. Jain K, Klier J, and Scranton AB, *Photopolymerization of Butyl Acrylate-in-Water Microemulsions: Polymer Molecular Weight and End-Groups.* Polymer, 2005. **46**(25): p. 11273-11278.

51. Jain K, Rasmussen P, Scranton AB, and Rethwisch DG, *Enhanced Epoxidation of Soybean Oil Through Microemulsion Technique.* Polymer Preprints, 2004. **45**(2): p. 579-580.

52. Depierro MA, Olson AJ, and Guymon CA, *Effect of Photoinitiator Segregation on Polymerization Kinetics in Lyotropic Liquid Crystals.* Polymer, 2004. **46**(2): p. 335-345.

53. Gou L, Opheim B, Coretsopoulos CN, and Scranton AB, *CONSUMPTION OF THE MOLECULAR OXYGEN IN POLYMERIZATION SYSTEMS USING PHOTOSENSITIZED OXIDATION OF DIMETHYLANTHRACENE.* Chemical Engineering Communications, 2006. **193**(5): p. 620 - 627.

54. Kim D and Scranton A, *The role of diphenyl iodonium salt (DPI) in three-component photoinitiator systems containing methylene blue (MB) and an electron donor.* Journal of Polymer Science Part A: Polymer Chemistry, 2004. **42**(23): p. 5863-5871.

55. Klein CA, *How accurate are Stoney's equation and recent modifications.* Journal of Applied Physics, 2000. **88**(9): p. 5487-5489.

56. Chen HY, Manhart J, Hickel R, and Kunzelmann KH, *Polymerization contraction stress in light-cured packable composite resins.* Dental Materials, 2001. **17**(3): p. 253-259.

57. Fano V, Ortalli I, Pizzi S, and Bonanini M, *Polymerization shrinkage of microfilled composites determined by laser beam scanning.* Biomaterials, 1997. **18**(6): p. 467-470.

58. Chappelow CC, Pinzino CS, Jeang L, Harris CD, Holder AJ, and Eick JD, *Photoreactivity of expanding monomers and epoxy-based matrix resin systems.* Journal of Applied Polymer Science, 2000. **76**(11): p. 1715-1724.

59. Schulze T and Klemm E, *Crosslinking copolymerization of cyclic ketenacetals with low shrinkage in volume.* Macromolecular Chemistry and Physics, 1995. **196**(2): p. 567-572.

60. Nichols ME, Seubert CM, Weber WH, and Gerlock JL, *A simple Raman technique to measure the degree of cure in UV curable coatings.* Progress in Organic Coatings, 2001. **43**(4): p. 226-232.

61. Fisher RA, *The Design of Experiment*. 1935, London: Oliver & Boyd.

62. Box GEP and Behnken DW, *Some New Three Level Designs for the Study of Quatitative Variables.* Technometrics, 1960. **2**(4): p. 455-475.

63. Minitab_Inc., *Minitab User's Guide 1: Data, Graphics, and Macros*. 2003.

64. Minitab_Inc., *Minitab User's Guide 2: Data Analysis and Quality Tools*. 2003.

65. Hahn E, Murphy G, and Bruckbauer G, *Method for Producing Coatings of Low Gloss*. 1979, PPG Industries, Inc.: US.

66. Matthews JC and Couch RW, *Method and Apparatus for Providing Low Gloss and Gloss Controlled Radiation-Cured Coatings*. 1982, Fusion Systems Corporation: United States.

67. Fletcher TE, *A simple model to describe relationships between gloss behaviour, matting agent concentration and the rheology of matted paints and coatings.* Progress in Organic Coatings, 2002. **44**(1): p. 25-36.

68. Sigel GA, Ross JS, Malkowski EA, Herr REJ, and Leininger LW, *Composition and process for providing a gloss controlled, abrasion resistant coating on surface covering products*. 2001, Armstrong World Industries, Inc.: Europe.

69. Johnson J and Mercier D, *Interior Automotive Laminate with Thermoplastic Low Gloss Coating*. 1998, Avery Dennison Corporation: US.

70. Palmer D and Oliver J, *Method for Controlling Laminate Gloss*. 2002, Premark RWP Holdings: US.

71. Lee D and Hendershot R, *Method for Producing Low Sheet Gloss Coated Paper*. 1988, The Dow Chemical Company: US.

72. Hansen L, *Novel Display Device*. 1973: US.

73. Takamiya N, Kunimitsu Y, Adachi K, Mori K, Noda I, and Wakabayashi A, *Transparent Conductive Film, Low-Reflectivity Transparent Conductive Film, and Display Device*. 2000, Sumitomo Osaka Cement Co., Ltd.

74. O'Brien AK and Bowman CN, *Modeling the Effect of Oxygen on Photopolymerization Kinetics.* Macromolecular Theory and Simulations, 2006. **15**(2): p. 176-182.

75. Cook WD, *Kinetics and properties of a photopolymerized dimethacrylate oligomer.* Journal of Applied Polymer Science, 1991. **42**(8): p. 2209-2222.

76. Jakubiak J, Sionkowska A, Linden L, and Rabak J, *Isothermal Photo Differential Scanning Calorimetry. Crosslinking polymerization of multifunctional monomers in presence of visible light photoinitiators.* Journal of Thermal Analysis and Calorimetry, 2001. **65**(2): p. 435-443.

77. Scott TF, Cook WD, and Forsythe JS, *Photo-DSC cure kinetics of vinyl ester resins. I. Influence of temperature.* Polymer, 2002. **43**(22): p. 5839-5845.

78. Hohne G, Hemminger W, and Flammersheim H, *Differential Scanning Calorimetry*. 2nd ed. 2003: Springer.

79. Koenig JL, *Spectroscopy of Polymers*. Second ed. 1999, New York: Elsevier. 491.

80. Hachey M, Bogomolov A, Gordon K, and Rades T, *How Using Raman Spectroscopy and SIMPLISMA Can Accelerate the Study of Polymorphs: A Case Study Using Carbamazepine.* Raman Technology For Today's Spectroscopists, 2004. **June**: p. 16-21.

81. Mantini AR, Marzocchi MP, and Smulevich G, *Raman excitation profiles and second-derivative absorption spectra of beta-carotene.* The Journal of Chemical Physics, 1989. **91**(1): p. 85-91.

82. O'Donnell K, *Effects of Finite Stylus Width in Surface Contact Profilometry.* Applied Optics, 1993. **32**(25): p. 4922.

83. Inc. C, *COMSOL 3.3 Multiphysics Modeling*. 2006.

84. Software CA, *FEMLAB Documentation*. 2005: Stockholm, Sweden.

85. MathWorks, *R2007a*. 2007: Natick, MA.

86. Fang N, Sun C, and Zhang X, *Diffusion-limited photopolymerization in scanning micro-stereolithography.* Applied Physics A: Materials Science & Processing, 2004. **V79**(8): p. 1839-1842.

87. Leewis CM, de Jong AM, van Ijzendoorn LJ, and Broer DJ, *Simulations with a dynamic reaction--diffusion model of the polymer grating preparation by patterned ultraviolet illumination.* Journal of Applied Physics, 2004. **95**(12): p. 8352-8356.

88. Leewis CM, Mutsaers PHA, De Jong AM, Van Ijzendoorn LJ, De Voigt MJA, Ren MQ, Watt F, and Broer DJ, *The mutual diffusion coefficient for (meth)acrylate monomers as determined with a nuclear microprobe.* The Journal of Chemical Physics, 2004. **120**(4): p. 1820-1825.

89. Moreau V, Renotte Y, and Lion Y, *Characterization of DuPont Photopolymer Determination of Kinetic Parameters in a Diffusion Model.* Applied Optics, 2002. **41**: p. 3427-3435.

90. van Nostrum CF, Nolte RJM, Broer DJ, Fuhrman T, and Wendorff JH, *Photoinduced Opposite Diffusion of Nematic and Isotropic Monomers during Patterned Photopolymerization.* Chem. Mater., 1998. **10**(1): p. 135-145.

91. Zhou L-M and Mai Y-W, *Analysis of Fiber Frictional Sliding in Fiber Bundle Pushout Test.* Journal of the American Ceramic Society, 1994. **77**(8): p. 2076-2080.